PERFORMANCE ANAYLSIS OF AN INTERMEDIATE TEMPERATURE SOLID OXIDE FUEL CELL

A THESIS SUBMITTED TO
THE GRADUATE SCHOOL OF NATURAL AND APPLIED SCIENCES
OF
MIDDLE EAST TECHNICAL UNIVERSITY

BY

BORA TİMURKUTLUK

IN PARTIAL FULFILLMENT OF THE REQUIREMENTS
FOR
THE DEGREE OF MASTER OF SCIENCE
IN
MECHANICAL ENGINEERING

SEPTEMBER 2007

Approval of the thesis:

PERFORMANCE ANALYSIS OF AN INTERMEDIATE TEMPERATURE SOLID OXIDE FUEL CELL

submitted by **BORA TİMURKUTLUK** in partial fulfillment of the requirements for the degree of **Master of Science in Mechanical Engineering, Middle East Technical University** by,

Prof. Dr. Canan Özgen ________________
Dean, Graduate School of **Natural and Applied Sciences**

Prof. Dr. Kemal İder ________________
Head of Department, **Mechanical Engineering Dept., METU**

Asst. Prof. Dr. İlker Tarı ________________
Supervisor, **Mechanical Engineering Dept., METU**

Prof. Dr. Mahmut D. Mat ________________
Co-Supervisor, **Mechanical Engineering Dept., Niğde Uni.**

Examining Committee Members:

Prof. Dr. M. Haluk Aksel ______________________
Mechanical Engineering Dept., METU

Asst. Prof. Dr. İlker Tarı ______________________
Mechanical Engineering Dept., METU

Asst. Prof. Dr. Almıla G. Yazıcıoğlu ______________________
Mechanical Engineering Dept., METU

Asst. Prof. Dr. Cüneyt Sert ______________________
Mechanical Engineering Dept., METU

Prof. Dr. Mahmut D. Mat ______________________
Mechanical Engineering Dept., Niğde Uni.

Date: **06.09.2007**

I hereby declare that all information in this document has been obtained and presented in accordance with academic rules and ethical conduct. I also declare that, as required by these rules and conduct, I have fully cited and referenced all material and results that are not original to this work.

Name, Last name :Bora Timurkutluk

Signature :

ABSTRACT

PERFORMANCE ANAYLSIS OF AN INTERMEDIATE TEMPERATURE SOLID OXIDE FUEL CELL

Timurkutluk, Bora
M.S., Department of Mechanical Engineering
Supervisor : Asst. Prof. Dr. İlker Tarı
Co-Supervisor: Prof. Dr. Mahmut D. Mat

September 2007 , 105 pages

An intermediate temperature solid oxide fuel cell (SOFC) is developed and its performance is investigated experimentally and theoretically. In the experimental program, a gadolinium doped ceria based membrane electrode group is developed with the tape casting and screen printing methodology and characterized. An experimental setup is devised for the performance measurement of SOFCs and the performance of produced cells is investigated over a range of parameters including the electrolyte thickness, the sintering temperature, the operation temperature etc. The experimental setup is then further modified to measure the temperature distribution in the large SOFC single cells. The effects of operating parameters on the temperature distribution are investigated and the parameter spaces leading high efficiency without cracking the ceramic membrane are identified.

In theoretical study a mathematical model is developed to represent the fluid flow, the heat transfer, the species transport and the electrochemical reaction in intermediate temperature of solid oxide fuel cells.The differential equations are solved numerically with a commercial CFD code which employs a control volume based approach. The temperature distribution and species distribution during the

SOFC operation is analyzed. The effects of operation parameters on critical SOFC characteristics and the performance are numerically investigated over a range of parameter space.

The experimental and numerical results are compared to validate the mathematical model. The mathematical model is found to agree reasonable with experimental data.

Keywords: SOFC, modeling, GDC, performance, CFD

ÖZ

ORTA SICAKLIK KATI OKSİT YAKIT PİLİ PERFORMANS ANALİZİ

Timurkutluk, Bora
Yüksek Lisans, Makina Mühendisliği Bölümü
Tez Yöneticisi : Yrd. Doç.Dr. İlker Tarı
Ortak Tez Yöneticisi: Prof. Dr. Mahmut D. Mat

Eylül 2007, 105 sayfa

Orta sıcaklık katı oksit yakıt pili deneysel ve teorik olarak incelenmiştir. Deneysel programda gadolinium ekli ceria elektrolit tabanlı membran elektrot grupları şerit döküm ve serigrafi metotları ile geliştirilmiş ve karakterize edilmiştir. Tasarlanan deney düzeneği ile üretilen katı oksit yakıt pilleri elektrolit kalınlığı, fırınlama ve çalışma sıcaklığı gibi parametreler üzerine incelenmiştir. Revize edilen deney düzeneği ile pil içi sıcaklık dağılımları elde edilmiştir. Sıcaklık dağılımına etkileyen parametreler araştırılmış ve yüksek verimde kırılmadan çalışabilecek pil için parametre aralıkları belirlenmiştir.

Teorik çalışmada, orta sıcaklık katı oksit yakıt pilleri için akış, ısı transferi, madde transportu ve elektrokimyasal reaksiyonları içeren matematiksel model geliştirilmiştir. Diferansiyel denklemler kontrol hacim mantığı ile çalışan CFD programı yardımı ile çözülmüştür. KOYP çalışması sırasında madde dağılımları ve sıcaklık profilleri analiz edilmiştir. Önemli KOYP özelliklerine ve performansına etkisi olan çalışma parametreleri geniş bir aralıkta nümerik olarak incelenmiştir.

Deneysel ve nümerik sonuçlar matematiksel modeli doğrulamak için karşılaştırılmıştır. Matematiksel model, deneysel sonuçlarla yakın değerler ortaya koymuştur.

Anahtar Kelimeler: KOYP, model, GDC, performans, CFD

To My Parents

ACKNOWLEDGMENTS

This work would not be possible without the support, advice and assistance of my family, friends and colleagues. Although this cannot be adequate to express my thought exactly, below I would like to acknowledge individuals who have made specific contribution to this thesis.

I would like to thank to my advisor Dr.İlker Tarı for his guidance and support throughout the duration of my work.

I would like to give my deep gratitude to Dr. Mahmut D. Mat and Dr. Yüksel Kaplan. Besides their truly advice and assistance, they provided a great research environment at Fuel Cell Laboratory at Nigde University and gave me freedom to explore.

I appreciate my friends and colleagues, especially Adem Cicek and Ersen Göktürk, for their always readiness to help.

I wish to give my special thanks to my family for their constant support and encouragement.

I also extend my thanks to TUBITAK for financial support under project number 105M096 and VESTEL Savunma A.Ş. for equipment and materials support.

TABLE OF CONTENTS

PLAGIARISM iii
ABSTRACT iv
ÖZ……….. vi
DEDICATION viii
ACKNOWLEDGEMENTS ix
TABLE OF CONTENTS x
LIST OF TABLES xiii
LIST OF FIGURES xiv
LIST OF SYMBOLS xvii
LIST OF ABBREVIATIONS xx

CHAPTER

1. INTRODUCTION 1
    1.1 Technology Overview 1
        1.1.1 Fuel Cell Description 1
        1.1.2 Fuel Cell Types 2
    1. 2 Solid Oxide Fuel Cells (SOFCs) 4
        1.2.1 SOFC Elements 4
        1.2.2 SOFC Configuration Options 7
        1.2.3 SOFC Materials 11
        1.2.4 SOFC Applications 12
    1.3 Objectives 15
    1.4 Methodology 16
    1.5 Thesis Outline 17
2. LITERATURE SURVEY 18
    2.1 Macro Modeling 19

2.2 Micro Modeling 26

3. FUNDAMENTALS OF SOFC: OPERATION AND DESCRIPTIONS 28

3.1 Basic Operation Principles of SOFCs 28

3.2 Open Circuit Potential 30

3.3 Polarizations 32

3.1.1 Ohmic Polarization 33

3.1.2 Activation Polarization 33

3.1.3 Concentration/Mass Transport Polarization 34

3.4 Actual Cell Potential 35

3.5 Cell Efficiency 37

4. MATHEMATICAL MODELING AND NUMERICAL ANALYSIS 39

4.1 General Governing Equations 41

4.1.1 Conservation of Mass 41

4.1.2 Species Balance 42

4.1.3 Momentum Equation 43

4.1.4 Charge Balance 43

4.1.5 Energy Balance 44

4.1.6 Electrochemical Model 44

4.1.7 Chemical Reactions 45

4.1.8 Boundary Conditions 45

4.2 Numerical Solution Method 46

4.2.1 Finite Volume Method 46

4.2.1.1 Transient Term 47

4.2.1.2 Convection Term 47

4.2.1.3 Diffusion Term 48

4.2.1.4 Source Term 49

4.2.2 Finite Difference Equation 49

4.2.3 Geometry of the Cell 50

4.2.4 Material and Parameter Setting 50

4.2.5 Numerical Accuracy 51

4.3 Numerical Results 53

4.3.1 Species Distribution 53

4.3.2 Temperature Distribution 56
4.3.3 Parametric Study 58
4.3.3.1 Effect of Operating Pressure 58
4.3.3.2 Effect of Fuel Gas Composition 60
4.3.3.3 Effect of Flow rate 62
5. EXPERIMENTAL ANALYSIS 64
5.1 The Experimental Set-up 64
5.2 Experimental Results 70
5.2.1 Performance Measurements 70
5.2.1.1 PEN Development 70
5.2.1.2 Parametric Study 73
5.2.2 Results and Discussions 73
5.2.2.1 Effect of Operation Temperature 73
5.2.2.2 Effect of Electrolyte Thickness 76
5.2.2.3 Effect of Sintering Temperature 78
5.3 Temperature Measurements 80
6. COMPARISON OF EXPERIMENTAL AND NUMERICAL RESULTS 84
7. CONCLUSION AND FUTURE STUDIES 87
REFERENCES 90

LIST OF TABLES

Table 1.1 Technical characteristics of different fuel cells [7] 3
Table 1.2 The tubular and planar SOFCs, advantages and disadvantages 10
Table 3.1 Example constants for equation (3.24) [129] 36
Table 4.1 Porous Media Setting 51
Table 4.2 Transport Parameter Setting 51

LIST OF FIGURES

Figure 1.1 Schematic of a fuel cell 1
Figure 1.2 Simple block representation of PEN structure (a) front and (b) isometric view 5
Figure 1.3 (a) SOFC single cell (b) SOFC stack with 3 cells 6
Figure 1.4 Schematic diagram of an IP-SOFC module [10] 7
Figure 1.5 Tubular SOFC design [11] 8
Figure 1.6 Monolithic SOFC design [13] 8
Figure 1.7 Flat-planar SOFC design [12] 9
Figure 1.8 Radial-planar SOFC design [7] 9
Figure 1.9 SOFC PEN structure configurations (a) cathode supported (b) anode supported (c) electrolyte supported (d) porous substrate supported 10
Figure 1.10 A schematic of the future GE SOFC hybrid [90] 13
Figure 1.11 The MHI SOFC hybrid units with its co-gen unit [90] 14
Figure 1.12 Nano Dynamic’s portable solid oxide fuel cell unit [90] 14
Figure 1.13 ITN 15-Cell Palm Power SOFC Stack [92] 15
Figure 2.1 Schematic diagrams of the one cell stack and the single-unit cell model for the anode-supported SOFC [98] 20
Figure 2.2 Photograph of 20-cell test rig [107] 22
Figure 2.3 (a) SOFC schematic configuration (b) BMW APU schematic layout [117] 25
Figure 2.4 Orientation of a flat-tube SOFC in a cell bundle [118] 25
Figure 3.1 Schematic of SOFC working principle 29
Figure 3.2 Cell voltage of a typical SOFC operating at 800°C 37
Figure 4.1 SOFC system of interest (not to scale) (a) cross section of one channel (b) 3D view) 40

Figure 4.2 The dimensions of SOFC model considered 41
Figure 4.3 2-D control volumes 48
Figure 4.4 Meshed structure of the domain of interest (+ : volumes).......... 50
Figure 4.5 Hydrogen consumption depending on grid spacing 52
Figure 4.6 Carbon monoxide consumption depending on grid spacing 53
Figure 4.7 Hydrogen concentration along the fuel gas channel.......... 54
Figure 4.8 CO concentration along the fuel gas channel 55
Figure 4.9 H_2O concentration along the anode gas channel 55
Figure 4.10 Carbon dioxide concentration along the gas channel 56
Figure 4.11 Temperature distribution on the anode through anode gas channels...... 57
Figure 4.12 Anode channel temperature through anode gas channels (left: in the middle of the gas channel and right: at the top of the gas channel) 57
Figure 4.13 Temperature distribution along gas channel under various operation pressure (P=1Bar) 59
Figure 4.14 H_2 consumption along anode channel under various operating pressures (P=1Bar) 59
Figure 4.15 CO consumption along anode channel under various operating pressures (P=1Bar) 60
Figure 4.16 Temperature distribution along gas channel under various hydrogen content in the fuel (H=0.096 (wt.%)) 61
Figure 4.17 Hydrogen consumption along the anode gas channel under various hydrogen content in the fuel (H=0.096 (wt.%)) 61
Figure 4.18 Temperature distribution along gas channel under various mass flow rates ($\dot{m}_{air}$= 2.1x10^{-5} kgs^{-1} and $\dot{m}_{fuel}$=3.4x10^{-5} kgs^{-1}) 62
Figure 4.19 H_2 consumption along anode channel under various mass flow rates ($\dot{m}_{air}$= 2.1x10^{-5} kgs^{-1} and $\dot{m}_{fuel}$=3.4x10^{-5} kgs^{-1}) 63
Figure 5.1 The block diagram of the experimental set up for the first group 66
Figure 5.2 Experimental set up components photos (a) an example of the interconnector channel design (b) electrolyte before sintering (c) electrolyte after sintering (d) cathode after sintering (e) anode after sintering (f) sealing material 67
Figure 5.3 Interconnects gas channel design.......... 67

Figure 5.4 Thermocouples placement on the interconnector 68
Figure 5.5 Experimental set up photo 69
Figure 5.6 Schematic of fabricated single cell configuration 69
Figure 5.7 Compact single cell (not to scale)... 70
Figure 5.8 Ball milling instrument 71
Figure 5.9 Laboratory scale tape casting equipment.. 72
Figure 5.10 SEM pictures of the PEN (a) Electrolyte (b) Electrolyte (left)-anode (right) 73
Figure 5.11 Effect of operating temperature on current density at V=0.7V 74
Figure 5.12 Effect of operating temperature on OCV.. 75
Figure 5.13 I-V characteristics of fabricated PEN 76
Figure 5.14 Effect of electrolyte thickness on current density at V=0.7V................. 77
Figure 5.15 Effect of electrolyte thickness on OCV 77
Figure 5.16 Effect of electrolyte sintering temperature on current density at V=0.7V 78
Figure 5.17 Effect of electrolyte sintering temperature on OCV 79
Figure 5.18 Temperature distributions over PEN before and after load ($\dot{m}_{\text{air}}$= 2.1x10^{-5} and $\dot{m}_{\text{fuel}}$=3.4x10^{-6}) 80
Figure 5.19 Temperature distributions over PEN under no load ($\dot{m}_{\text{air}}$= 2.1x10^{-5} and $\dot{m}_{\text{fuel}}$=3.4x10^{-6}) 81
Figure 5.20 Temperature distributions over PEN under load ($\dot{m}_{\text{air}}$= 4.2x10^{-6} and $\dot{m}_{\text{fuel}}$=6.8x10^{-7}) 82
Figure 5.21 Temperature distributions over PEN under load ($\dot{m}_{\text{air}}$=3.15x10^{-5} and $\dot{m}_{\text{fuel}}$=5.1x10^{-6}) 82
Figure 5.22 Temperature distributions over PEN under load ($\dot{m}_{\text{air}}$=4.2x10^{-5} and $\dot{m}_{\text{fuel}}$=6.8x10^{-6}) 83
Figure 6.1 Temperature profile on the anode under various mass flow rates 84
Figure 6.2 Temperature profile on the anode when $\dot{m}_{\text{air}}$= 4.2x10^{-6} and $\dot{m}_{\text{fuel}}$=6.8x10^{-7} 85

LIST OF SYMBOLS

x,y,z	Primary Cartesian coordinates
ΔG	Change in Gibbs free energy
ΔG^0	Change in Gibbs free energy at standard pressure
ΔH	Change in enthalpy
ΔS	Change in entropy
ΔV_{act}	Activation overpotential
ΔV_{con}	Concentration overpotential
ΔV_{ohm}	Ohmic overpotential
A	Activation overpotential equation constant
c_i	Concentration
c_p	Specific heat
F	Faraday constant
$\vec{g}$	Gravity vector
I	Current
i	Current density
i_{exc}	Exchange current density
i_{exc}^a	Anode exchange current density
i_{exc}^c	Cathode exchange current density
i_{lm}^a	Anode limited current density
i_{lm}^c	Cathode limited current density
$\vec{J}_{el}$	Electronic current density
$\vec{J}_i$	Diffusion flux
$\vec{J}_{io}$	Ionic current density
$\vec{J}_o$	Exchange current density at equilibrium
k	Thermal conductivity
M_i	Molecular weight

m	Mass flow rate
$\dot{m}_{\text{air}}$	Air mass flow rate
$\dot{m}_{\text{fuel}}$	Fuel mass flow rate
N	Avogadro number
n	Number of electrons
$\vec{n}$	Normal vector to the boundary
P	Pressure
P_o	Standard pressure
P_{elec}^{max}	Maximum electrical power
R	Ideal gas constant
S_c	Source term for the charge
S_e	Source term for the energy
S_m	Source term for the mass
$S_{s,i}$	Source term for the concentration
S_{Φ}	Source term for a generic variable
T	Temperature
t	Time
V	Voltage
V^0	Electromotive force at standard pressure
V_{cell}	Actual cell potential
V_{theor}	Theoretical cell potential
$\vec{V}$	Velocity vector
α	Activation of the reaction gases
α	Charge transfer coefficient
ξ , λ , γ	Actual cell potential equation constants
ρ	Density
ε	Porosity
Φ	Generic variable
μ	Dynamic viscosity
σ	Conductivity
ζ	Permeability
Γ	Mass diffusivity

ϕ	Electric potential
$\vec{\tau}$	Shear stress tensor
η_{cell}	Cell efficiency
μ_{fuel}	Fuel utilization

LIST OF ABBREVIATIONS

AFC	Alkaline Fuel Cell
APU	Auxiliary Power Unit
ASR	Area Specific Resistance
CFD	Computational Fluid Dynamics
DMFC	Direct Methanol Fuel Cell
EDB	Erbia Doped Bismuth Oxide
EMF	Electromotive Force
FDE	Finite Difference Equation
GE	General Electric
GDC	Gadolinium Doped Ceria
HPD	High Power Density
IP-SOFC	Integrated Planar Solid Oxide Fuel Cell
LSF	Strontium Doped Lanthanum Ferrite
LSM	Strontium Doped Lanthanum Manganite
MCFC	Molten Carbonate Fuel Cell
MEA	Membrane Electrode Assembly
OCV	Open Circuit Voltage
PAFC	Phosphoric Acid Fuel Cell
PCFC	Protonic Ceramic Fuel Cell
PEMFC	Proton Exchange Membrane Fuel Cell
PEN	Positive Electrode-Electrolyte-Negative Electrode
SAFC	Sulfuric Acid Fuel Cell
SEM	Scanning Electron Microscope
SOFC	Solid Oxide Fuel Cell
TEC	Thermal Expansion Coefficient
TPB	Three Phase Boundary
YSZ	Yttria Stabilized Zirconia

CHAPTER 1

INTRODUCTION

1.1 Technology Overview

1.1.1 Fuel Cell Description

Fuel cells are electrochemical devices that convert the chemical energy of a fuel reaction directly into electrical energy (with heat as a byproduct). The fundamental physical structure of a fuel cell consists of an electrolyte in contact with porous anode and cathode electrodes and catalyst layers on both sides. A schematic representation of a fuel cell is shown in Figure 1.1.

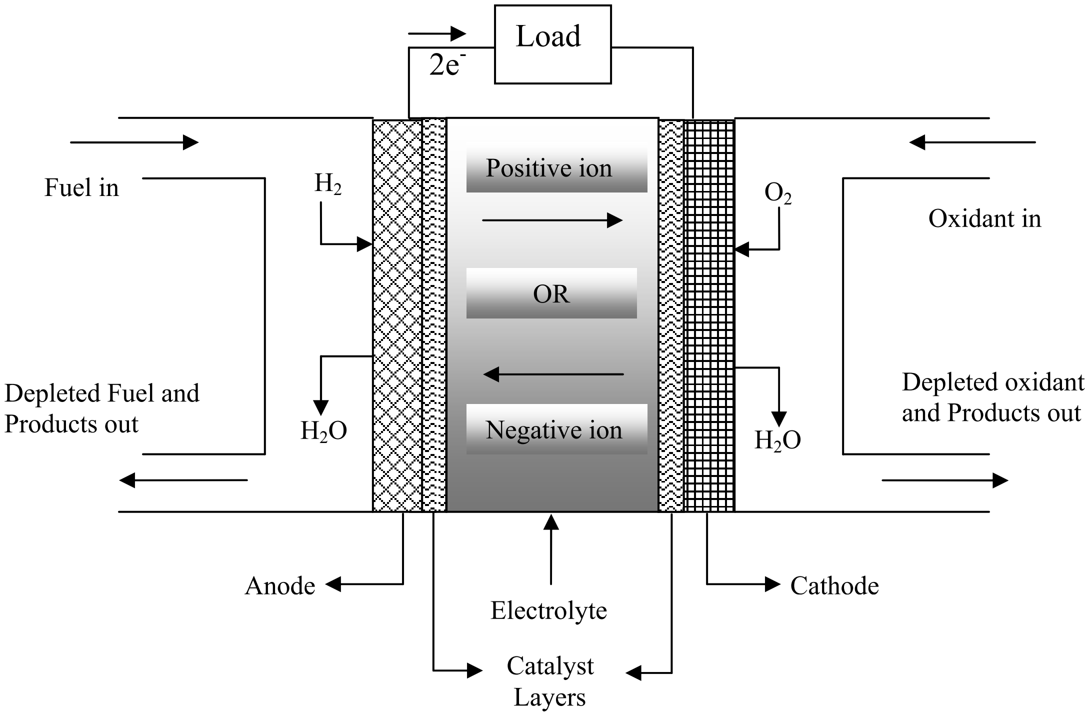

Figure 1.1 Schematic of a fuel cell

In a typical fuel cell, the fuel is fed to the anode compartment and the oxidant is supplied to the cathode compartment continuously, while the electrochemical reactions occur at the catalyst layers, the anode/electrolyte and cathode/electrolyte interfaces also known as three phase boundaries (TPBs). One of the biggest advantages of the fuel cells is their high efficiency which is not thermodynamically restricted by the Carnot efficiency [1-6]. Therefore, most of the chemical energy of the fuel can be converted into electricity in a fuel cell operation.

1.1.2 Fuel Cell Types

Their modular nature combined with the ability to generate electricity efficiently and cleanly, make fuel cells attractive for a wide variety of applications and markets. There are six major types of fuel cells in different stages of development. They can mainly be classified by the electrolyte employed and the operating temperature. The well known fuel cells are:

- Alkaline fuel cell(AFC)
- Proton exchange membrane fuel cell(PEMFC)
- Direct methanol fuel cell(DMFC)
- Phosphoric acid fuel cell(PAFC)
- Molten carbonate fuel cell(MCFC)
- Solid oxide fuel cell(SOFC)

The main characteristics of major fuel cells are given in comparison Table 1.1.

Table 1.1 Technical characteristics of different fuel cells [7]

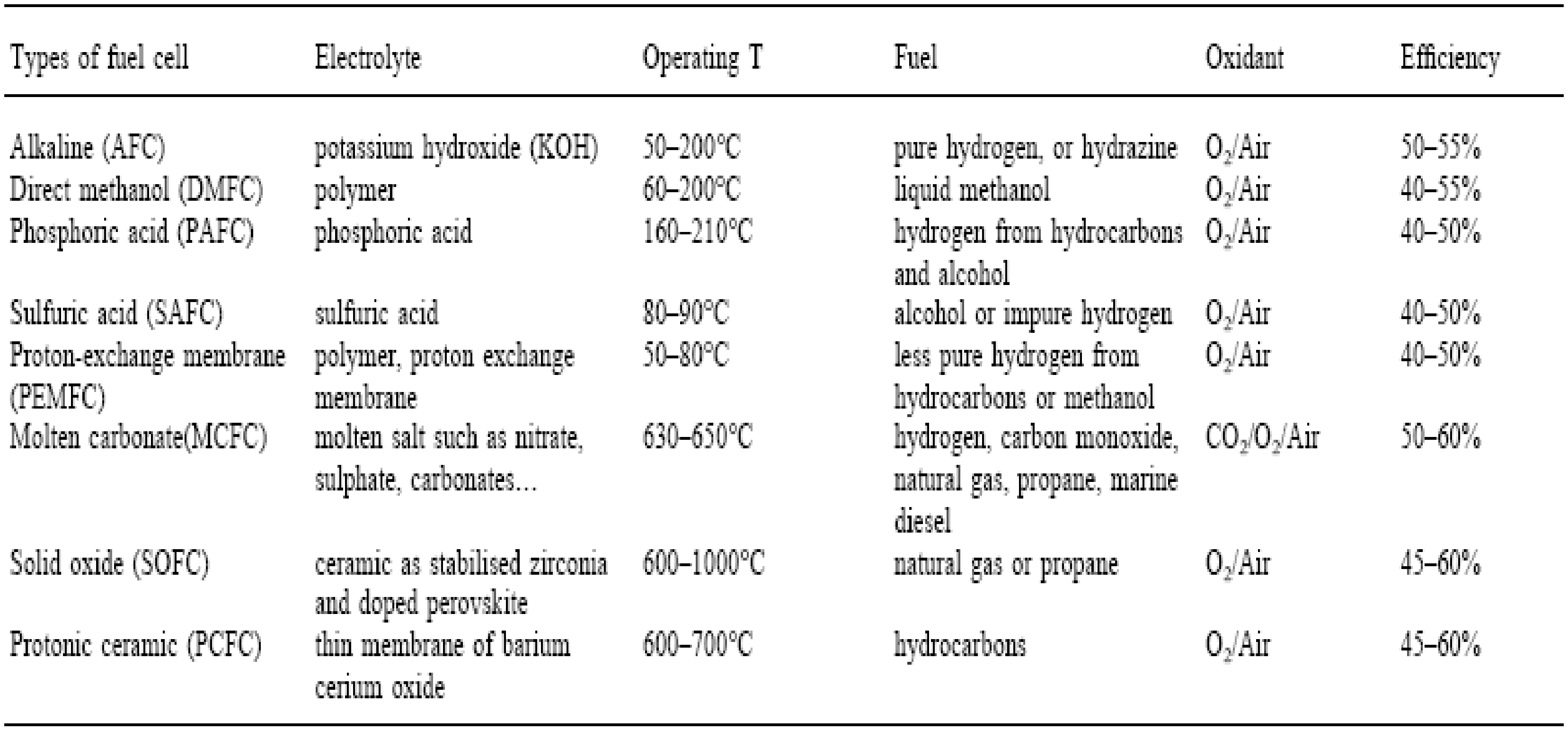

Types of fuel cell	Electrolyte	Operating T	Fuel	Oxidant	Efficiency
Alkaline (AFC)	potassium hydroxide (KOH)	50–200°C	pure hydrogen, or hydrazine	O_2/Air	50–55%
Direct methanol (DMFC)	polymer	60–200°C	liquid methanol	O_2/Air	40–55%
Phosphoric acid (PAFC)	phosphoric acid	160–210°C	hydrogen from hydrocarbons and alcohol	O_2/Air	40–50%
Sulfuric acid (SAFC)	sulfuric acid	80–90°C	alcohol or impure hydrogen	O_2/Air	40–50%
Proton-exchange membrane (PEMFC)	polymer, proton exchange membrane	50–80°C	less pure hydrogen from hydrocarbons or methanol	O_2/Air	40–50%
Molten carbonate(MCFC)	molten salt such as nitrate, sulphate, carbonates…	630–650°C	hydrogen, carbon monoxide, natural gas, propane, marine diesel	CO_2/O_2/Air	50–60%
Solid oxide (SOFC)	ceramic as stabilised zirconia and doped perovskite	600–1000°C	natural gas or propane	O_2/Air	45–60%
Protonic ceramic (PCFC)	thin membrane of barium cerium oxide	600–700°C	hydrocarbons	O_2/Air	45–60%

1. 2 Solid Oxide Fuel Cells (SOFCs)

Among the fuel cell types available, in recent years, much attention has been given to SOFCs as new electricity generating devices due to their high conversion efficiency, high operation temperature, clean and quiet operation with fuel flexibility. One of the major characteristics that puts SOFCs to a different category and makes them attractive is their high operating temperature (600-1000°C) which brings in rapid reaction kinetics without precious catalysts and byproduct of heat. The high operating temperature also allows using hydrocarbons as a fuel by means of reforming. Although CO has a poisonous effect for PEM fuel cells, SOFCs can use CO as a fuel.

Even in a small capacity, SOFC can reach 50% electrical efficiency and the electrical efficiency of SOFC combined with bottom cycle (usually with a turbine) working in the range of high pressure and large capacity (in the order of MW power output) is predicted as 70% [8]. High exhaust gas temperature (around 600-1000ºC) allows cogeneration; therefore the combined heat and power total efficiency can reach 90% [9]. Another advantage of SOFCs is that they employ a ceramic PEN (positive electrode-electrolyte-negative electrode) which does not require expensive platinum catalyst as in PEM fuel cell. Therefore, they are potentially cheaper and ease to manufacture.

1.2.1 SOFC Elements

The membrane-electrode assembly (MEA) or PEN structure is the key element for SOFC systems. PEN structure consists of a solid oxygen ion conducting electrolyte with porous anode and cathode electrodes which includes fuel and oxygen catalysts respectively printed on each side (Fig. 1.2).

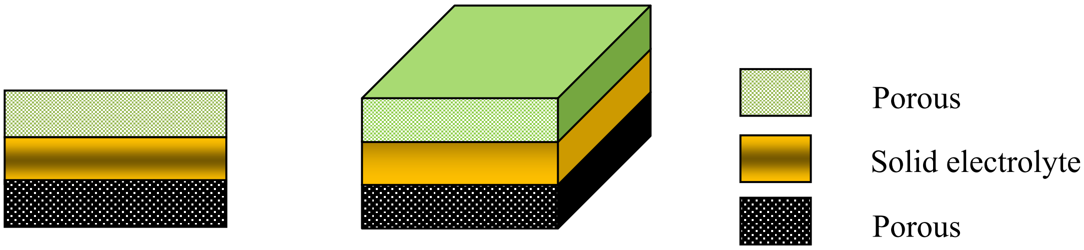

(a) (b)

Figure 1.2 Simple block representation of PEN structure (a) front and (b) isometric view

In order to collect current from electrodes, interconnector application is required. Interconnectors also known as current collectors have gas flow channels to feed fuel and oxidant to anode and cathode compartments respectively. SOFC composed of PEN structure and two interconnects with gas seals is called as a single cell producing, 0.5–0.9 V DC voltage. In order to have high power as well as high cell potential, single cells are serially connected to form SOFC stacks. A SOFC stack and a single cell are illustrated in Fig. 1.3 with system elements.

The main electrochemical reaction takes place in the electrodes. Oxygen is reduced in the cathode catalyst layer while oxygen ions react with hydrogen and carbon monoxide in the anode catalyst layer to form water, carbon dioxide and electrons. The structure of the anode must be porous to enable the gas to penetrate the reaction sites. The electrochemical reaction occurs at locations where the gas phase meets with the electrode and the electrolyte phases which are called as three phase boundaries (TPBs). To increase three phase boundary, electrode materials are usually mixed with the electrolyte materials. The free electrons produced must easily be transported to the current collector side. Therefore, the structure and tailoring of the electrodes are very important for both high electrochemical activities and electron transport.

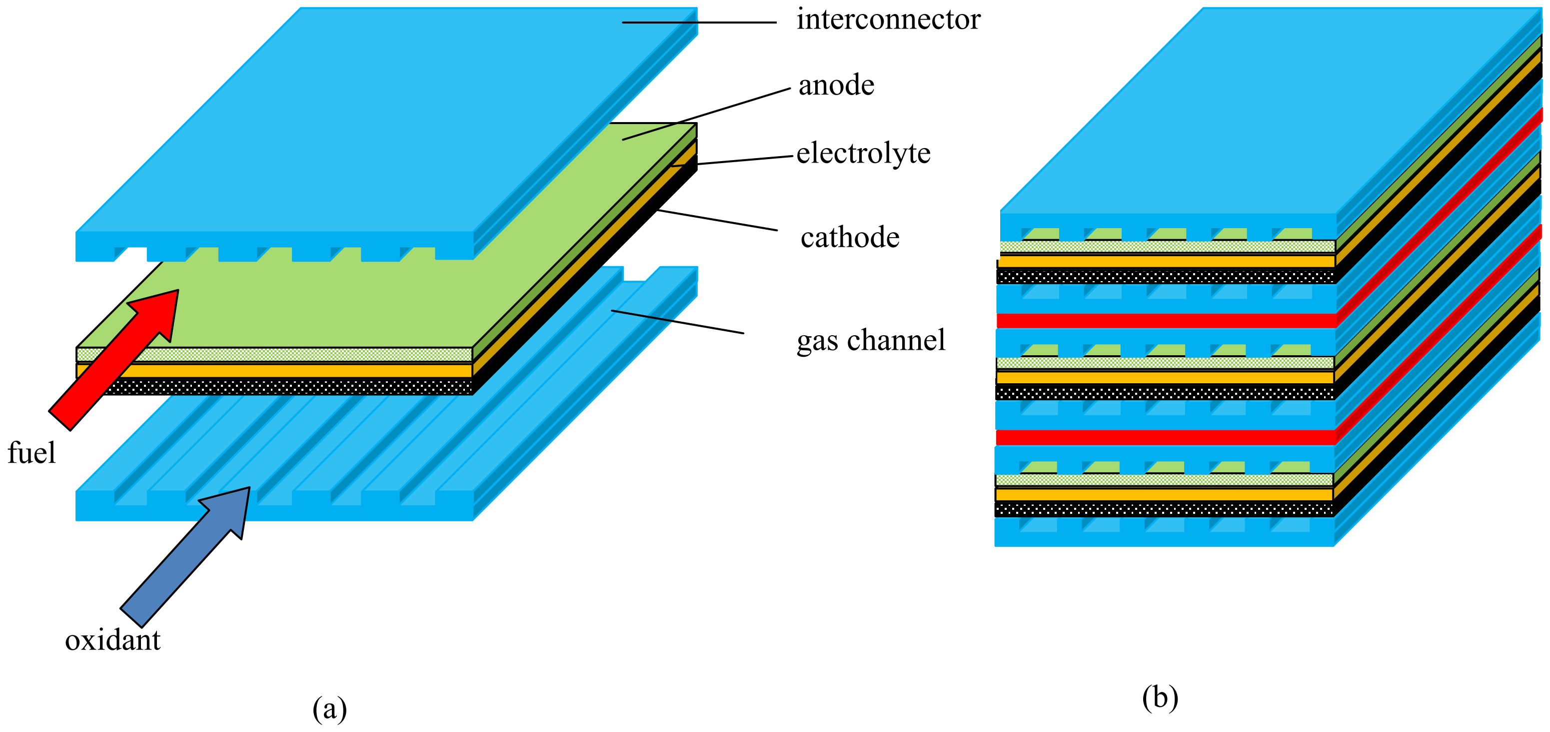

Figure 1.3 (a) SOFC single cell (b) SOFC stack with 3 cells

The solid oxide electrolyte must be free of porosity so that the fuel and the oxidant can react only by the electrochemical reaction. The electrolyte conducts oxygen ions from a vacancy mechanism in the lattice structure. The ion conduction mechanism is activated at high temperatures. Due to high operating temperature electrolyte should tolerate quick temperature rise or drop. In addition, the oxygen ion conductivity of the electrolyte must be as close to unity as possible whereas its electronic conductivity must be as close to zero as possible. In the SOFC system view, all elements must have chemical stability and compatibility with other system elements, including the thermal expansion coefficient (TEC).

1.2.2 SOFC Configuration Options

There exist three major SOFC design configurations: tubular, planar and monolithic structures. Siemens-Westinghouse Company has been developing tubular SOFC technology for over 20 years. However, a new SOFC concept namely integrated planar SOFC (IP-SOFC) (Fig. 1.4), developed by Rolls-Royce has gained a lot of attention [10]. To date, of the three main types, the tubular SOFC (Fig. 1.5) is the well-known type SOFC. Although it is problematic in that it is very difficult to produce similar to monolithic type (Fig. 1.6) and it has low power density in comparison with the planar or the monolithic type, it is somewhat advantageous in that it is easy to accomplish both gas sealing and interconnection application of single cells during stack manufacturing.

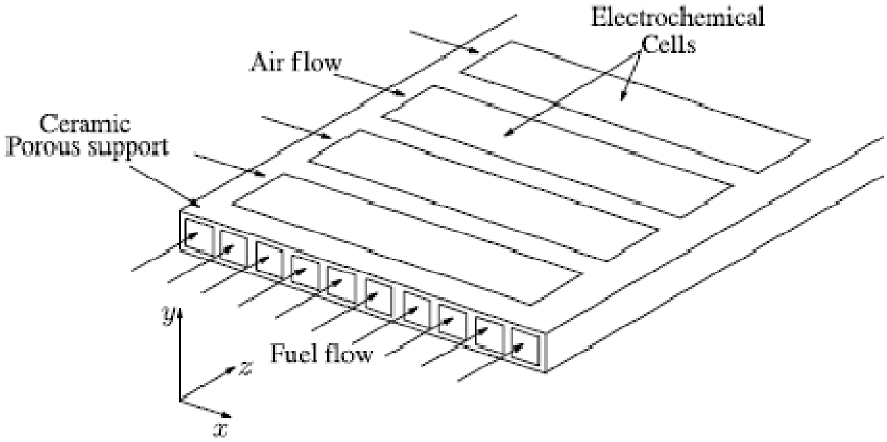

Figure 1.4 Schematic diagram of an IP-SOFC module [10]

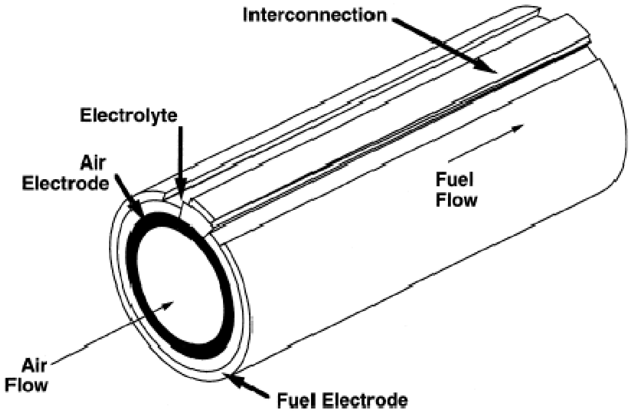

Figure 1.5 Tubular SOFC design [11]

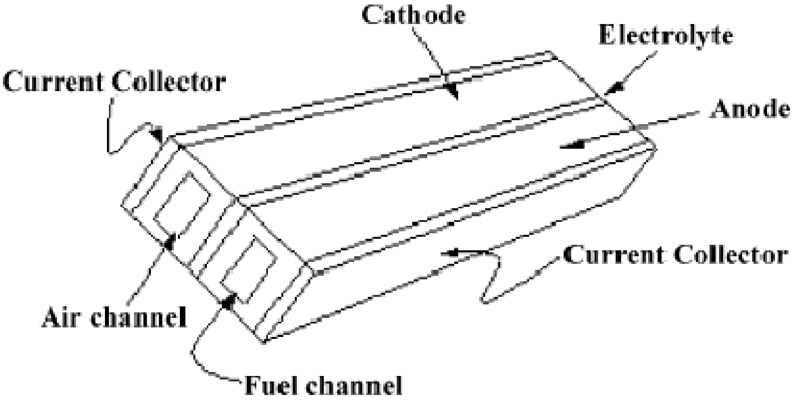

Figure 1.6 Monolithic SOFC design [13]

On the other hand in addition to easier fabrication, the planar type can give the power density at an extent which cannot be reached by the tubular or monolithic types due to their structural disadvantages. In this regard, recently, the planar SOFC rather than the tubular or the monolithic types have been studied and developed in two forms of radial and flat types (Fig. 1.7-8). The comparison of the tubular and the planar SOFCs is summarized in Table 1.2.

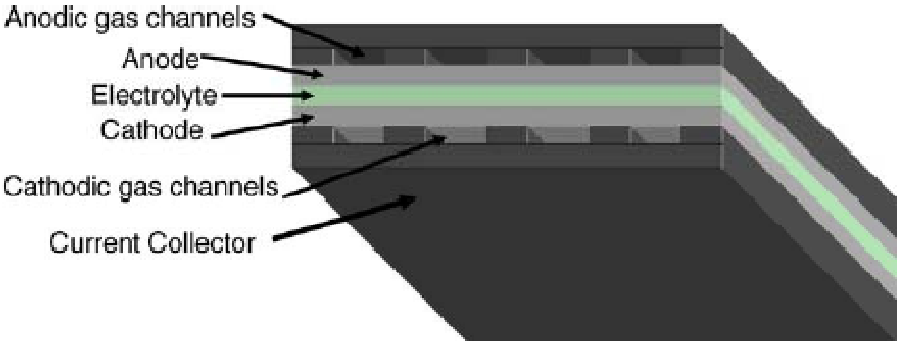

Figure 1.7 Flat-planar SOFC design [12]

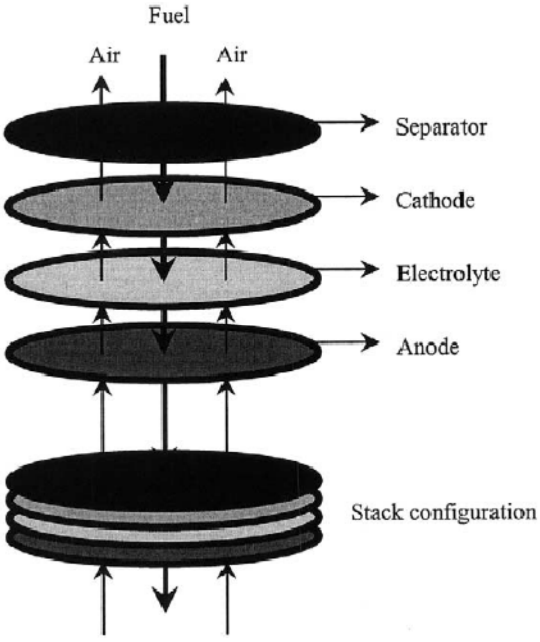

Figure 1.8 Radial-planar SOFC design [7]

Table 1.2 The tubular and planar SOFCs, advantages and disadvantages

Property	**Tubular**	**Planar**
Power density	Low	High
Volumetric power density	Low	High
High temperature sealing	Not necessary	Necessary
Start up and shut down	Fast	Slow
Interconnector fabrication	Hard	High cost
Production cost	High	Low

The planar SOFCs can mainly be manufactured either electrolyte or electrode supported (Fig. 1.9). For electrode supported cells, mass limitation problems arise due to thick electrodes. The use of a new material to support the two electrodes and the electrolyte increases the complexity in the porous supported design. The electrolyte supported SOFCs, however, have relatively strong structures and are less susceptible to failure. In addition to these four types, the interconnect supports can also be used. Although the structure is as strong as that of electrolyte supported configurations, it is problematic in that the design of the flow-field is restricted by the cell support requirement [14].

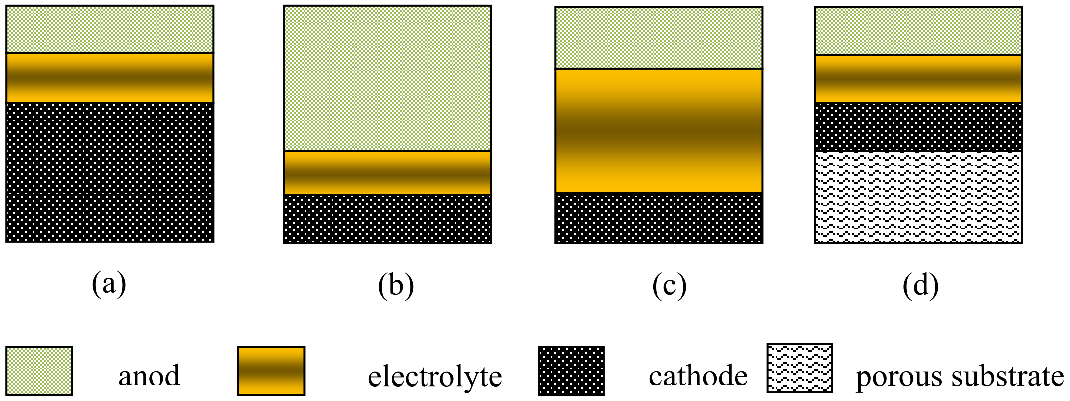

Figure 1.9 SOFC PEN structure configurations (a) cathode supported (b) anode supported (c) electrolyte supported (d) porous substrate supported

1.2.3 SOFC Materials

The typical SOFC single cell PEN structure is composed of a YSZ (Yittria stabilized zirconia: Y_2O_3-ZrO_2) electrolyte, a Ni/YSZ (nickel and YSZ) cermet anode and a LSM/YSZ (strontium doped lanthanum manganite and YSZ) cathode.

YSZ has been a promising and widely used electrolyte material for SOFCs. In addition to showing pure ionic conductivity [11,15-24], YSZ has very good chemical stability [15,17-21, 23,25] and good mechanical properties [16-18,21,26]. The highest ionic conductivity is obtained from 8YSZ (%8 Y_2O_3-ZrO_2) at around 1000°C [20,27-30]. Therefore, YSZ supported SOFCs require high operating temperatures around 1000°C for acceptable performance and ionic conductivity [31,32].

At hydrogen fueled SOFC operating conditions, Ni/YSZ anode shows excellent catalytic activity [33-48] and good chemical stability [33,35,39,42,45,48]. Moreover, Ni is reported as a very good current collector [43,48] in addition to its low cost [35,36,38-40,44,47,49]. In the case of hydrocarbon fueled SOFC with Ni anode, however, carbon deposition is seen [33,35,50-71] covering the anode active sites thus reducing the cell performance. Even at 400°C, carbon deposition is observed [72]. The studies in the literature on addition of Ru [36], Mo [35,54], Au [35], Cu[51,53,73] and CeO_2 [53,57,74] to Ni/YSZ anode show no or less carbon deposition indicating that direct utilization of hydrocarbons is possible. The other problem when hydrocarbons used as a fuel for SOFC is sulfur poisoning. The small amount of S that hydrocarbon fuels have reacts with H to form H_2S resulting in the loss of cell performance by blocking the active sites of anode like in carbon deposition[33-35,38,43,60,65,73,75]. Therefore, the addition of a sulfur removal unit to a hydrocarbon fueled Ni/YSZ anode-SOFC system is considered as unavoidable.

The high operating temperatures of conventional SOFC systems based on YSZ electrolyte (~1000°C) lead to high production costs [15-17,32,76-82] due to difficulties in production [15,32,78,80,83,84]. At such a high temperature that is required for the YSZ electrolyte to achieve adequate ionic conduction, it is difficult to expect a good long-term stability [16,17,28-32,77,78,80,81,84,86]. It is also not easy to reach that high temperature during start up and to cool down the system during shut down. Both necessitate long times limiting the SOFC application areas. In addition, high temperature-resistant materials are limited and this is the chief obstacle for interconnect and sealing elements.

Therefore, it is essential to lower the SOFC operating temperature from the viewpoint of cost reduction and long-term stability. By lowering SOFC working temperatures, low-cost stainless steels and glass based materials can be used as interconnect and sealing materials, respectively. Furthermore, due to wider choices of materials more production techniques can be used and complex shaped SOFC elements can be designed and fabricated. The reduced operating temperature serves in reducing the time and energy for start-up and quick shut-down behaviors enabling SOFCs to have wider application areas from automobile industry to stable power generation plants.

Thus, the reduction in the operation temperature of SOFCs is one of the key issues in the aspects of the cost reduction and the long term operation without degradation as well as commercialization of the SOFC systems. One way to reduce SOFC operation temperature is replacing YSZ with alternative electrolyte materials that are showing similar characteristics at low temperatures. Gadolinium doped ceria (Gd doped Ce_2O_3=GDC) has been regarded as the most promising electrolyte candidate for intermediate temperature (~500-600°C) SOFCs. GDC exhibit higher ionic conductivity than YSZ at this intermediate temperature range [16,86].

1.2.4 SOFC Applications

SOFCs have been considered as stationary power generating systems due to high operating temperatures, high energy conversion efficiency and hot exhaust gases. Siemens Westinghouse has been leading this technology. There exist many SOFC power stations installed by Siemens Westinghouse working with a power output ranging from 25kW to 1MW [87-89].

Since an SOFC system can provide efficient, quiet and clean power, it can be used for military applications. Owing to their low sensitivity to contaminant poisoning, SOFCs may be used with a number of hydrocarbons as fuel for auxiliary power units as well. Owing to these highlights of the SOFCs, many companies in the world have been developing this technology.

General Electric (GE) is working on the US Department of Energy Clean Coal Initiative, which aims by 2013 to have an efficient Multi-MW SOFC in combination with coal gasification and it has recently announced that as part of the project has delivered a 49% efficient 6kW prototype to the National Energy Technology Laboratory for testing [90]. A schematic of the future GE SOFC hybrid is shown in Fig.1.10.

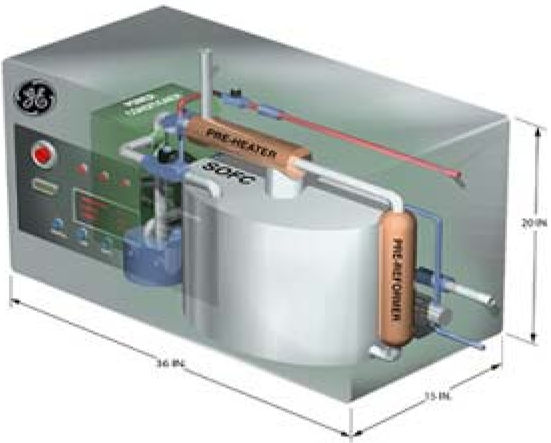

Figure 1.10 A schematic of the future GE SOFC hybrid [90]

Mitsubishi Heavy Industries (MHI) planned to manufacture a 200kW SOFC-MGT during 2006 and undertake verification tests in 2007 [90].

Figure 1.11 The MHI SOFC hybrid units with its co-gen unit [90]

US firm NanoDynamic has been working on its portable solid oxide fuel cell (Fig. 1.12). The company also gained a patent on SOFC structures [90]. Besides these companies, Unitel Technologies, Franklin Fuel Cells, Versa Power Systems and ITN Energy Systems have been developing SOFCs for use in military applications [91]. ITN has now fabricated a 15-cell SOFC stack (Fig. 1.13) and integrated it with balance-of-plant components [92].

Figure 1.12 Nano Dynamic’s portable solid oxide fuel cell unit [90]

Figure 1.13 ITN 15-Cell Palm Power SOFC Stack [92]

1.3 Objectives

Solid oxide fuel cells are receiving much attention in recent years as a means of electricity generation devices with high efficiency. It is modular nature allows application from mili-watt to megawatts. The main problem of SOFC is high operation temperature and brittle ceramic membrane electrode group which makes SOFC are expensive and unreliable compared to conventional electricity generators.

Using gadolinium doped ceria instead of Yittria stabilized zirconia as electrolyte significantly decreases the operation temperature down to 600 ºC from 1000 ºC. At 600ºC, it is possible to use a cheaper stainless steel in interconnectors; cheaper sealing materials which will be significantly reduce high cost of SOFCs. The lower operating temperatures also enable fast start up/ slow down and also reliable operation.

Although there are many experimental and theoretical works for high temperature SOFC which employs YSZ electrolyte there is only a few studies available for gadolinium doped ceria based SOFCs. Therefore the objectives of this study can be summarized as;

1. Develop a SOFC cell based on gadolinium doped ceria which is not available in the market.
2. Extend dimension of GDC based PEN to be able to use in practical applications.

3. Devise an experimental set up for performance determination of PEN and cell developed.
4. Devise an experimental set up to measure the temperature distribution in the SOFC cells. This data will be very important for identification of safe operation SOFC without breaking ceramic PEN and high performance.
5. Develop a mathematical model to estimate performance of a SOFC which employs GDC based PEN and investigate temperature distribution, species distribution and effects of operating conditions on the performance of SOFC cell.
6. Compare and validate numerical results with experimental data and improve the mathematical model.

1.4 Methodology

In this study, the performance of a GDC based SOFC cell is investigated experimentally and numerically. Since there is no commercial GDC available, in first step of the study, PENs with GDC electrolyte are produced and characterized to improve performance of PEN, a range of parameter are investigated.

To be able to understand the basic mechanisms of SOFC operation at intermediate temperatures, a mathematical model which considers fluid flow, heat transfer, species transport and electrochemical reactions is developed and differential equations are numerically solved with a commercial CFD code which employs a control volume based methodology. The effects of operating conditions on the SOFC performance are then numerically investigated.

An experimental set up is designed and established to understand the details of SOFC operation, to measure single SOFC cells performance depending on operation condition. The experimental set up is then modified to measure temperature distribution on the SOFC cell. The data is used to study the effects of some parameters on the temperature distribution and comparison with numerical results.

1.5 Thesis Outline

In the following two chapters, literature survey and introduction to SOFC is given. The mathematical modeling, governing equations, simulation solutions and the details of the experimental study are provided in Chapters 4 and 5. The validation of the cell model and the comparison of the numerical and experimental results are presented in the Chapter 6. Chapter 7 concludes the present study with a summary of findings and recommendations for further work.

CHAPTER 2

LITERATURE SURVEY

Due to the brittle nature of the ceramic PEN and high operating temperature, it is crucial to control the temperature inside the cell. Although the cell components have been selected such that all have similar thermal expansion coefficient, during operation the temperature fluctuations inside the cell result in thermal stresses that may cause cracks in the cell components leading failure of the SOFC. Another point resulting from high operating temperature is that radiation becomes important.

The electrochemical reaction taking place in the cell depends on the temperature; therefore the temperature gradient affects both the current distribution and the species distribution in the system. To be able to predict the cell performance hence to better the cell design, the temperature distribution, the species distribution and the flow characteristics must be accurately calculated.

Most of the studies in the literature, therefore, have been focused on the thermal management of single cells or SOFC stacks as well as their performance. There have been numerous modeling studies in the literature to investigate the critical parameters such as thermal behavior, fluid flow, species distribution and electrochemistry of SOFCs. As SOFC technology has been developing, various SOFC models for different scales, SOFC types and components also have become available in the literature. It is possible to categorize these studies into two as micro and macro scale modeling. Micro scale models have focused on the behavior of individual SOFC components whereas macro models have considered all operational behaviors of SOFCs. Among these studies, Bove and Ubertini [94] offer a 3D, time dependent SOFC model considering all processes occurring in each cell component. The entire mathematical model is independent from the cell geometry (planar, tubular) and the modeling approaches (2D, 3D), thus can be conducted for any SOFC. The most commonly used numerical techniques are also well explained. Kakaç et al. [95] summarized the present status of the SOFC. Hussain et al. [96] purposed a general mathematical model for the planar SOFC. Their simulations have showed similar results with the experimental studies in the literature.

2.1 Macro Modeling

Macro models consider macroscopic fluid flows, temperature and species distributions as well as electrochemical reactions in SOFC operation. Generally, differential forms of mass, momentum, charge, species and energy conservation equations are solved to obtain temperature, charge and species profiles in a system. Due to the complexity of the physical phenomena and the structure of SOFC, some of the studies consider only a part of an SOFC system mainly the anode channel and the anode catalyst layer.

The studies considering only the anode sides assume a constant ionic flux across the membrane and symmetrical conditions for the heat flux. This assumption although gives reasonable results for the anode side and for understanding the phenomena, is limited due to the uniform heat flux at the membrane side boundary. Lehnert et al. [97], Yakabe et al. [98] and Virkar et al. [99] consider the electrode performance. Lehnert et al. [97] focused on the inhomogeneous temperature distribution that may result in a mechanical failure during SOFC operation running by internal steam reforming. A 1D numerical simulation program was developed for the SOFC anode using experimentally determined reaction rates and structural properties of the anode. They emphasized that the gas transport in the SOFC anode is important in order to have uniform temperature profiles during internal steam reforming. Yakaba et al. [98] developed a single unit with a double channel (Fig. 2.1) model for a counter flow pattern of the anode of the Ni/YSZ anode supported SOFC. They assumed that the gas flow in the anode is governed by Darcy's Law and the species are transferred to the electrolyte/anode interface mainly by diffusion in a multi component mixture system. The estimated concentration polarization was found to be comparable for binary H_2–H_2O and CO–CO_2 systems. Virkar et al. [99], on the other hand, studied the effect of Ni/YSZ anode microstructure on activation and concentration losses for the anode of an anode supported SOFC. They concluded that the micro structural control of the anode is essential for polarizations.

Ji et al. [100] developed a 3D mathematical model, studied the dependence of the temperature, the mass transport, the local current and power densities on the gas channel size for a planar SOFC and considered the cathode and the electrolyte. They concluded that (i) when the channel height is decreased, the higher cell efficiency is obtained due to a shorter current length together with the higher heat and mass transfer coefficients; (ii) the smaller ratios of the flow channel width to rib width improves the cell due to a reduced ohmic loss at the interface; (iii) the higher gas inlet temperature improves the cell performance and the thermal stress is reduced.

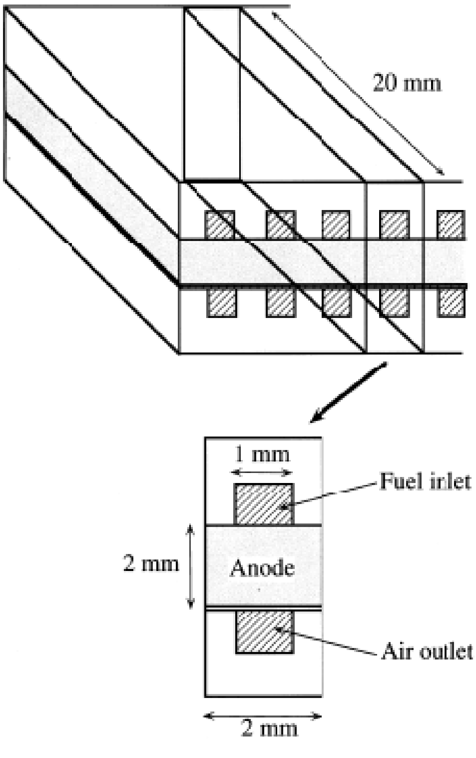

Figure 2.1 Schematic diagrams of the one cell stack and the single-unit cell model for the anode-supported SOFC [98]

Yuan et al. [101] have improved Ji study [100] by adding interconnector effect to a planar SOFC composed of a gas channel, an anode and an interconnector. Thermal boundary conditions on solid walls, mass transfer and gas permeation across the interface were applied in the analysis. Characteristic ratios: hydraulic diameter ratio and the permeation ratio, permeation rate ratios are proposed as the important parameters affecting the SOFC performance. The gas flow and the heat transfer were investigated based on these ratios considering the friction factors and Nusselt numbers. The anode characteristics and the channel size are shown to have great importance for mass transport and the heat transfer. Achenbach [102] who is mentioned almost in all SOFC modeling papers introduced a mathematical model and numerical simulation for a planar SOFC. However, interconnects were not included in this study. Chyou et al. [103] tried to establish a 2D steady state model with an integrated electrochemical and thermal analysis of a planar SOFC. Different from Achenbach [102], the insulation material and the interconnector were also taken into account. The planar SOFC performance considering the different flow patterns have been obtained. Chyou et al. [103] model is improved by Li et al. [104] by developing a new design for the interconnector of the planar SOFC and bipolar plates of PEM fuel cells. They added cylindrical current collecting elements perpendicular to the gas flow direction. The size and shape of the gas channels have been optimized. The simulation results of the designed PEM plates have showed a higher performance than that of available experimental studies in the literature.

Iwata et al. [105] predicted temperature and current density distributions in a planar SOFC with co-flow and counter flow (2D), and with cross flow (3D) configurations. When the upper and the lower surfaces of the unit cell is assumed adiabatic surfaces, corresponding to the central cells in an SOFC stack, the temperature increase was determined in all flow configurations. However, it is suppressed by the increased operation pressure. On the other hand, when the cell outer surfaces are modeled by considering the radiative heat transfer, corresponding to an SOFC in a furnace, almost flat temperature profiles were observed. Costamagna [106] numerically investigated a planar SOFC with integrated air pre-heater systems. Their model offers a nearly uniform temperature gradient along the cell without increasing the operation pressure unlike the result of to Iwata et al. [105] study.

Lockett et al. [107] installed a tubular SOFC stack composed of 20 micro tubes for an experimental unit (Fig 2.2) on thermal controlling. The numerical analysis was also included by using of FLUENT on single micro tubes. However, the comparison of the experimental and the numerical analysis is not given in the study. Burt et al. [108] discovered the cell to cell variation of the voltage in a planar SOFC stack with 5 cells, numerically. They found that the radiative heat transfer mode gives uniform temperature distribution which is essential for a higher cell performance.

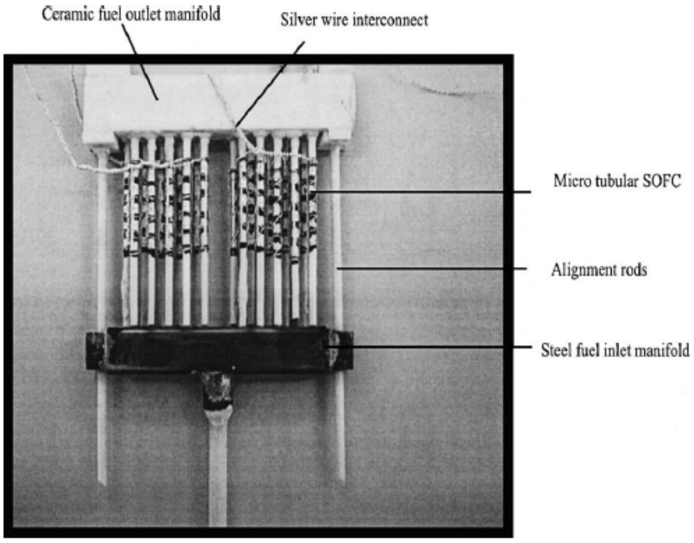

Figure 2.2 Photograph of 20-cell test rig [107]

Due to the high operating temperature of SOFCs, the radiative heat transfer becomes important. Most of the modeling studies neglected the radiative heat transfer for either after an order of magnitude analysis between the convective and the radiative heat transfer modes or simply ignored due to non-linear nature of the radiative heat transfer term. However, it is shown that radiative heat transfer homogenizes the temperature distribution in the cell. Tanaka et al. [109] studied the numerical simulations for a planar SOFC stack in order to verify the dependence of the cell performance on its operating conditions. The model includes the radiative heat transfer which is important for high temperature operation. The effect of ambient temperature on the cell voltage is investigated by a 3D simulation code that controls the whole stack. An alternative planar stack level approach was presented by Recknage et al. [110] in which PENs, interconnectors and gas seals were 3D modeled for different flow patterns. The effect of radiation was neglected due to being small relative to other heat transfer modes. The walls of the domain of interest were assumed as adiabatic surfaces and STAR-CD was used for thermo-fluid calculations. The current and temperature distributions were obtained for different flow patterns. Murthy and Federov [111] studied the radiation for a monolithic SOFC. The main governing equations were solved by FLUENT but a new code was developed for the radiation. The numerical results showed that addition of the radiation term resulted in a higher cell potential coming from the uniform temperature distribution in the monolithic cell. However, Daun et al. [112] proposed that the radiation effect is very small for the planar SOFC electrolyte and electrodes. A similar study by Xue et al. [113] for the tubular SOFC single cell also showed that the radiation term can be neglected comparing with the convection term. On the other hand, the numerical study by Damm and Federov [114] for a tubular cell suggested that the radiation effects are essential in order to obtain accurate temperature variations and cell voltages.

Damm and Federov [115] numerically investigated the temperature variations in the SOFC during start up and shut down. On the other hand, the temperature gradient inside the planar SOFC under different load conditions which is one of the important operating parameters has been studied by Inui et al. [116]. The authors have proposed a new cell temperature control method that is based on the optimization of the air utilization and the inlet gas temperature for each average current density. The simulation results for co-flow and counter-flow type cells showed that the temperature variation in the cell is suppressed, thus this new method enables SOFCs to operate under variable load conditions.

Some of the authors have been focused on modeling of SOFCs that are still under development by some companies in the world. One of them is a 3D numerical study performed by Petruzzi et al. [117] on BMW AG high temperature SOFC as an auxiliary power unit (APU) for high class car conveniences (Fig. 2.3). The simulation code has been developed in MATLAB and the SOFC APU system behaviors have been investigated during heat-up, start-up, cool down, on load and steady state. The study by Lu et al. [118] numerically investigated the flat-tube high power density (HPD) SOFC, a new design developed by Siemens Westinghouse (Fig. 2.4). The variation of the temperature, the concentration and the flow-field with the current is given. They propose a basis for an overall simulation and optimization of the flat-tube HPD-SOFC. Haberman and Young [119] have investigated 3D steady state air flow through the integrated planar SOFC developed by Rolls Royce (Fig. 1.8). SOFCs serve various fuel options, thus some modeling studies in the literature considers SOFCs under different fuel operations. Sanchez et al. [120] has offered an internal methane direct reforming tubular SOFC modeling, whereas Sang et al. has developed a 2D model for methane fueled indirect internal reforming bundles of tubular SOFCs to predict its performance. Chan and Ding [121] investigated a methane fueled SOFC power station composed of heat exchangers, an evaporator, a reformer, a mixer, piping and the fuel cell unit. The mathematical models for the system components have been developed. Suwanwarangkul et al. [122] has analyzed a syngas fueled SOFC experimentally and numerically. The similar study by Monder et al. [123] has been interested in the hydrogen sulfur fueled SOFC.

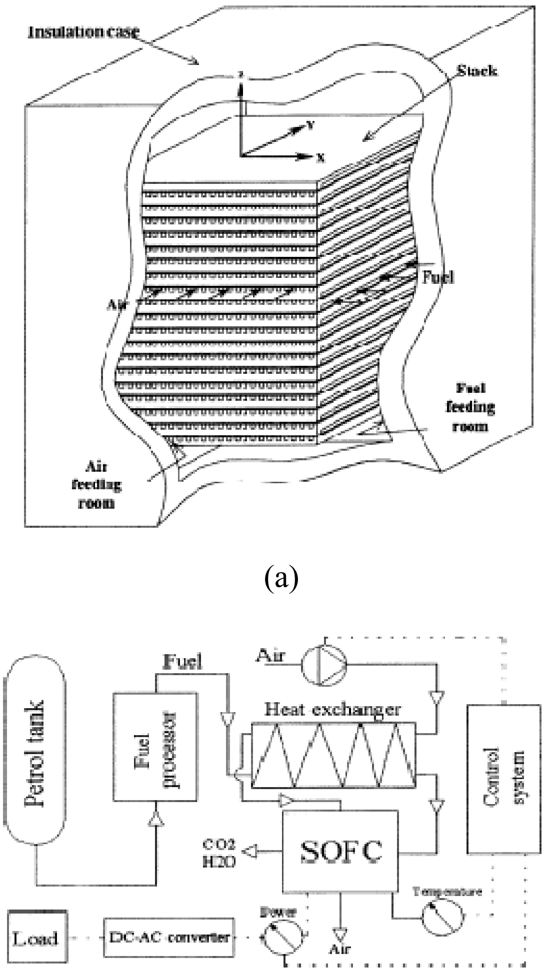

(a)

(b)

Figure 2.3 (a) SOFC schematic configuration (b) BMW APU schematic layout [117]

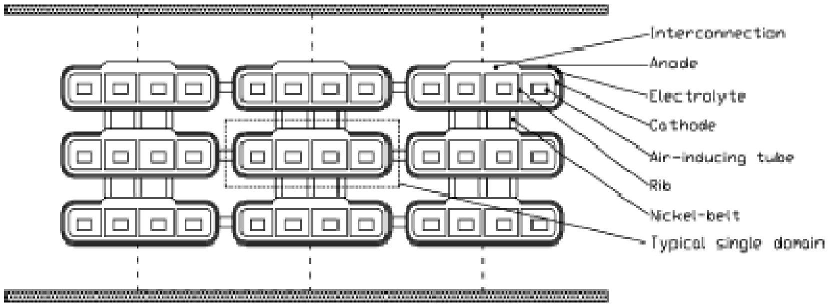

Figure 2.4 Orientation of a flat-tube SOFC in a cell bundle [118]

2.2 Micro Modeling

The micro scale models [124-126] enable to investigate micro characteristics of the PEN structure such as the porosity of the electrodes, the powder size and the thickness of the components which are believed to be critical in the PEN performance. Costamagna et al. [125] developed a micro modeling for SOFC electrodes namely EDB (Erbia-Doped Bismuth Oxide)/Pt and YSZ/LSM cathodes and YSZ/Ni anodes. They found that the morphology of the electrodes strongly influences the electrode resistance and the thickness of the electrodes should be optimized in the limits of the maximum active area and the minimum ohmic losses. Chen et al. [126] developed a complete micro model for a YSZ/LSM cathode considering all forms of polarizations related to the transport phenomena, the electrochemical processes and the microstructure of the composite cathode. They also fabricated a single cell for validation of the model. Like in Costamagna's study [125], too thin cathodes result in poor performance due to insufficient electrochemical active areas. The larger particle size is suggested to obtain reduced overpotentials.

The numerical studies in the literature are essential for detailed understanding of SOFC components and SOFC systems. These studies have been concentrated mostly on the parameters that affect the SOFC performance. One of the most important parameters has been considered is the cell temperature. The cell temperature should be under control during start-up, shut-down and load change so that no degradation is seen in the cell components or the cell performance due to temperature fluctuations. For this reason, the electrolyte, the electrodes, the interconnectors, the sealing materials and the gas channels have been modeled and solved simultaneously. However, there exist some studies focused on a single component. In the mathematical modeling, heat and mass transport, momentum, conservation of mass, energy and electrochemical equations have been involved according to the domain of interest. For the solution of these governing equations, mostly a readily available computer program has been preferred. The authors also have been developed new codes where the detailed analysis is required. In the most of the studies, the simulation results have been validated with the experimental results from directly performed experiments or other available ones in the literature. However, some authors have focused on the special SOFC configurations that some companies have been developing. In any case, the numerical investigations are indispensible for the fuel cells and their systems design for optimization of the parameters having influence on the system performance.

Although numerous numerical studies on various aspects of SOFC and SOFC systems are available in the literature, there is little work on the temperature measurements during SOFC operation especially for intermediate temperature SOFCs. These measurements are very essential for both the determination of the temperature profile in the system under various operational conditions and the validation of numerical studies and mathematical modeling efforts.

Therefore, the main objective of this study is to adapt/develop a mathematical model for intermediate temperature SOFCs in order to investigate, in detail, the temperature profile, the fluid flow and the species distribution on the SOFC performance and to develop an experimental system to measure critical parameters such as the cell temperature distribution and the voltage-current depending on various operational parameters. The measurements will be used to validate the mathematical model and to determine the parameters for the optimal cell performance.

CHAPTER 3

FUNDAMENTALS OF SOFC: OPERATION AND DESCRIPTIONS

3.1 Basic Operation Principles of SOFCs

In order to understand how the reaction between hydrogen and oxygen creates electrical current and where the electrons come from, the electrochemical reactions occurring at the anode and the cathode should be taken into consideration separately. When hydrogen is used as a fuel these reactions at the anode and the cathode are:

$$\text{Anode:} \quad H_2 + O^{2-} \rightarrow H_2O + 2e^- \tag{3.1}$$

$$\text{Cathode:} \quad \tfrac{1}{2} O_2 + 2e^- \rightarrow O^{2-} \tag{3.2}$$

$$\text{Overall:} \quad H_2 + \tfrac{1}{2} O_2 \rightarrow H_2O \tag{3.3}$$

The electrons produced at the anode must pass through an electrical circuit to the cathode. In addition, oxygen ions created at the cathode must go through the electrolyte. The electrons coming from the external circuit create an electrical current whereas the oxygen ions traveling through electrolyte react with hydrogen fuel at the anode to form water. These are shown in Figure 3.1.

If the electrons that are produced passed through the electrolyte, the same electrochemical reactions would occur. However, in the absence of an external circuit, it is not possible to obtain power. Therefore, the electrolyte must be electronically insulating, otherwise all would be lost.

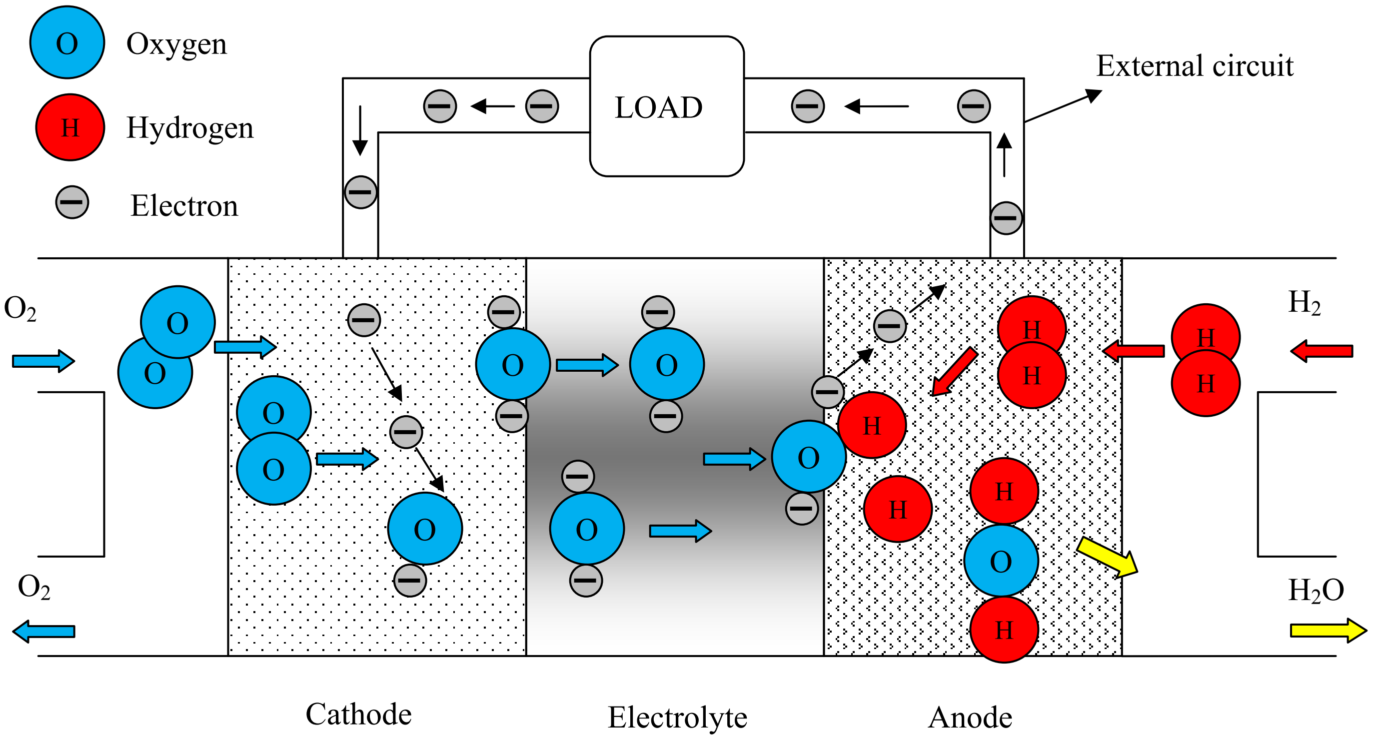

Figure 3.1 Schematic of SOFC working principle

SOFCs generally run with hydrogen as a fuel and air or directly pure oxygen as an oxidant. In addition to hydrocarbons, carbon monoxide can be used as a fuel in SOFCs. The electrochemical oxidation of carbon monoxide in SOFCs occurs via the reactions:

Anode: $CO + O^{2-} \rightarrow CO_2 + 2e^-$ (3.4)
Cathode: $\frac{1}{2} O_2 + 2e^- \rightarrow O^{2-}$ (3.5)
Overall: $CO + \frac{1}{2} O_2 \rightarrow CO_2$ (3.6)

3.2 Open Circuit Potential

Consider the overall SOFC reaction running with hydrogen:

$$H_2 + \frac{1}{2} O_2 \rightarrow H_2O$$

The maximum theoretical work is equal to the change in molar Gibbs free energy of the reaction:

$$\Delta G = \Delta H - T.\Delta S \tag{3.7}$$

where ΔH is the enthalpy change or the total energy that can be obtained theoretically, T is the temperature in Kelvin and ΔS is the entropy change by the reaction. Since work done is in the form of electrical power; i.e. the Gibbs free energy is converted to the electrical energy:

$$P_{elec}^{max} = \Delta G = VI \tag{3.8}$$

where V is the cell potential difference and I is the current passing through the external circuit.

If the reactions occurring at the anode and the cathode are taken into account, it is obvious that for each molecule of water produced and hydrogen used, $2e^-$ pass through the circuit. In the molar basis, it becomes for one mole of hydrogen, 2 moles of electrons or 2N electrons where N is the Avagadro's number. If the charge contained by one electron is –e, the charge passing round the external circuit is then:

$$I = -nNe = -2Ne = -2F \tag{3.9}$$

where F is known as Faraday constant meaning the charge on one mole of electron and n is the number of moles of the electrons transferred.

Then the equation (3.7) becomes after substituting for I:

$$\Delta G = -2FV \tag{3.10}$$

or can be arranged for V:

$$V = \frac{-\Delta G}{2F} \tag{3.11}$$

The equation (3.11) gives the electromotive force (EMF) or reversible/no loss open circuit potential (OCP). In other words, V is the maximum potential difference can be reached. Although equation (3.11) shows that V is only dependent on the nominator, it is also dependent on the temperature, pressure and concentrations of the substances due to again the term of ΔG.

In order to see how they affect the OCV, consider the general reaction described as:

$$xX + yY \ \rightarrow zZ \tag{3.12}$$

where x and y are the moles of X and Y respectively to produce z mol Z. For this equation change in Gibbs free energy can be calculated as:

$$\Delta G = \Delta G^0 - \ RTln\left(\frac{a_X^x a_Y^y}{a_Z^z}\right) \tag{3.13}$$

In the equation (3.13), ΔG^0 and R represent change in molar Gibbs free energy at standard pressure, universal gas constant, while a is the activity and defined as the ratio of the partial pressure of the substance to standard reference pressure of 1atm:

$$a = \frac{P}{P_o} \tag{3.14}$$

If equation (3.13) is rewritten:

$$\Delta G = \Delta G^0 - RTln\left(\frac{P_X^x P_Y^y}{P_Z^z}\right) \tag{3.15}$$

Thus, in the case of SOFC reaction (3.3), equation (3.15) becomes:

$$\Delta G = \Delta G^0 - RTln\left(\frac{P_{H_2}(P_{O_2})^{1/2}}{P_{H_2O}}\right) \tag{3.16}$$

Then substituting the above equation into equation (3.11), one can get after some manipulation:

$$V = -\frac{\Delta G^0}{2F} + \frac{RT}{4F}ln\left(\frac{P_{O_2}(P_{H_2})^2}{(P_{H_2O})^2}\right) \tag{3.17}$$

The first term at the right hand side of the equation is known as V^0, the EMF at standard pressure, and the whole reaction is known as Nernst equation giving Nernst voltage, V.

3.3 Polarizations

When a fuel is put to use and the current is drawn, the fuel cell operates at voltages below that of the Nernst potential owing to irreversible losses. These irreversibilities commonly called polarizations or overpotentials cause a voltage drop and are functions of the current density. The current density is the convention used for fuel cells instead of the current and usually in unit of mA/cm^2, meaning the current drawn per electrode/active area. There exist three dominant polarizations: ohmic polarizations, activation polarizations and mass/concentration polarizations.

3.1.1 Ohmic Polarization

Ohmic losses/polarizations/overpotentials occur due to electronic conduction of the current and ionic conduction of oxygen anions. The former is observed in the interconnectors and electrodes while the latter is occurred through the solid electrolyte. Therefore, the conductivity of the materials plays a very important role for the ohmic polarization. Nevertheless, the ohmic polarizations are the simplest to understand and model. The voltage drop as a result of ohmic polarizations is:

$$\Delta V_{ohm} = iR \tag{3.18}$$

where i is the current density and R is the area specific resistance (ASR) corresponding to 1cm^2 of the cell.

3.1.2 Activation Polarization

Activation polarizations occur at each electrode and are linked with slow electrode reaction kinetics at TPBs. They can be considered as a resistance to initiating electrode reactions. Chemical reactions including electrochemical reactions involve energy barriers. The activation overpotentials can be viewed as extra potential necessary to overcome that energy barrier. The activation overpotential is given as:

$$\Delta V_{act} = Aln(\frac{i}{i_{exc}}) \tag{3.19}$$

where i is the current density, i_{exc} is the exchange current density and it has different values for the anode and the cathode. A is the equation constant and can be calculated as:

$$A = \frac{RT}{n\alpha F} \tag{3.20}$$

In the above equation n is the number of electrons transferred so it is 2 for hydrogen fueled SOFCs and α is the charge/electrochemical transfer coefficient. Thus the final form of the equation (3.19) giving total activation polarizations, after combining the anode and cathode activation polarizations:

$$\Delta V_{act} = \frac{RT}{2\alpha_a F} ln\left(\frac{i}{i_{exc}^{a}}\right) + \frac{RT}{2\alpha_c F} ln\left(\frac{i}{i_{exc}^{c}}\right) \qquad (3.21)$$

The significant parameters in the equation (3.21) are the exchange current densities (i_{exc}^{a} and i_{exc}^{c}, for the anode and the cathode respectively) and charge transfer coefficients (α_a and α_c, for the anode and the cathode, respectively). Both are dependent on the electrode materials and the electrochemical reactions involved. The charge transfer coefficient is usually 0.5 for both the anode and the cathode in fuel cell applications [127]. The exchange current density is the current density at which the overpotential begins to move from zero and it reflects the electrochemical reaction rate. Thus it is crucial to make its value as high as possible. In addition, for the hydrogen fueled fuel cells, like SOFC, the activation polarization of the anode is negligible compared to that of the cathode moreover it becomes less important polarization due to high temperature resulting in higher reaction kinetics [128].

3.1.3 Concentration/Mass Transport Polarization

Due to gradual consumption of the fuel and the oxidant, their fraction will decrease in the fuel and oxidant streams respectively. This concentration change in the direction of the gas flow brings about partial pressure drop of both the hydrogen and oxygen in the anode and the cathode gas channels respectively. These pressure drops cause a reduction in the cell voltage called concentration polarization. The total potential loss due to the concentration polarizations is written as:

$$\Delta V_{con} = -\frac{RT}{nF}[\frac{1}{2} ln\left(1 - \frac{i}{i_{lm}^{c}}\right) + \ln\left(1 - \frac{i}{i_{lm}^{a}}\right) - \ln\,(1 + \frac{P_{H_2}.i}{P_{H_2O}.i_{lm}^{a}})] \qquad (3.22)$$

where i_{lm}^{c} and i_{lm}^{a} are the limited current densities corresponding to the cathode and the anode in that order, while the other parameters have already explained. The anode limited current density is the current density at which the fuel is assumed to be fully consumed and the partial pressure of the hydrogen is nearly zero at the electrolyte/anode interface. Similarly, the cathode limited current density is the current density at which the oxidant is assumed to be fully used up and the partial pressure of the oxygen at the electrolyte/cathode interface is nearly zero. Both are dependent on the electrode microstructures such as porosity.

3.4 Actual Cell Potential

After combining three chief polarizations and subtracting from the Nernst voltage, one can write simply the real cell potential as:

$$V_{cell} = V - \Delta V_{ohm} - \Delta V_{act} - \Delta V_{con} \tag{3.23}$$

The equation (3.23) can be rewritten as a function of the current density only after inserting the polarizations equations and simplifying the constants in the polarization equations by some manipulation to give:

$$V_{cell} = V - iR - \lambda \ln(i) + \xi \exp\,(\gamma i) \tag{3.24}$$

The second term from the right hand side is the ohmic polarizations while the third and the fourth terms are representing the activation and concentration overpotentials. Figure (3.2) shows the cell potential obtained from the equation (3.24). The constants used are given in Table 3.1.

Table 3.1 Example constants for equation (3.24) [129]

Constant	Values for SOFC operating at 800°C
V(V)	1.01
R(kΩcm^2)	0.0002
λ (V)	0.002
ξ (V)	0.0001
γ (cm^2/mA)	0.008

One of the key points of Figure 3.2 is that the OCV is a little less than the theoretical voltage value given as a small initial fall in the voltage. The activation polarizations occur at all current densities but they are dominant at low current densities. In the case of SOFC, due to high operating temperature the electrochemical reaction rates are relatively high. Using more effective catalysts, in other words using a catalyst having high exchange current density value, is one of the major ways to reduce the activation polarizations. The concentration polarizations, however, are dominant at high current densities resulting the faster fall in voltage. When a SOFC is running at this regime, it is not possible to supply reactants at a rate that electrode reactions demand. For the fuel side, using a reformer may limit the quick increase in the hydrogen supply rate corresponding to the anode demand. Similarly, for the cathode side, using air instead of pure oxygen, the nitrogen in the air may block the oxygen supply. Both result in increase in the concentration polarizations. Finally, at moderate current densities at which SOFCs generally run, the ohmic polarizations are dominant. It can also be seen in the Figure 3.2 that at the moderate current densities, the voltage drop is fairly linear similar to the ohmic losses equation (3.18).

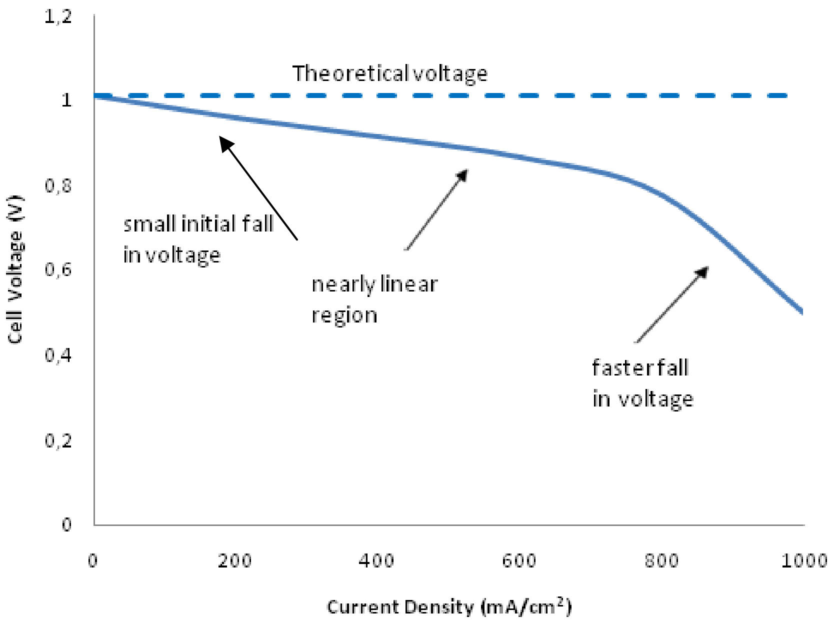

Figure 3.2 Cell voltage of a typical SOFC operating at 800°C

3.5 Cell Efficiency

Consider the equation (3.7) again, which was:

$$\Delta G = \Delta H - T.\Delta S$$

The maximum energy can be converted into electrical energy is the enthalpy change of the reaction denoted as ΔH. In other words, all of the energy that hydrogen possesses is converted into electrical energy theoretically. If this was the case then the theoretical voltage would be:

$$V_{theor} = \frac{\Delta H}{2F} \tag{3.25}$$

If higher heating value of the hydrogen is used Equation (3.25) gives 1.48V whereas for the lower heating value of the hydrogen, it gives 1.25V. Therefore, the cell efficiency can be written according to cell voltage as:

$$\eta_{cell} = \frac{V_{cell}}{V_{theor}} \tag{3.26}$$

where V_{cell} is the actual cell potential and V_{theor} is the theoretical voltage. However, when a SOFC is running, not all the fuel fed is consumed. Some fuel remains unused. So, the fuel utilization factor can be defined as:

$$\mu_{fuel} = \frac{fuel\ consumed\ in\ the\ cell}{fuel\ supplied\ to\ the\ cell} \tag{3.27}$$

Then, the cell efficiency can be rewritten by adding the fuel utilization factor μ_{fuel} :

$$\eta_{cell} = \mu_{fuel}\ \frac{V_{cell}}{V_{theor}} \tag{3.28}$$

CHAPTER 4

MATHEMATICAL MODELING AND NUMERICAL ANALYSIS

The SOFC system considered is schematically illustrated in Figure 4.1. The system consists of GDC electrolyte, NiO/GDC anode layer, LSF (strontium doped lanthanum ferrite)/GDC cathode layer, anode and cathode gas channels, current collectors and interconnectors in contact with anode and cathode. The dimensions of the considered model are shown in the Fig. 4.2. The thickness (z direction) of the system is 6.27mm.

In this study, the electrochemical reactions that are considered take place in all catalyst layers. This is a volumetric phenomenon not a boundary condition as usually assumed in the literature. We adopted a continuum kind of approach to the considered SOFC system. Mainly a single conservation equation is solved for the whole domain. The characteristics of each layer are incorporated as a source term. For example, a Darcy source term incorporated to the momentum equation at each anode and cathode layer while a very large porosity is imposed at the electrolyte layer. The main objective of this methodology is to eliminate the solution of excessive number of differential equations for each layer.

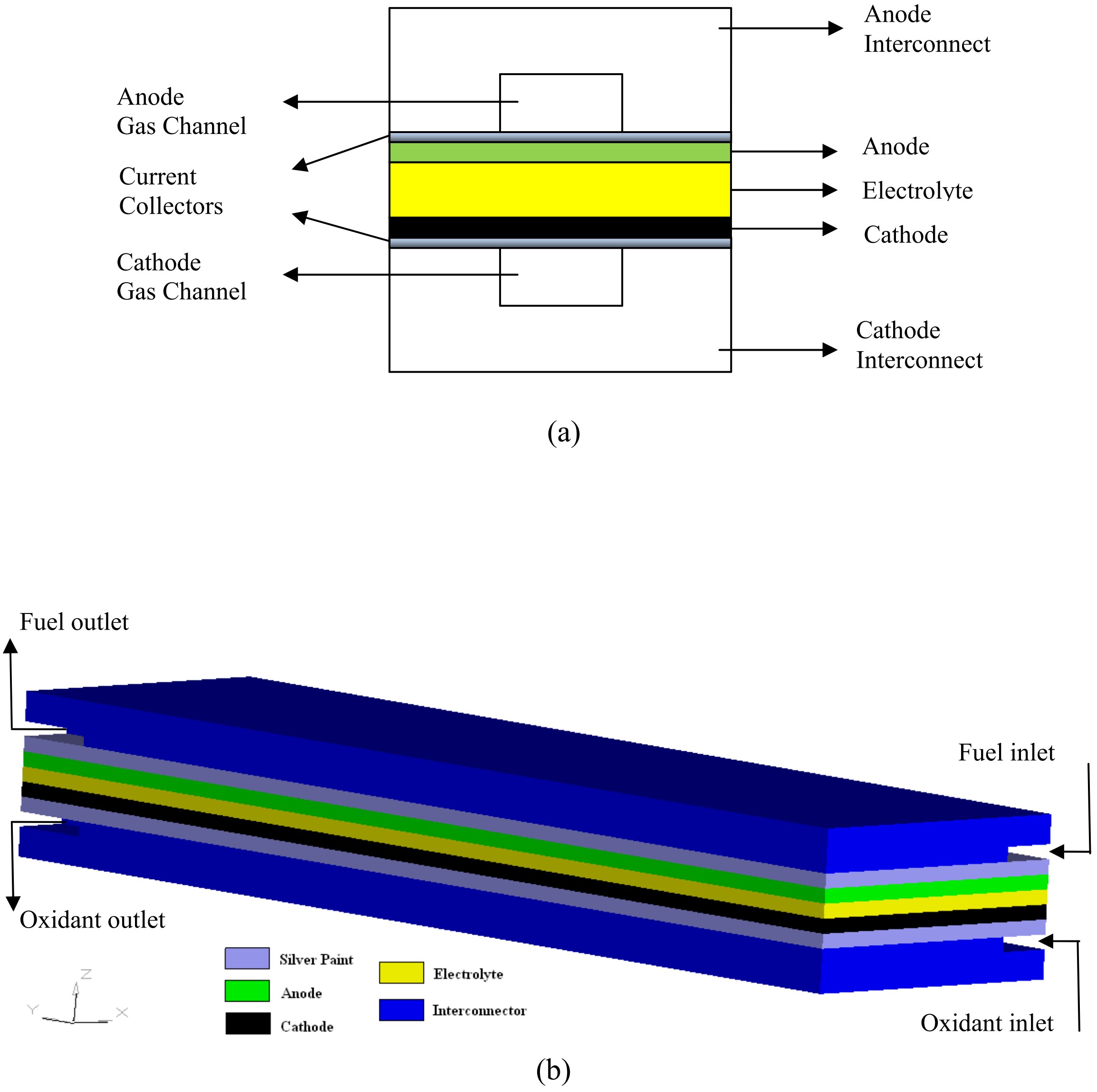

Figure 4.1 SOFC system of interest (not to scale)
(a) cross section of one channel (b) 3D view

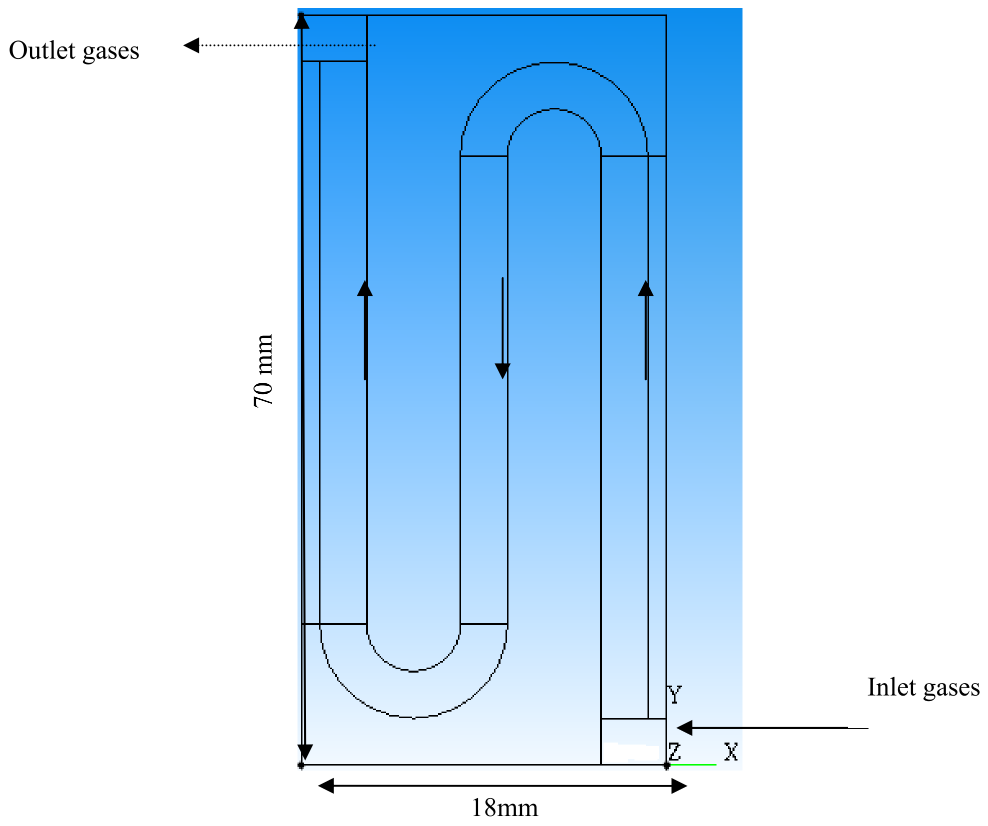

Figure 4.2 The dimensions of SOFC model considered

4.1 General Governing Equations

4.1.1 Conservation of Mass

The continuity equation for the all of the domains of a single cell i.e. the anode, the cathode, the electrolyte, the interconnectors and the gas channels is given:

$$\frac{\partial(\epsilon\rho)}{\partial t} + \nabla.\left(\rho\epsilon\vec{V}\right) = S_m \tag{4.3}$$

In the equation (4.3) ρ stands for density of the gas mixture as defined in the following equation, $\vec{V}$ and S_m represent velocity vector and additional mass source respectively, whereas ϵ is the porosity. Thus, the equation (4.3) is only valid for the anode, cathode and their gas channels, but for the totally solid parts (i.e. the electrolyte and two interconnects) it is not applicable.

Density is the mixture density representing each species in the system depending on their volumetric ratio:

$$\rho = \sum_{i=1}^{N} \rho_i c_i \tag{4.4}$$

In the above equation, ρ_i and c_i are the density and the concentration of the specie i and N is the number of the species as all giving density of the mixture. Density of the species on the other hand can be estimated from Ideal Gas Law:

$$P_i = \rho_i R_i T \tag{4.5}$$

4.1.2 Species Balance

The species balance equation is defined as:

$$\frac{\partial(\rho \epsilon c_i)}{\partial t} + \nabla.\left(\rho \epsilon \vec{V} c_i\right) = -\nabla.\epsilon \vec{J_i} + S_{s,i} \tag{4.6}$$

where $\vec{J_i}$ is the diffusive mass flux for the specie i and $S_{s,i}$ is the additional species source term which is a function of current density and expressed as:

$$S_{s,i} = i \frac{M_i}{nF} \tag{4.7}$$

where M_i is the molecular weight of the specie i, i is the local density and n is the number of electrons involved in the electrochemical reaction.

The diffusion term can be given simply by Fick's Law:

$$\vec{J_i} = \left[\rho D_i \vec{\nabla}(c_i)\right] \tag{4.8}$$

4.1.3 Momentum Equation

Assuming laminar flow in the system, the momentum equation can be expressed as:

$$\frac{\partial(\rho\epsilon\vec{V})}{\partial t}+\nabla.\left(\rho\epsilon\vec{V}\vec{V}\right)=-\epsilon\nabla p+\rho\epsilon\vec{g}\nabla.\vec{\tau}+\frac{\epsilon^2\mu V}{\zeta} \tag{4.9}$$

In the equation (4.8), μ is the viscosity obtained similar to the density calculation and p represents the static pressure. The third term on the right hand side of Equation (4.9) is the Darcy source term which represents the flow in porous medium depending on permeability ζ and porosity ϵ. $\vec{\tau}$ is the stress tensor defined as:

$$\vec{\tau}=\mu\left\{\left(\nabla\vec{V}+\nabla\vec{V}^T\right)-\frac{2}{3}\left(\overrightarrow{\nabla.V}\right)\right\} \tag{4.10}$$

4.1.4 Charge Balance

The charge is expressed by Ohm's Law and the conservation of charge as follows:

$$\vec{j}=\sigma\nabla\phi \tag{4.11}$$

$$\frac{\partial\rho_e}{\partial t}+\nabla.\vec{j}=S_c \tag{4.12}$$

where $\vec{j}$, σ and ϕ are the ionic or electronic current density, the conductivity and the electrical potential. On the other hand, ρ_e is the ionic or electronic charge density and S_c is the charge source term and equal to current density of the considered domain valid only in TPBs, otherwise it is equal to zero. In other words, S_c is equal to the anode or cathode current density calculated from Butler-Volmer equation for the electrodes whereas it is zero for the electrolyte or interconnects purely ionic and purely electronic conductive parts respectively. The electrodes, however, have both ionic and electronic conductivity. Therefore, charge balance equation is required as follows:

$$\vec{J}_{io} = -\vec{J}_{el} \tag{4.13}$$

4.1.5 Energy Balance

The energy conservation equation is:

$$\frac{\partial(\rho\epsilon e)}{\partial t} - \epsilon\frac{\partial p}{\partial t} + \nabla.\left(\rho\epsilon\vec{V}e\right) = \nabla.\epsilon(k\nabla T) + S_e \tag{4.14}$$

where k is the thermal conductivity and S_e denotes the energy due to a source term including Joule effect due to ohmic resistance, the electrochemical reactions or the radiation according to the domain of interest.

The total energy change resulting from the reaction is the difference in the enthalpy of formation (ΔH) and Gibbs free energy of the formation (ΔG) which is theoretically converted into the electricity, the remainder is converted into the heat.

The ohmic (electrical) and activation kinetic losses cause additional chemical energy to be irreversibly converted into heat. Thus if V is the overall heat source due to an electrochemical reaction then the losses can be expressed as:

$$S_e = i\left(\frac{\Delta H}{nF} - V\right) \tag{4.15}$$

The source term in the energy equation for the electrolyte layer is due to the ohmic heating and expressed as:

$$S_e = \frac{i^2}{k} \tag{4.16}$$

4.1.6 Electrochemical Model

The actual voltage of an SOFC is less than its open circuit voltage owing to irreversible losses as explained in Chapter 3:

$$V_{cell} = V - \Delta V_{ohm} - \Delta V_{act} - \Delta V_{con} \tag{4.17}$$

The current density is given by Butler-Volmer equation [130]:

$$i = j_o \left[\exp\left(\alpha \frac{nF\eta_{act}}{RT} \right) - \exp\left(-\alpha \frac{nF\eta_{act}}{RT} \right) \right] \tag{4.18}$$

where j_o is the exchange current density at the equilibrium, α denotes the charge transfer coefficient, η_{act} is the activation loss, n is the number of electrons involved and i is the current density.

4.1.7 Chemical Reactions

The electrochemical reactions in the anode and cathode are modeled as surface reactions as taking place inside the pores of the electrodes according to following reactions. The oxygen ions, however, are modeled as bulk species.

Anode: $$H_2 + O^{-2} \rightarrow H_2O + 2e^- \tag{4.1}$$

Cathode: $$O_2 + 2e^- \rightarrow O^{-2} \tag{4.2}$$

In the case of fuel mixture while benchmarking, the same electrochemical reaction in the cathode, whereas for the anode:

Anode: $$H_2 + CO + O^{-2} \rightarrow H_2O + CO_2 + 4e^- \tag{4.3}$$

4.1.8 Boundary Conditions

The boundary walls are assumed to be impermeable to species and no-slip condition is applied to velocities. Therefore velocities at the solid boundaries are set to zero:

$$\vec{V} = 0 \tag{4.19}$$

The impermeable boundary walls can be expressed in terms of no-flux in which:

$$\frac{\partial c_i}{\partial \vec{n}} = 0 \tag{4.20}$$

where $\vec{n}$ is the unit normal vector of the boundary walls.

All boundary walls are assumed as adiabatic surfaces and no flux condition is applied to the electric field at the boundaries as:

$$\frac{\partial \phi}{\partial \vec{n}} = 0 \tag{4.21}$$

4.2 Numerical Solution Method

4.2.1 Finite Volume Method

For the solutions of the governing equations introduced, a commercial CFD code, CFD-ACE+ is employed. The numerical solution technique of CFD-ACE+ is based on the finite volume approach. In this method, the solution domain is divided into a number of cells known as control volumes. The governing equations then are numerically integrated over each of these computational domains or control volumes within which the average value of any quantity is given by its value at the cell center. CFD-ACE solves following the general transport equation:

$$\frac{\partial(\rho\Phi)}{\partial t} + \nabla.\left(\rho\vec{V}\Phi\right) = \nabla.(\Gamma\nabla\Phi) + S_{\Phi} \tag{4.22}$$

where Φ is the generic variable, unity in continuity equation, U,V, W in momentum equation, h in energy equation and c_i concentration of each species in species conservation equation.

The above equation is also known as the generic conservation equation for a quantity Φ with a density of ρ and the integration of this equation over a control volume, ν, gives:

$$\int_{\nu} \frac{\partial(\rho\Phi)}{\partial t} d\nu + \int_{\nu} \left(\nabla.\left(\rho\vec{V}\Phi\right)\right) d\nu = \int_{\nu} \left(\nabla.\left(\Gamma\nabla\Phi\right)\right) d\nu + \int_{\nu} S_{\Phi}\, d\nu \qquad (4.23)$$

The terms in the given equations are the transient, the convection, the diffusion and the source terms from left to right, respectively. The integrations of these terms are discussed in the following sections one by one.

4.2.1.1 Transient Term

The transient term in Equation (4.23) is integrated as follows:

$$\int_{\nu} \frac{\partial(\rho\Phi)}{\partial t} d\nu = \frac{\rho\Phi\nu - \rho^{o}\Phi^{o}\nu^{o}}{\Delta t} \qquad (4.24)$$

where no superscript denotes the current or the new time, whereas the superscript "o" denotes an older time.

4.2.1.2 Convection Term

Similar to the transient term integration, the convection term is discretized as follows:

$$\int_{\nu} \left(\nabla.\left(\rho\vec{V}\Phi\right)\right) d\nu = \int_{A} \left(\rho\Phi\left(\vec{V}.\vec{n}\right)\right) dA = \sum_{f}\left(\rho_f\Phi_f V_f^{n}\right)A_f = \sum_{f} C_f\Phi_f \qquad (4.25)$$

where subscript "f" denotes one of the faces of the considered control volume, A_f is the area of face f, V_f^{n} stand for the velocity component in the direction which is normal to the face f and C_f is the mass flux through the face f.

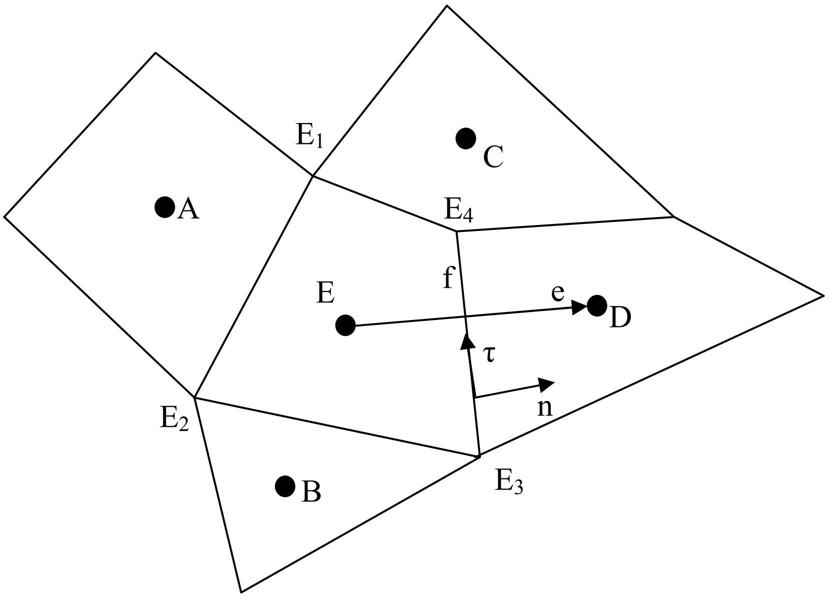

Figure 4.3 2-D control volumes

The most essential concern at this point is the determination of Φ at the control volume faces i.e. all Φ_f. The most stable scheme having a first order accuracy as its name implies, First Order Upwind Scheme is used to evaluate Φ at a given face f as shown in Fig. 4.3. The value of Φ at this face Φ_f is equal to either Φ_E or Φ_D depending on the flow direction at that face. It is expressed mathematically as follows:

$$\Phi_E = \begin{cases} \Phi_E, \; V_f^n < 0 \\ \Phi_D, \; V_f^n > 0 \end{cases} \tag{4.26}$$

4.2.1.3 Diffusion Term

The diffusion term is integrated as follows:

$$\int_v \left(\nabla.(\Gamma\nabla\Phi)\right) dv = \int_A \; \Gamma\nabla\Phi.\vec{n}dA = \sum_f \Gamma_f \left(\frac{\partial\Phi}{\partial n}\right)_f A_f \tag{4.27}$$

The unit vectors as shown in Figure 4.3 give:

$$\frac{\partial \Phi}{\partial n} = \frac{1}{\vec{n}\vec{e}}\left(\frac{\partial \Phi}{\partial e} - \vec{e}.\vec{\tau}\frac{\partial \Phi}{\partial \tau}\right) \tag{4.28}$$

Then Equation (4.27) becomes:

$$\int_v \left(\nabla.(\Gamma\nabla\Phi)\right) dv = \sum_f \frac{\Gamma_f}{\vec{n}.\vec{e}}\left(\frac{\partial \Phi}{\partial e}\right)_f A_f - \sum_f \frac{\vec{\tau}.\vec{e}\Gamma_f}{\vec{n}.\vec{e}}\left(\frac{\partial \Phi}{\partial \tau}\right)_f A_f \tag{4.29}$$

where:

$$\left(\frac{\partial \Phi}{\partial e}\right)_f = \frac{\Phi_D - \Phi_E}{\delta_{E,D}} \tag{4.30}$$

$$\left(\frac{\partial \Phi}{\partial \tau}\right)_f = \frac{\Phi_{E4} - \Phi_{E3}}{\delta_{E4,E3}} \tag{4.31}$$

In Equations 4.30 and 4.31 $\delta_{E,D}$ and $\delta_{E4,E3}$ represent the distance between E and D, and E4 and E3, respectively.

4.2.1.4 Source Term

The source term can be linearized as follows:

$$S_\Phi = S^U + S^E \Phi \tag{4.32}$$

such that S^E is negative. In the equation (4.32), both $S^U$and S^E are the functions of Φ. Similar integration of this equation over the control volume results in:

$$\int_v S_\Phi \, dv = S_U + S_E \Phi_E \tag{4.33}$$

where $S_U = S^U v$ and $S_E = S^E v$.

4.2.2 Finite Difference Equation

All numerically integrated transient, convection, diffusion and source terms are assembled together; it gives the following linear equation:

$$(a_E - S_E)\Phi_E = \sum_{nb} a_{nb}\Phi_{nb} + S_U \qquad (4.34)$$

The above equation is known as finite difference equation (FDE) that the numerical evaluations start with. In this equation, the subscripts nb denote values at neighboring cells and $a_{nb}$are called as the link coefficients. When an FDE is formulated for each control volume, it results in a set of nonlinear equations due to link coefficients being functions of Φ_E and Φ_{nb}, etc. The only method to solve these equations is an iterative procedure at every time step. In this method, a linear FDE is formulated by the link coefficients calculated with the value of Φ at the end of the previous iteration.

4.2.3 Geometry of the Cell

The dimensions of the co-flow geometry SOFC used in the present study are given in Fig. 4.2 whereas the model with mesh is shown in Figure 4.4. The system is composed of an electrolyte, an anode, a cathode, fuel and oxidant gas channels, anode and cathode interconnectors and current collectors.

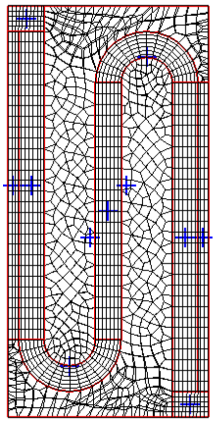

Figure 4.4 Meshed structure of the domain of interest (+ : volumes)

4.2.4 Material and Parameter Setting

The GDC-10 electrolyte, the Ni/GDC anode, the LSF/GDC cathode and the interconnects are modeled as porous media and their details are given Table 4.1. On the other hand, transport properties and conductance settings are summarized in Table 4.2.

Table 4.1 Porous Media Setting

Volume	Reaction	ϵ	ζ	S/V	Pore	k	σ
Anode	4.1/4.3	0.4	2	100	1e-6	6.23	100000
Cathode	4.2	0.5	2	100	1e-6	9.6	7700
Electrolyte	-	0.01	2	-	1e-6	2.7	1e-18
Interconnect	-	0.001	2	-	1e-6	9.6	1e-18

ϵ: porosity, ζ: permeability (m^2), S/V:surface to volume ratio(m^{-1}), pore: average pore size (m), k: thermal conductivity ($Wm^{-1}K^{-1}$), σ: solid electrical conductivity ($ohm^{-1}m^{-1}$)

The humidified reformate gas (wt. % CO:26, CO_2:21.6, H_2O:42.8 and H_2:9.6) and air (wt. % N_2:79 and O_2:21) are used as the fuel and the oxidant in the numerical study, respectively. For the comparison of the experimental and the numerical results, however, pure hydrogen and oxygen are used as a fuel and oxidant, respectively.

Table 4.2 Transport Parameter Setting

Volume	ρ	μ	σ	c_p	k	Γ
Anode	IGL	MixKin	10	JANNAF	MixKin	SCH
Cathode	IGL	MixKin	10	JANNAF	MixKin	SCH
Electrolyte	IGL	MixKin	10	JANNAF	MixKin	SCH
Fuel Channel	IGL	MixKin	1e-20	JANNAF	MixKin	SCH
Oxidant Chanel	IGL	MixKin	1e-20	JANNAF	MixKin	SCH
Interconnect	IGL	MixKin	1e-20	JANNAF	MixKin	SCH

ρ: density,μ: dynamic viscosity ($kgm^{-1}s^{-1}$),MixKin:kinetic theory, c_p: specific heat ($Jkg^{-1}K^{-1}$) by JANNAF curve fits, k: thermal conductivity $Wm^{-1}K^{-1}$, Γ: mass diffusivity ($kgm^{-1}s^{-1}$) by Schmdt number

4.2.5 Numerical Accuracy

A numerically accurate result is obtained with the 50x50x50 grid system for all considered cases. This grid system is selected from a systematic grid refinement test for only a half of the first channel from the inlet section of the cell. The results of mess independency tests that are performed for 5x15x5, 10x30x10, 15x50x15 and 30x50x30 grid systems are shown in Figs. 4.5 and 4.6. It is seen that the change in the results (H_2 and CO concentration along the channel) is not significant after the

15x50x15 mesh system. Therefore, this mesh system is applied to the whole solution domain of the cell with the same grid dimension as 125,000 mesh points for the whole domain.

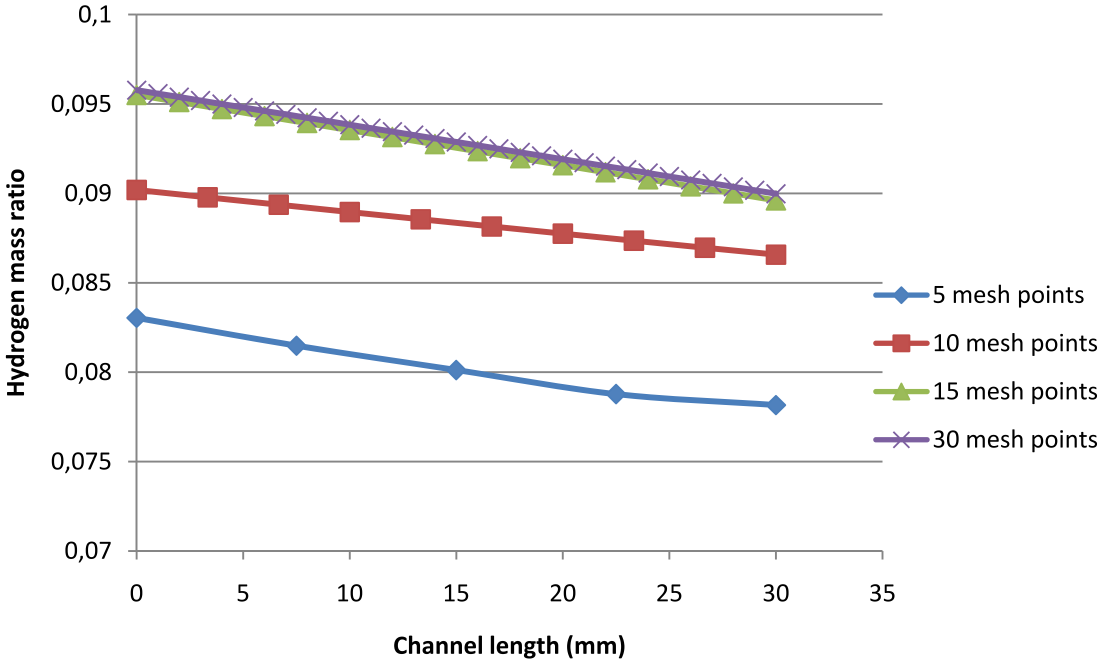

Figure 4.5 Hydrogen consumption depending on grid spacing

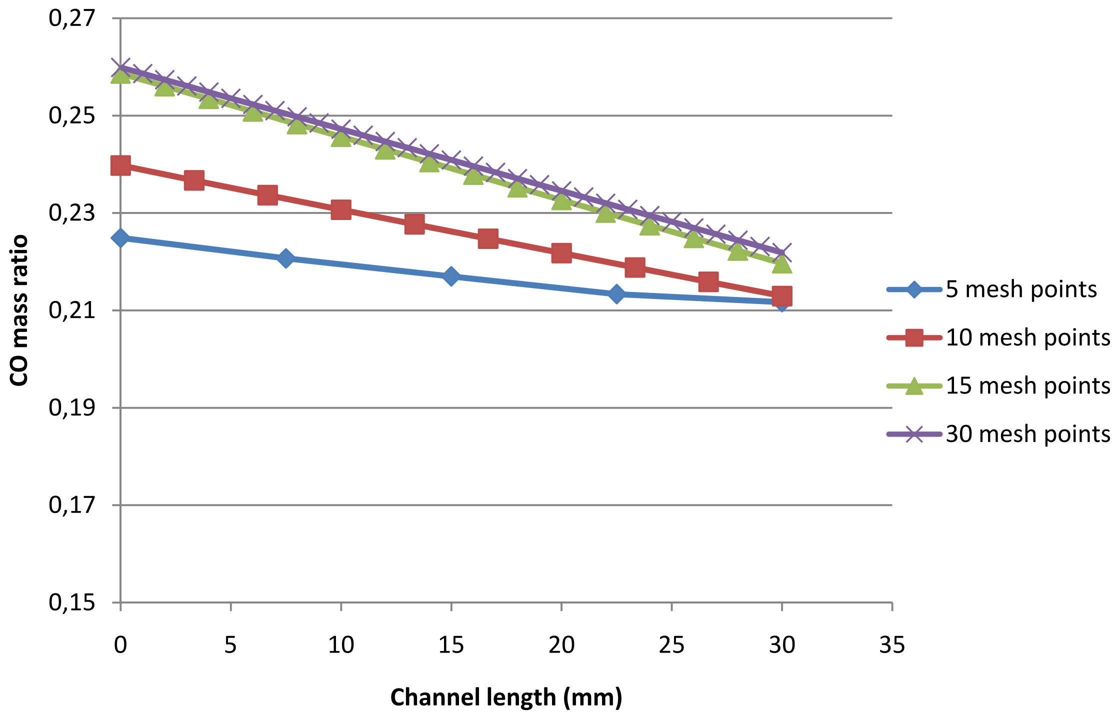

Figure 4.6 Carbon monoxide consumption depending on grid spacing

4.3 Numerical Results

In the numerical studies, the species calculated, the temperature and flow distributions in the cell are presented. The effects of operation parameters on the temperature distribution, the fuel consumption and the performance are investigated.

4.3.1 Species Distribution

The species distributions in terms of mass ratios along the anode channel close to the electrolyte interface are shown in Figs. 4.1-4.10. A mixture of humidified H_2, CO fuel with some amount of CO_2 is introduced at the anode inlet which simulate reformate gas used in SOFC application. Figure 4.7 shows H_2 distribution along the anode channel. It is seen that the concentration of H_2 decreases along the channel length. The concentration drops are more pronounced close to the inlet section due to the direct contact of fuel with anode catalyst layer. Through the exit section there is less fuel available for the electrochemical reactions. Figure 4.8 shows the distribution of CO in the anode channel. Although it has poisonous effects in PEM fuel cells, it is used as a fuel in SOFCs. It is seen that CO concentration drops along the channel.

However, this drop is lower than that of H_2 indicating a slower electrochemical reaction of CO compared to H_2 oxidation.

Steam formation as a result of the electrochemical reactions along the anode channel is presented in Fig. 4.9. Opposite to PEM fuel cells, water forms in the anode catalyst layer in SOFCs. It is seen that the water content increases along the channel due to the accumulation of the water formed from the continuous electrochemical reactions. This water may react with CO in the system with the water shift mechanism resulting in a further increase in H_2 content and can also be used in reformation of methane in the channel. However, due to the complexity of the situation, the water shift reaction is not included in the present study.

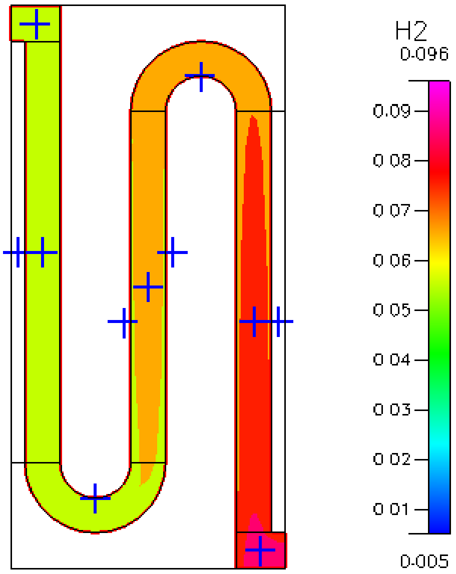

Figure 4.7 Hydrogen concentration along the fuel gas channel

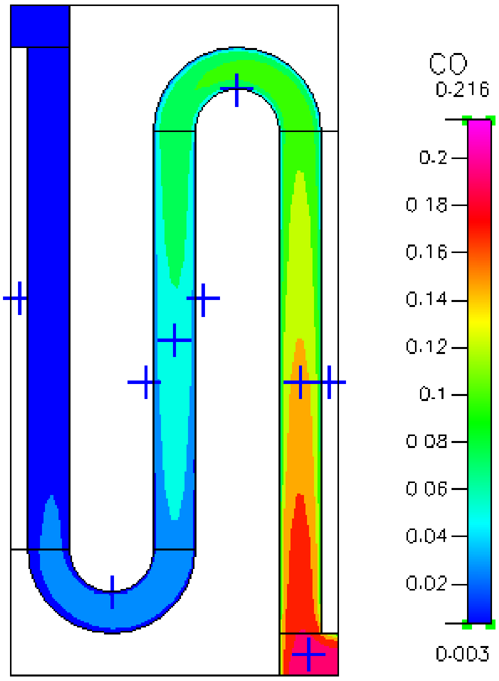

Figure 4.8 CO concentration along the fuel gas channel

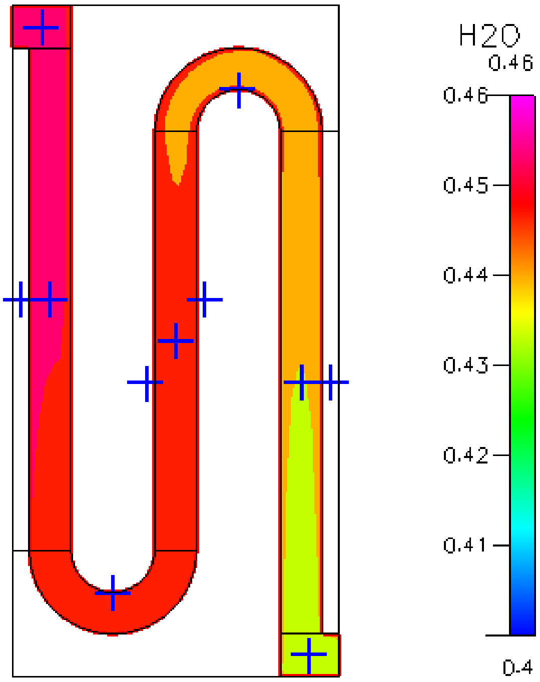

Figure 4.9 H_2O concentration along the anode gas channel

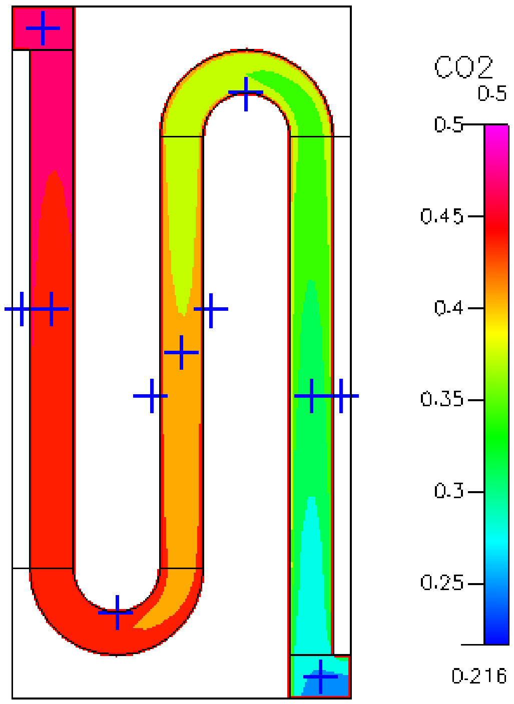

Figure 4.10 Carbon dioxide concentration along the gas channel

Corresponding CO_2 formation and distribution along the anode channel is presented in Fig. 4.10. It is seen that the CO_2 concentration and formation increase along the channel as a result of the electrochemical reaction of CO and O^{2-} ions traveled from cathode side.

4.3.2 Temperature Distribution

The temperature profile on the anode-anode gas channel interface where experimental measurements are taken is shown in Fig. 4.11 while the anode channel temperatures along the gas channel flow direction at different sections are given in Fig. 4.12. Due to the exothermic nature of the anode reaction the temperature increases in the anode channel. However, the rate of increase in the temperature is decreasing. This may be due to consumption of the fuel introduced at the inlet. Since the fuel is used continuously, its concentration decreases resulting in slower or limited electrochemical reaction taking place as leaving from inlet. Therefore, the temperature near to inlet section is higher than the rest of the cell.

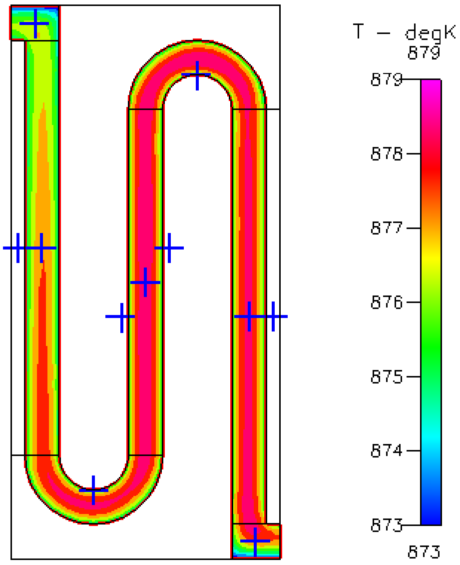

Figure 4.11 Temperature distribution on the anode through anode gas channels

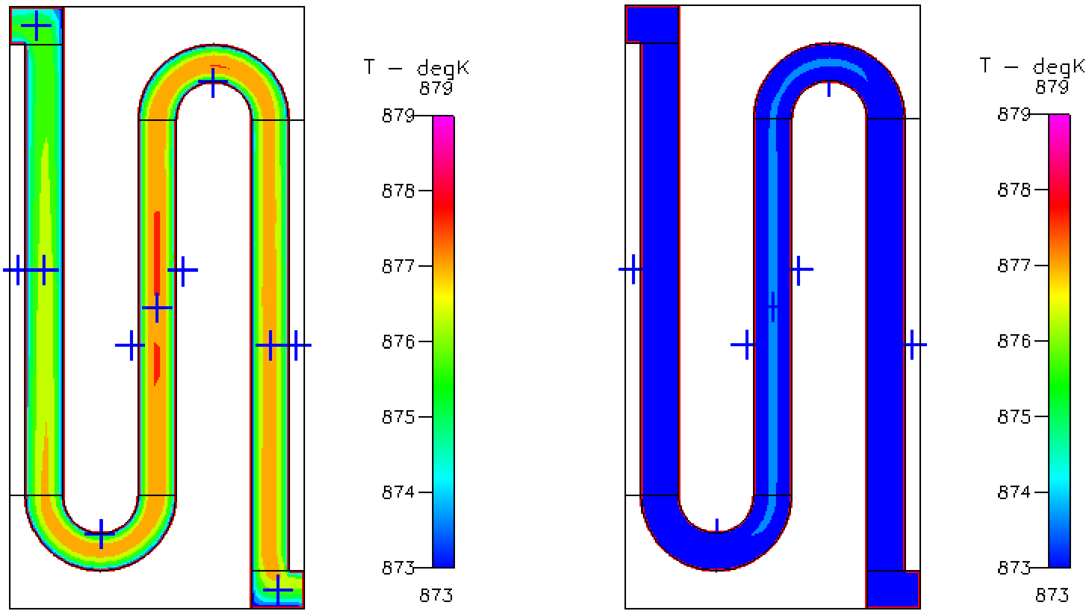

Figure 4.12 Anode channel temperature through anode gas channels (left: in the middle of the gas channel and right: at the top of the gas channel)

4.3.3 Parametric Study

A parametric study is performed to investigate the effects of some of the operation parameters such as fuel consumption, operating pressure and mass flow rate. Values in the first channel from inlet section are used in all plots due to curved section of the channel. The values plotted are also chosen at the mid-section of the anode channel close to the anode catalyst layer.

4.3.3.1 Effect of Operating Pressure

The effects of pressure on the temperature distribution and the hydrogen and CO consumption are presented in Figs. 4.13-4.15, respectively. Figure 4.13 shows that the temperature in the cell increases at high pressure operation due to the enhanced chemical reaction at higher pressures. Relatively a flat temperature distribution is observed along the channel almost for all considered cases due to high electrochemical activity in the first channel. Figure 4.14 shows the hydrogen consumption in the first anode channel. It is seen that the hydrogen consumption increases at high pressures again due to enhanced electro chemical reaction at elevated pressures. The consumption of CO also follows the same trend as hydrogen behavior for the same reason (Fig.4.15)

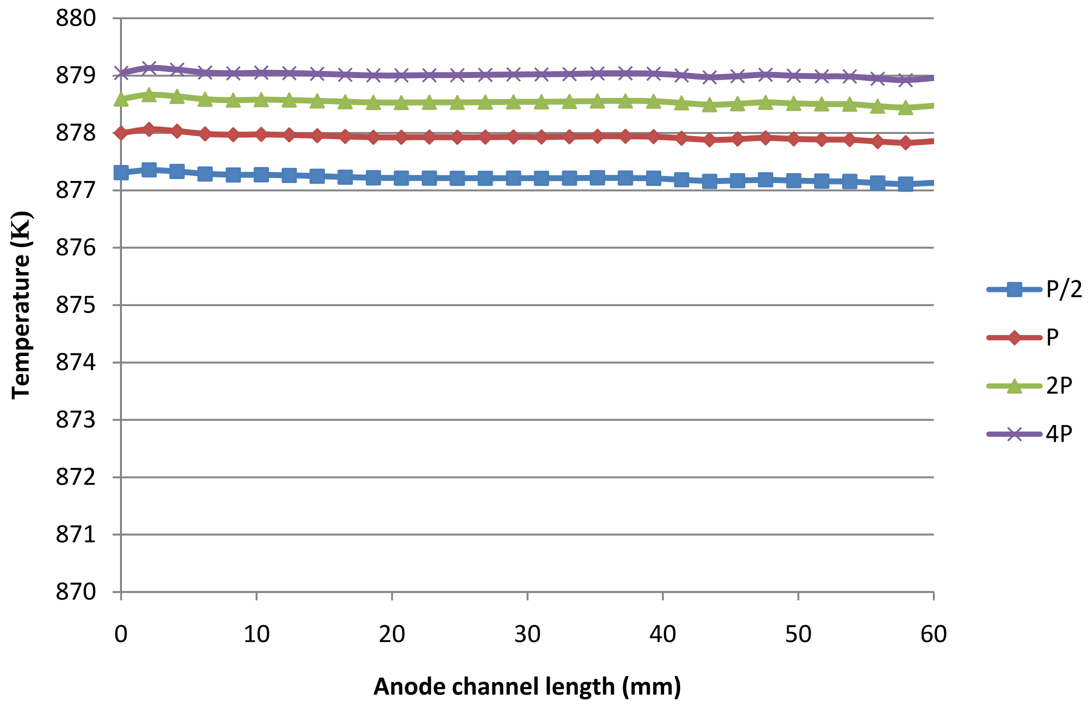

Figure 4.13 Temperature distribution along gas channel under various operation pressure (P=1Bar)

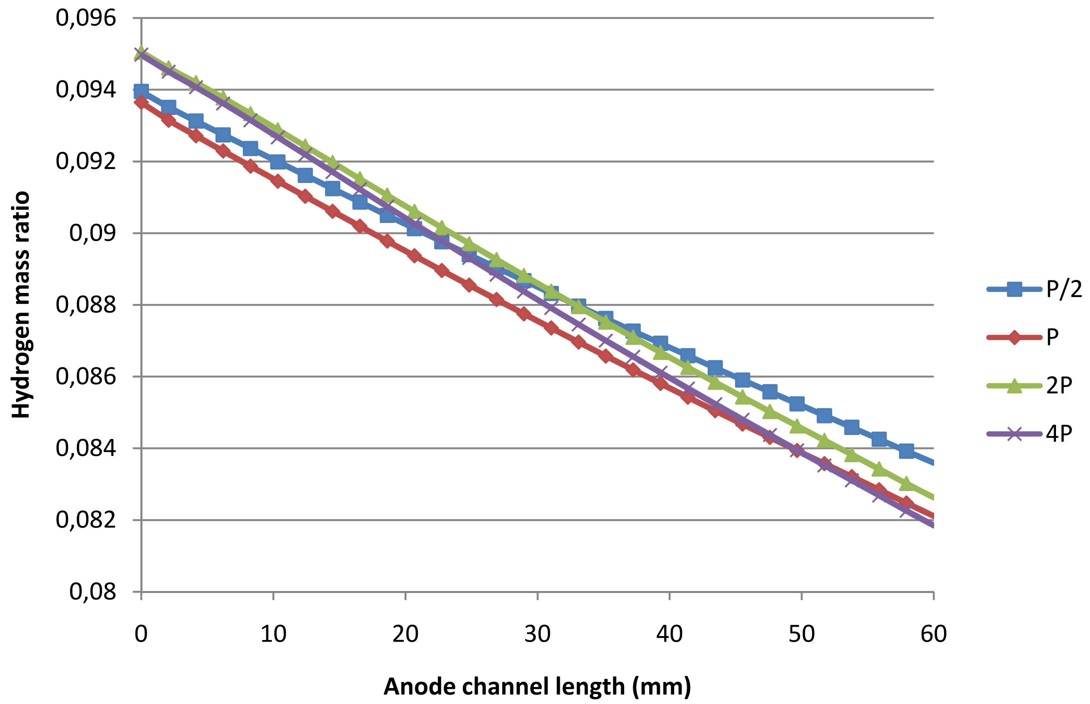

Figure 4.14 H_2 consumption along anode channel under various operating pressures (P=1Bar)

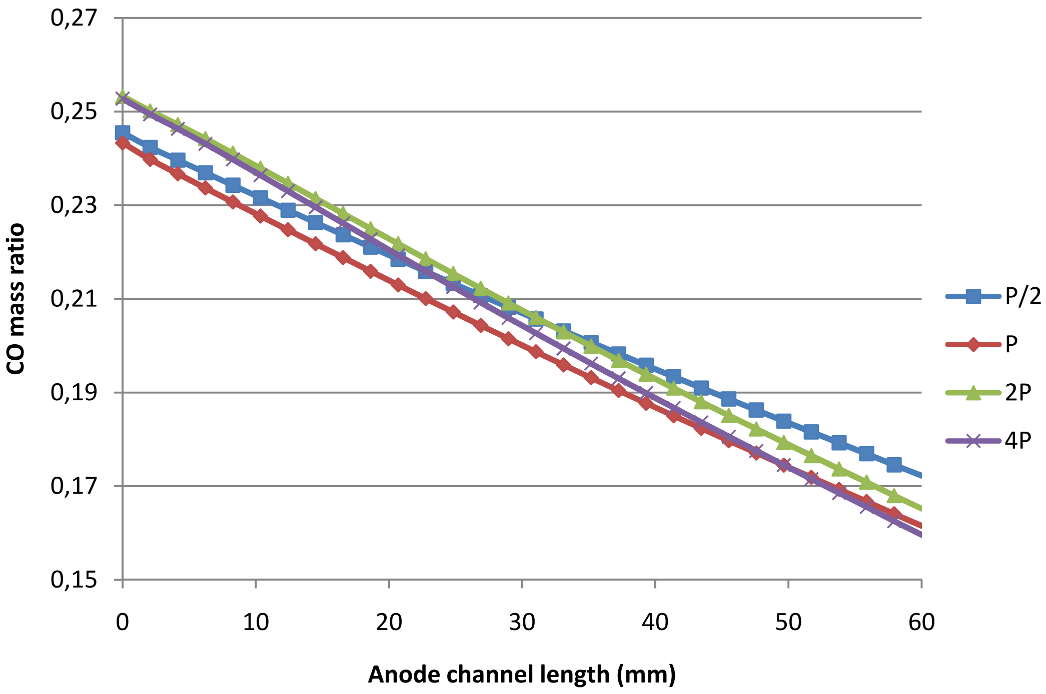

Figure 4.15 CO consumption along anode channel
under various operating pressures (P=1Bar)

4.3.3.2 Effect of Fuel Gas Composition

The effects of the fuel composition are presented in Fig. 4.16 and 4.17. In all cases hydrogen mass ratio increased 2, 3 and 4 times in the fuel mixture composed of hydrogen, carbon monoxide and carbon dioxide. Figure 4.16 shows temperature distribution in the first channel for three cases considered. It is seen that the temperature in the first channel does not change significantly with the increasing hydrogen content in the fuel due to the rate limiting electrochemical reaction in the anode catalyst layer. Figure 4.17 shows that the hydrogen consumption does not significantly change along the channel due to again the rate limiting process.

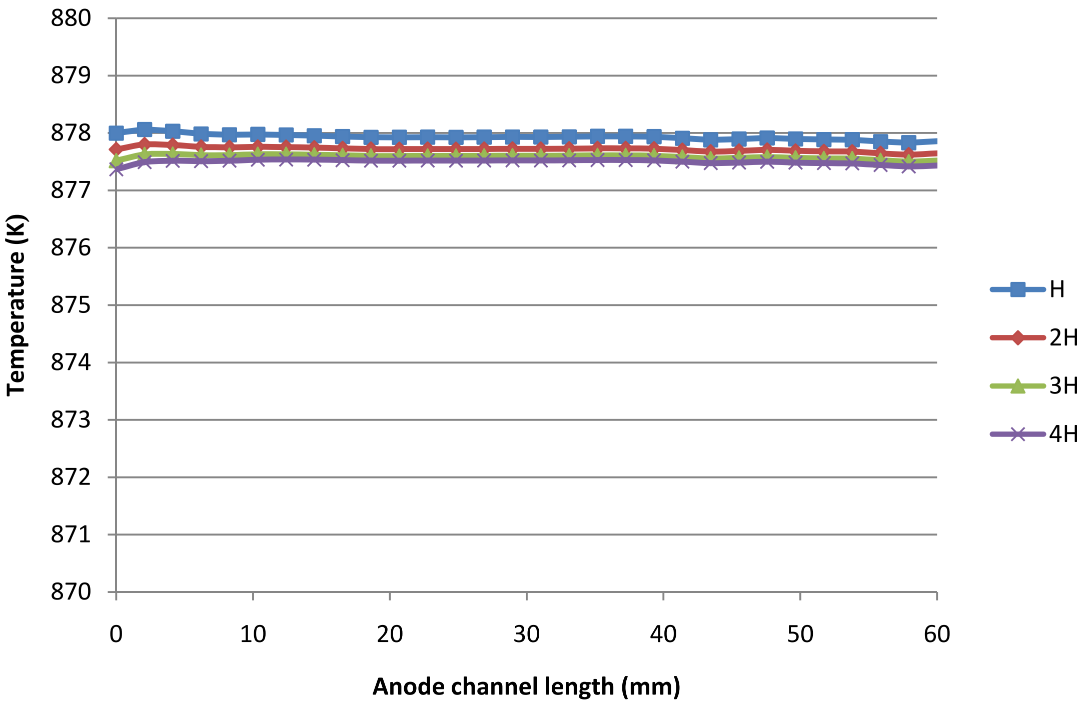

Figure 4.16 Temperature distribution along gas channel under various hydrogen content in the fuel (H=9.6 (wt.%))

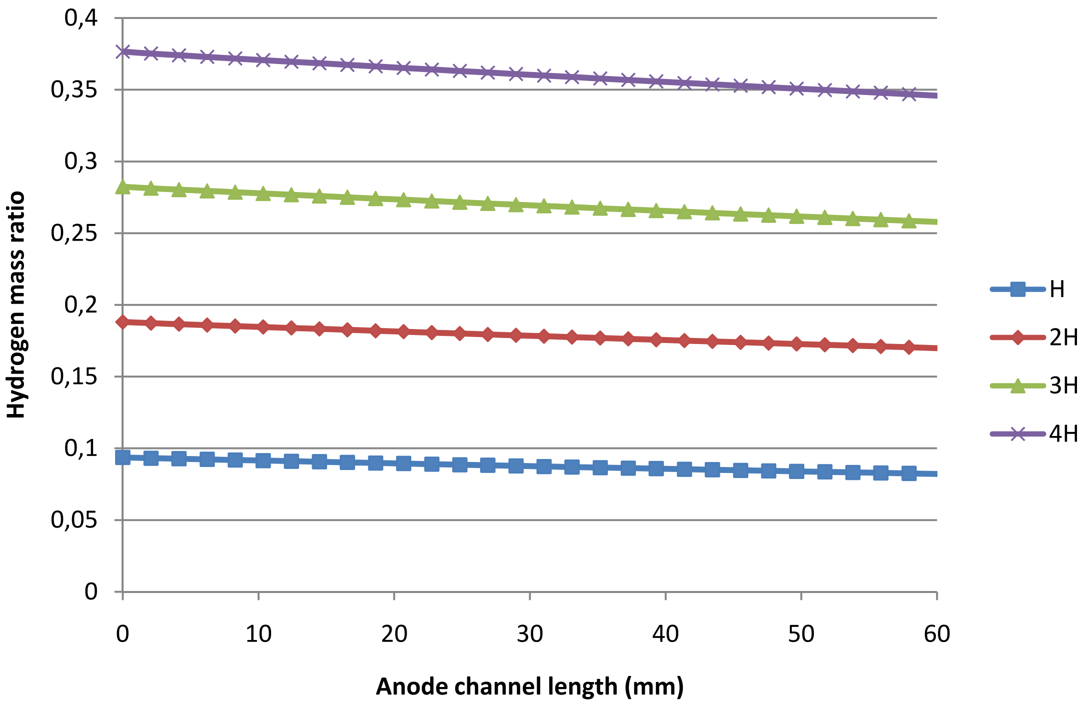

Figure 4.17 Hydrogen consumption along the anode gas channel under various hydrogen content in the fuel (H=9.6 (wt.%))

4.3.3.3 Effect of Flowrate

Effects of mass flow rate are investigated in Fig. 4.18 and 4.19. Figure 4.18 shows the effects of mass flow rate on the temperature. In this study the mass flow rate increased 1.5 and 2 times and decreased to half and 1/5. It is seen that mass flow rates half, 1.5 and 2 times does not change the temperature in channel significantly since the electrochemical reaction is rate limited. Increasing the amount of fuel does not significantly affect the performance after a reasonable flow rate. However, if the mass flow rates are too low (m/5 case), most of the fuel is consumed at the first section of the channel and temperature decreases significantly at later sections due to due to low electrochemical reactions and fuel starvation. Similar trend is observed in the hydrogen consumption along the channel. It is seen that the hydrogen concentration does not change significantly along the first channel.

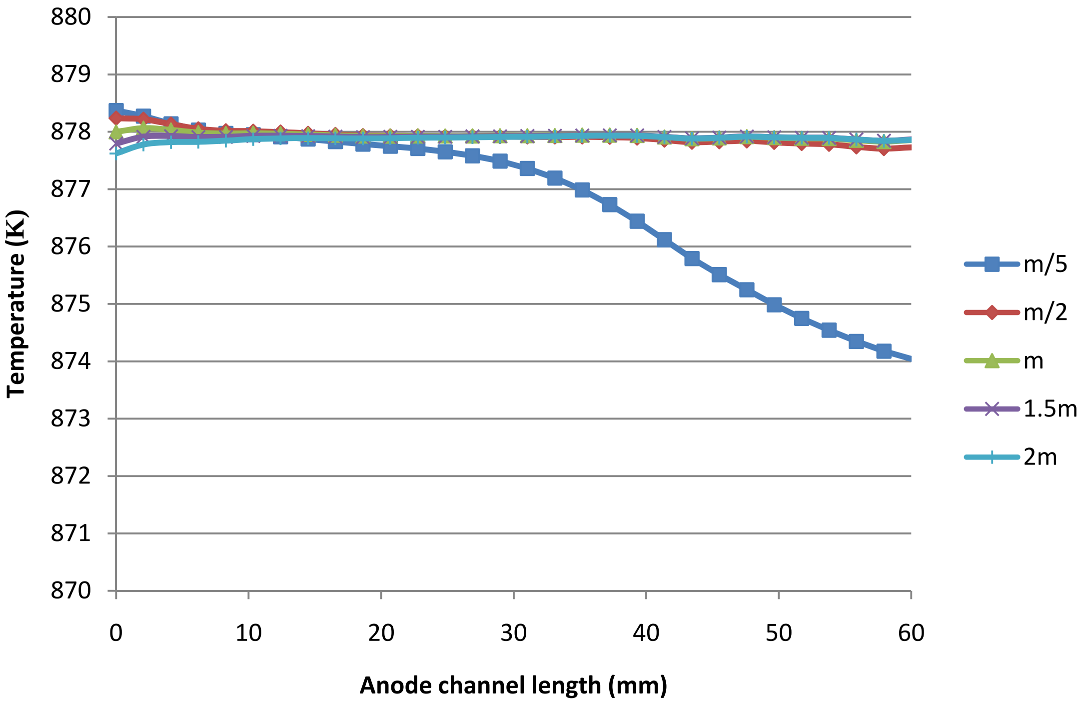

Figure 4.18 Temperature distribution along gas channel under various mass flow rates ($\dot{m}_{air}$= 2.1x10^{-5} kgs^{-1} and $\dot{m}_{fuel}$=3.4x10^{-6} kgs^{-1})

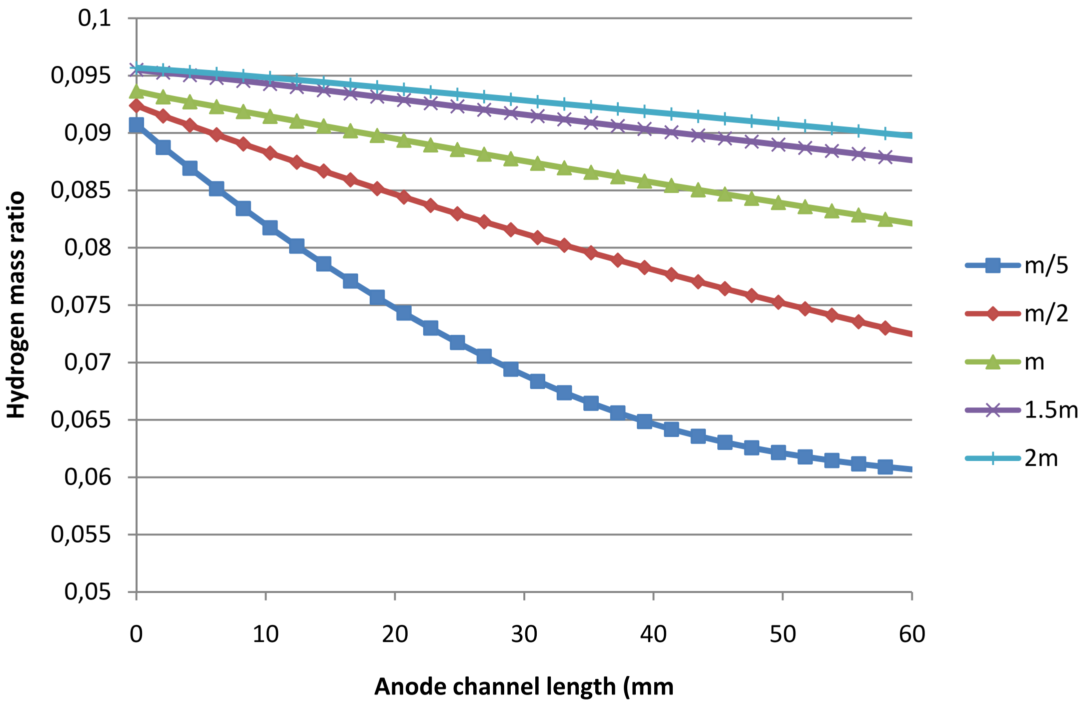

Figure 4.19 H_2 consumption along anode channel under various mass flow rates ($\dot{m}_{air}$= 2.1x10^{-5} kgs^{-1} and $\dot{m}_{fuel}$=3.4x10^{-6} kgs^{-1})

CHAPTER 5

EXPERIMENTAL ANALYSIS

Since there are a few experimental studies in the literature to measure the temperature distribution and the effects of operational parameters on intermediate temperature SOFCs, an experimental set-up is designed and established. The experimental set-up is aimed to collect data for validation of the mathematical model and for comparison with the numerical study. The experimental data will also be used for better cell and interconnector designs and for the optimization of operational parameters for a better cell performance. The validation of the model with the experimental data makes simulation a functional tool to predict the process parameters, potentially enabling the SOFC to be fabricated to reach high performance values. Therefore, experimental studies are indispensible for the SOFC technology research and development stages before commercialization. Due to high temperature operation of SOFCs, special concerns are required for the experimental set up in the viewpoints of material selection as well as temperature and reaction gas control.

5.1 The Experimental Set up

Mainly two groups of experiments are performed. In the first group, the performance of the PEN structure fabricated in our lab was determined. In the second one cell temperature measurements are performed. The performance of the PEN is characterized with open circuit voltage (OCV) measurements, I-V curves and current- temperature measurements. The experimental set up for the performance measurements is shown in Fig. 5.1. The experimental set-up consists of a PEN that is fully produced in our lab, a current collector, an electronically controlled furnace to control the operating temperature and to heat up the system till operating temperature, a fully automated fuel cell test station for I-V curve and OCV measurements.

The experimental procedure is started with the fabrication of the GDC-10 electrolyte by tape casting. Then the prepared anode and cathode slurries are screen printed on the electrolyte so that the active area of the PEN is around 57 cm^2 (the area of the anode/cathode). After that, the active areas of the electrodes were painted with a silver high conducting paste in order to obtain a better current collection.

The details of the PEN fabrication are given in the following section of this chapter and the PEN structure used in this study was prepared according to the optimized parameters some of which are explained in the same chapter. The photos of the PEN structure are shown in Fig. 5.2. The second step of the first group of experiments is the production of the interconnectors. The gas channels on both anode and cathode interconnect that are made out of S314 are machined and surface finished to ensure the flatness of the surface in order not to break brittle PEN structure. The fuel and oxidant inlet and outlet pipes are welded to the interconnectors as shown in Fig. 5.3. The voltage and current measurements are performed connecting the test station probes on the pipes. The silver painted PEN is then inserted inside the soft sealing material and sandwiched between two interconnects to form SOFC single cell unit as shown.

The only difference between the two groups of experiments is that the second group is designed also to measure the temperature inside the cell by means of thermocouples as shown in the Fig. 5.4 with given numbers which will be used in the rest of the study. The thermocouples are covered by a ceramic pipe with a high temperature resistance adhesive and then inserted into the metal pipe through interconnector holes again by means of the adhesive to prevent gas leakage while their probes are kept in contact with the PEN structure. In both experiment groups, the single cell unit is placed into furnace. Its temperature is set to 600ºC.

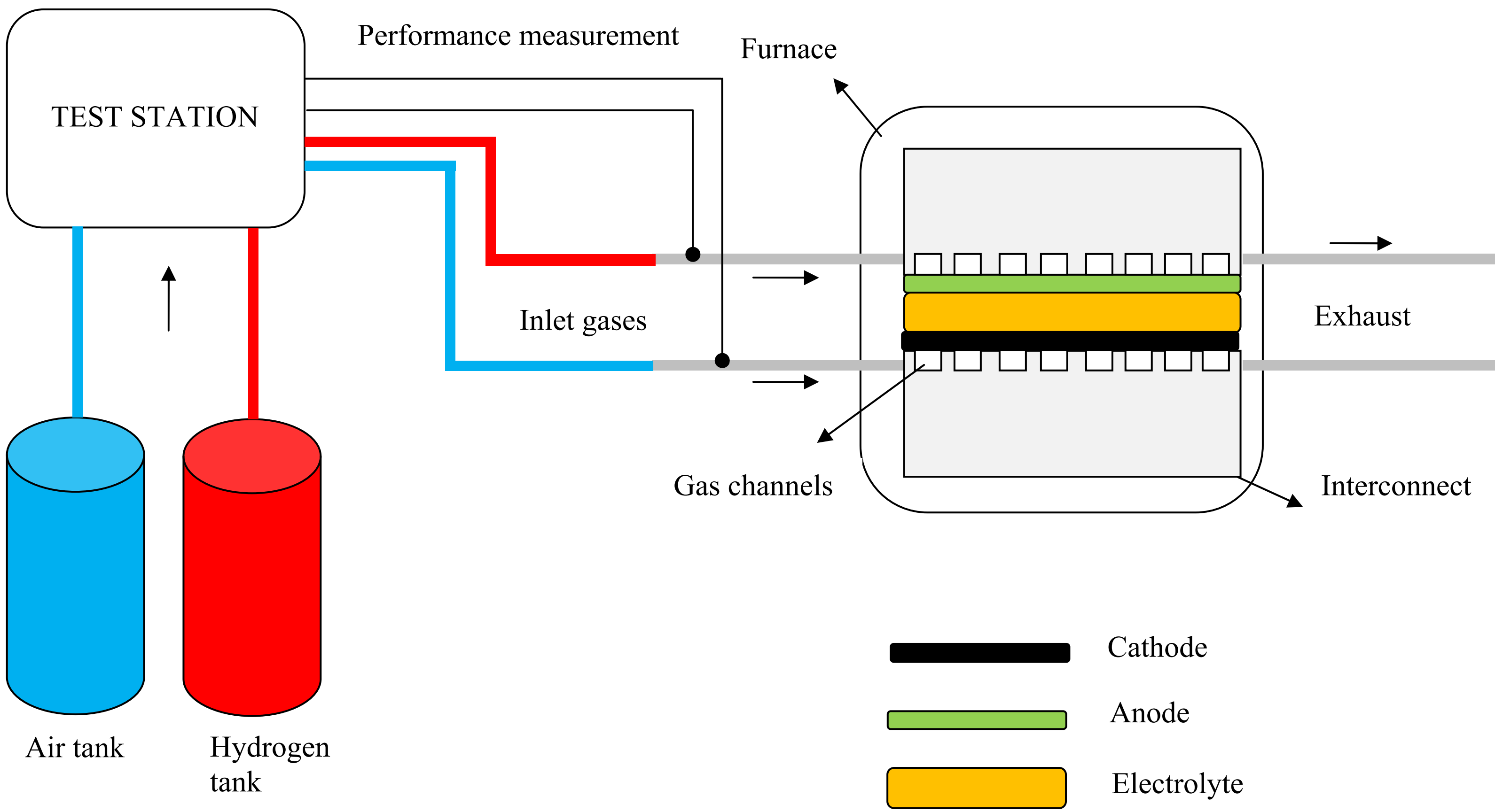

Figure 5.1 The block diagram of the experimental set up for the first group

After reaching the set temperature, hydrogen and oxygen are supplied from the storage tanks to the test station as a fuel and an oxidant, respectively.

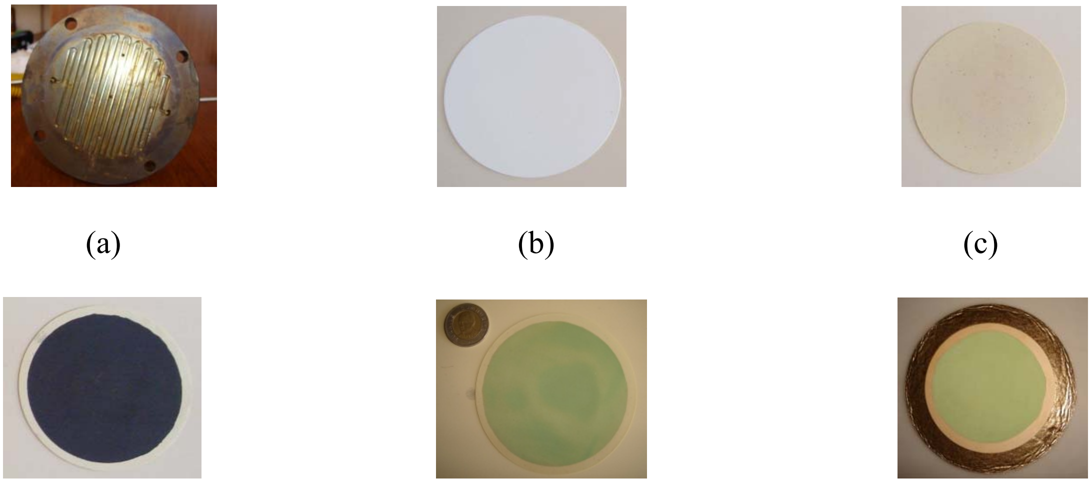

(a) (b) (c)

(d) (e) (f)

Figure 5.2 Experimental set up components photos (a) an example of the interconnector channel design (b) electrolyte before sintering (c) electrolyte after sintering (d) cathode after sintering (e) anode after sintering (f) sealing material

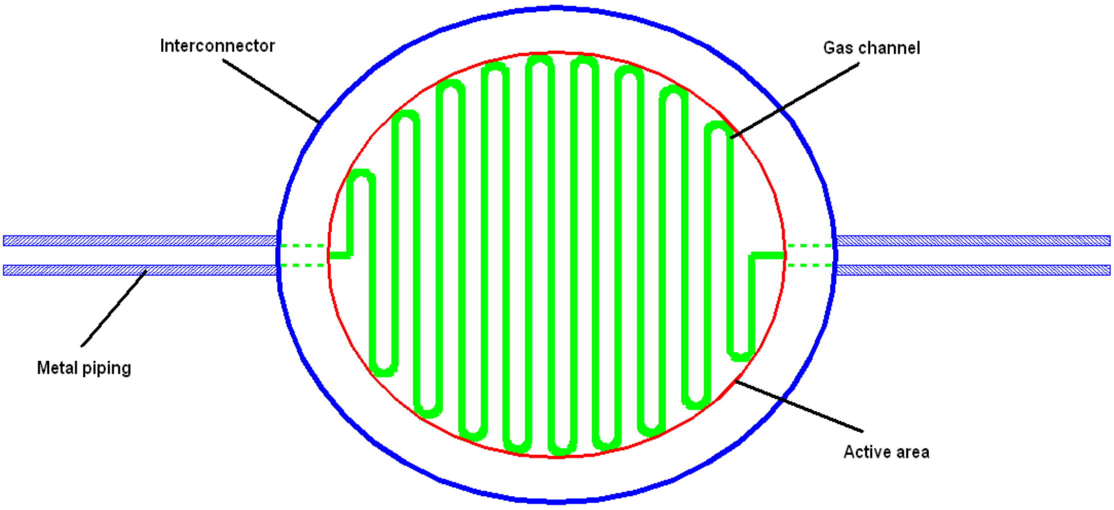

Figure 5.3 Interconnects gas channel design

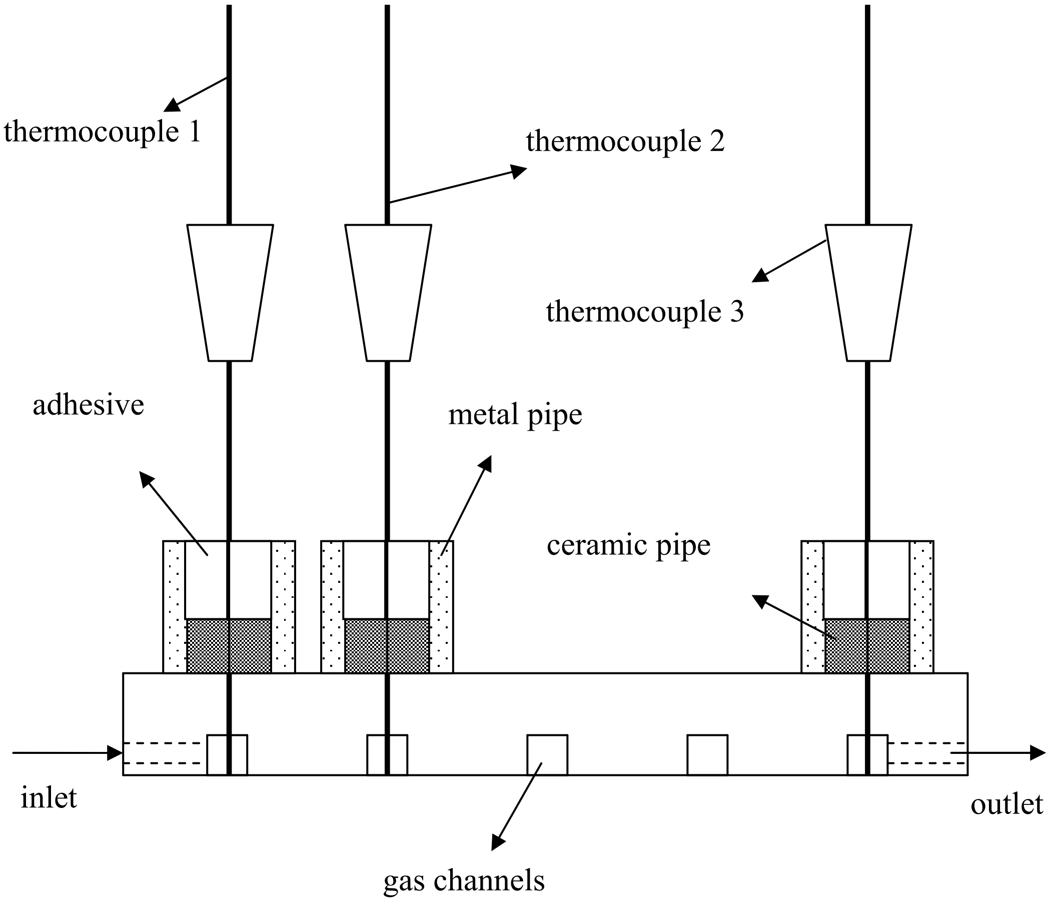

Figure 5.4 Thermocouples placement on the interconnector

The gas flows are controlled by the test station. In the second group additional computer is required for the temperature measurements and for storing the measured data. The experimental set-up photo for the second group is shown in Fig. 5.5 while single cell demonstrations are shown in Figs. 5.6-7.

Figure 5.5 Experimental set up

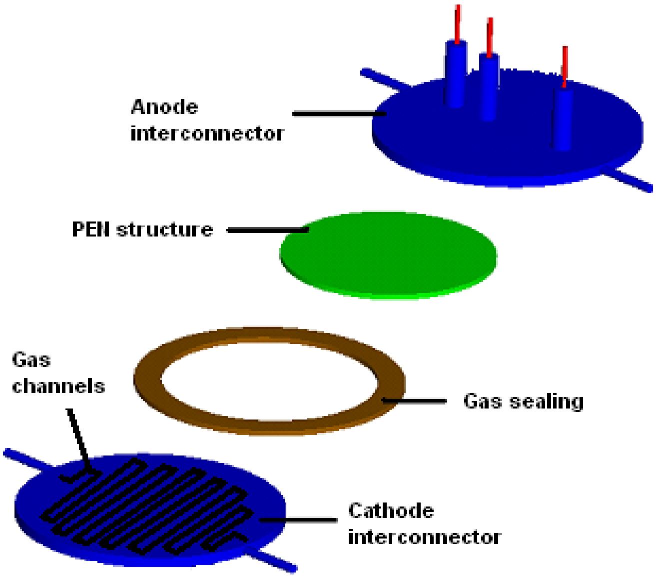

Figure 5.6 Schematic of fabricated single cell configuration

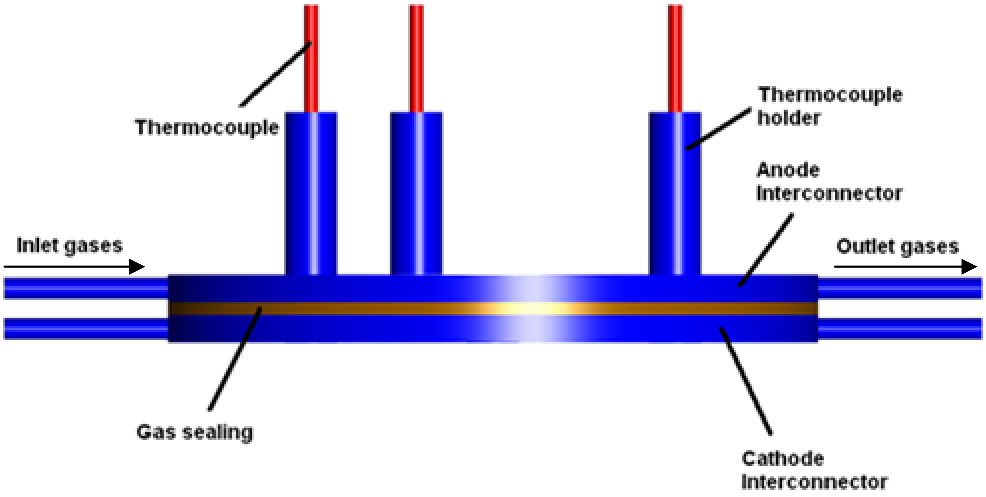

Figure 5.7 Compact single cell (not to scale)

5.2 Experimental Results

5.2.1 Performance Measurements

5.2.1.1 PEN Development

One of the main objectives of this study was to develop a GDC based PEN for an intermediate temperature solid oxide fuel cell to operate at 600-700ºC. Such PEN is not commercially available; therefore, it is produced in our lab. To produce the PEN, the tape casting and screen printing methods are employed. The high purity electrolyte material 10% gadolinium doped ceria (GDC10, $Ce_{0.9}Gd_{0.1}O_{1.9}$) is purchased from Nextech Materials and ball milled (Fig. 5.8) for around 24h with an organic dispersant, plasticizer and binder to form a slurry. The purpose of the dispersant is to prevent agglomeration of particles and obtain homogenous particle distribution. The binder added to the slurry is to form a workable, plastic like composite system and to give the desired shape of the final product. The plasticizer is added to the casting solution to provide green ceramic softness and workability. The slurries then are casted by a laboratory scale tape casting equipment (Fig. 5.9). The electrolyte tapes are stacked together and laminated under 20MPa pressure for 20 min via a laboratory press. After the lamination and pressing, a two stage sintering procedure is applied to fabricate a fully dense electrolyte layer. In the first step, added organic materials are burned with a slow heating schedule up to 800ºC. After this stage, the half sintered electrolytes are transferred to the high temperature furnace. The fully densified electrolyte is obtained after a relatively fast heating schedule (3ºC/min) up to 1500ºC. The electrolyte is found to be 98% dense after the measurement employing Archimet method.

Figure 5.8 Ball milling instrument

The anode and cathode layers are produced with the screen printing method. The anode powders NiO-GDC10 (wt%, 60NiO : 40GDC10) are purchased from Nextech Materials Co. and a screen printable solution obtained with mixing the powders with a certain amount of terpineol and ethyl cellulose solution. The screen printing is then performed with silk screen with an 80 meshes per centimeter square. After the printing process, the printing is dried and sintered again in a temperature controlled furnace at 1200ºC. The same procedure is applied for the cathode layer. LSF-GDC10 (wt%, 50LSF : 50GDC10) is purchased from the same company, however, it is sintered at 900ºC, at a relatively lower temperature compared to that of anode layer.

Figure 5.9 Laboratory scale tape casting equipment

At the end, the electrolyte supported intermediate temperature SOFC membrane electrode groups that are fabricated with an active area of 8 cm radius disk are ready for the single cell tests for the performance measurements.

The SEM (Scanning Electron Microscope) pictures of the produced PEN are given in Fig. 5.10. Figure 5.10a shows the micro structure of the electrolyte layer. It is seen that the particles are well attached to each other; there are no cracks or porosity visible at almost 20,000 magnification. Figure 5.10b shows the transverse section of the PEN. It is seen that the anode layer around 10µm thickness are porous as desired and well attached to the electrolyte. The 300µm thick electrolyte layer is seen as porosity free and neither cracks nor through holes are observed.

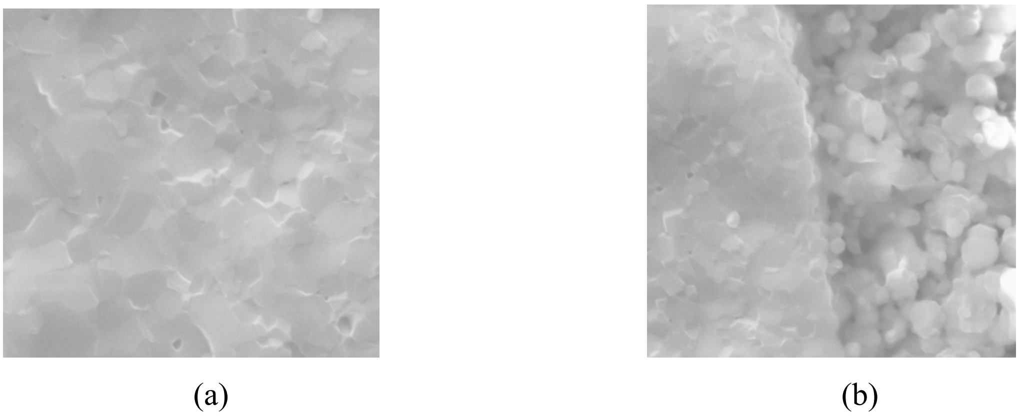
(a) (b)

Figure 5.10 SEM pictures of the PEN (a) Electrolyte (b) Electrolyte (left)-anode (right)

5.2.1.2 Parametric Study

To produce PENs with higher performance, a range of PENs are produced with different thicknesses and sintering temperatures. The sintering temperatures of the anode and cathode are also investigated together with their effects on the cell performance of the PEN. The performances of produced PENs are determined with some OCV and current density measurements.

5.2.2 Results and Discussions

5.2.2.1 Effect of Operation Temperature

To determine the operation temperature of the PEN, a single cell with the PEN and the interconnectors are placed in an electronically controlled furnace and it is connected to the test station. The open circuit potential and the current density are measured in a range of temperatures between room temperature and 650ºC. The current density as a function of temperature is given in Fig. 5.11. There was no current up to 400ºC and therefore current values are not recorded. All current is started to be produced after 400ºC but value was not significant until 450ºC, then the data recording is started at this temperature. The current values are obtained at 0.7V which is usually the operational voltage of SOFCs. It is seen that the produced current increases exponentially with the temperature up to 640ºC and decreases at the higher temperatures, and measurements are stopped after 650ºC. The highest current density at 640ºC is found to be 0.21 A/cm^2 which corresponds to 0.47 W/ cm^2. These current and power density values are lower than the data reported in the literature. Considering the performance data in the literature usually given for pellet size PENs with 1-2 cm^2 active area, the measured values are quite reasonable for a PEN with around 57 cm^2 active area. The relatively low power density may also be attributed to the measurement equipment used in the experiments. To enhance the conductivity silver paint is employed in this study, a higher power density value may be measured with a platinum mesh which is usually employed in the literature.

Figure 5.12 shows how the operating temperature affects the open circuit voltage (OCV) of the cell. Up to the temperature of 450ºC, the fabricated single cell gives almost zero OCV. However, after that point, the OCV increases with the increasing temperature up to almost 600ºC. Further increase in the operating temperature results in a decrease in the OCV of the cell. Therefore, the operation temperature of the fabricated single cell unit should be around 600ºC.

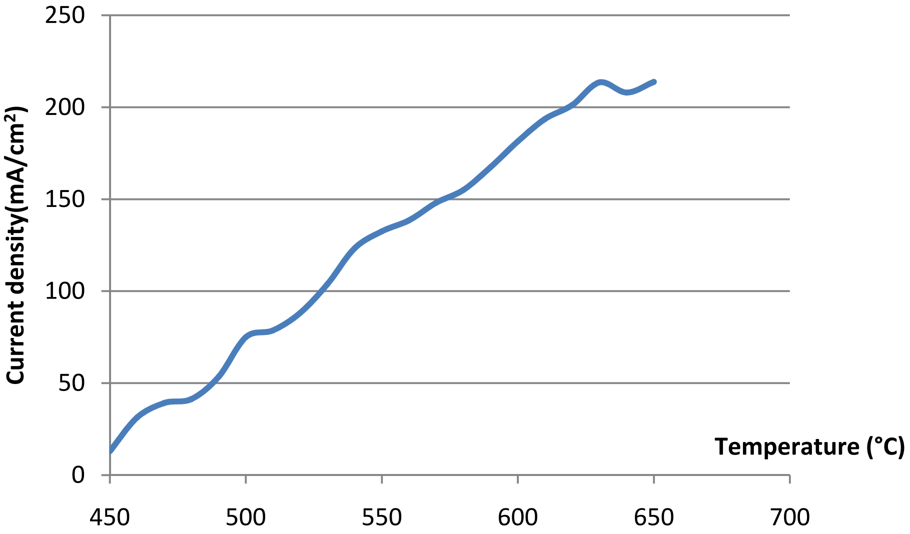

Figure 5.11 Effect of operating temperature on current density at V=0.7V

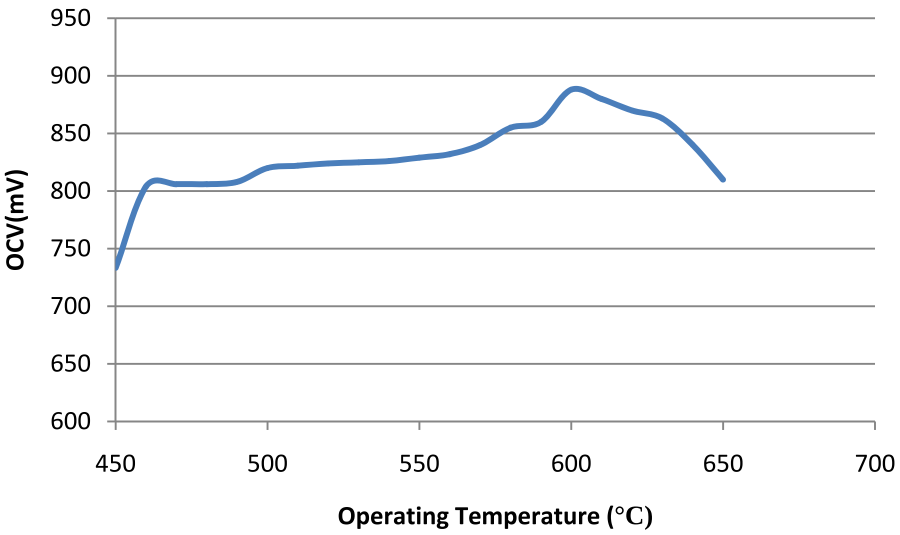

Figure 5.12 Effect of operating temperature on OCV

The measured I-V curve at 640 ºC is given in Figure 5.13. The I-V curve is obtained by measuring the current response of the cell while changing the operational voltage. The current values are recorded after the current stabilization at each voltage value. The performance values are measured at the voltage values of practical importance. It is seen that the maximum voltage is obtained when no current is drawn also known as OCV. The voltage of the cell drops at the high current densities due to the concentration and ohmic losses as explained in detail in Chapter 3. The operating point of the cell is chosen close to the point where the power reaches to the maximum.

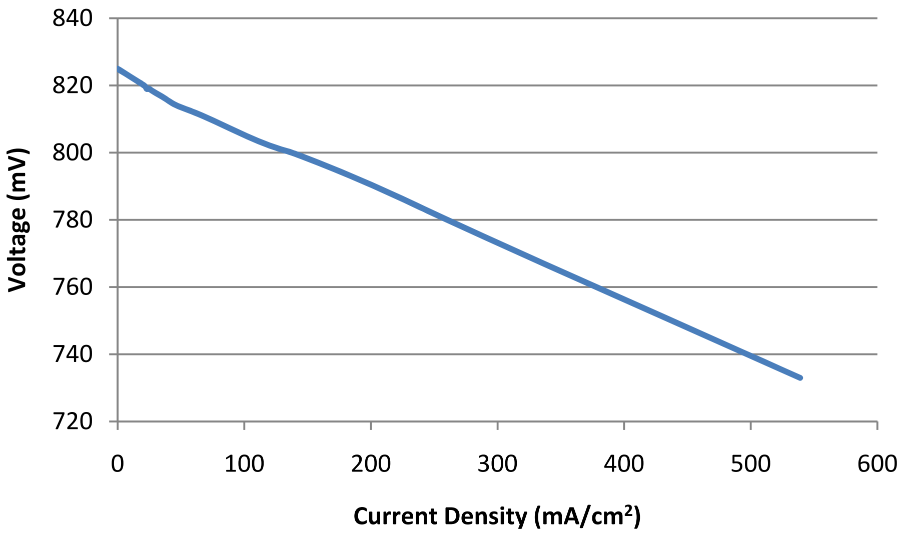

Figure 5.13 I-V characteristics of fabricated PEN

5.2.2.2 Effect of Electrolyte Thickness

The electrolyte thickness plays a major role in the PEN performance since there are power losses during the ion transfer from the anode layer to cathode layer. Therefore, three kinds of electrolytes are produced with 150, 200 and 300µm thicknesses. Figure 5.14 shows the results of the current density measurements of the three types of electrolytes that are fabricated. It is seen that PEN with a 300µm electrolyte thickness produces more power until around 620ºC however after that temperature, the PEN with a 200µm thick electrolyte performs better. This may be attributed to high conductivity at high temperatures and low resistance in thinner electrolytes. The PEN with a 150µm thick electrolyte performs significantly lower than the other two PENs. The low power is attributed to the micro cracks formed in the electrolyte due to the reducing atmosphere of the anode.

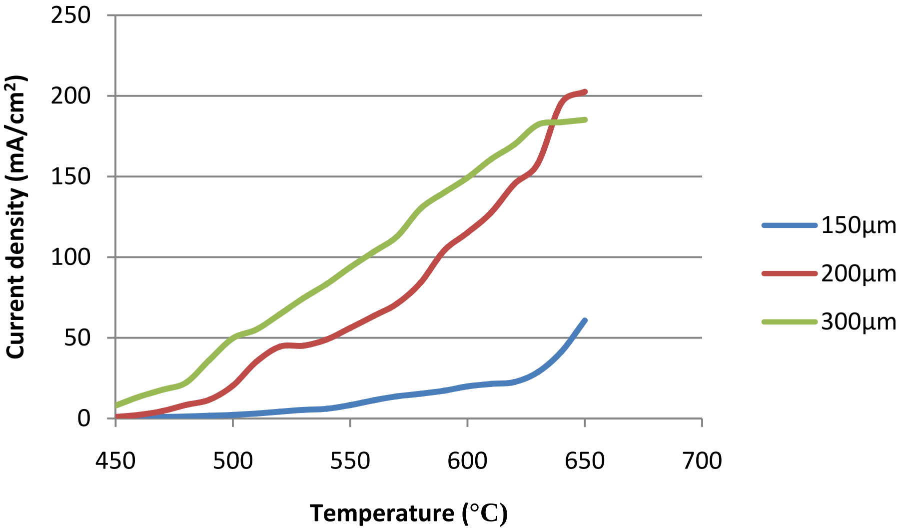

Figure 5.14 Effect of electrolyte thickness on current density at V=0.7V

The OCV measurements of the three PENs are presented in Fig. 5.15. Similar to the current density, the 200µm electrolyte performs better after around 620ºC. The unstable behavior of the thinner electrolyte is again attributed to the micro cracks developed during the operation.

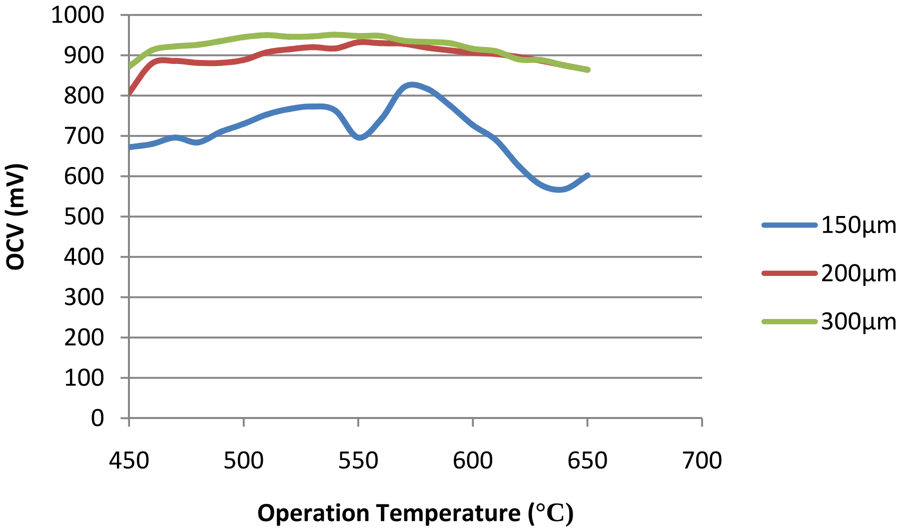

Figure 5.15 Effect of electrolyte thickness on OCV

5.2.2.3 Effect of Sintering Temperature

The sintering temperature of the electrolyte significantly affects the performance of the PEN. The fully dense electrolyte without open porosity is desired for better performance. Open porosity results in local short circuits and gas leaks from the anode side to the cathode side or vice versa. The higher sintering temperature gives a higher density, but leads to grain growth which decreases the performance due to increase in resistance. The recent findings are shown that bulk conduction is not the main ion conduction mechanism; grain boundary condition also plays a major role in overall conductivity. Therefore, bigger grains may result in lower cell performance. The sintering temperatures of the electrolytes are changed from the 1350ºC to 1450ºC and their performances are measured. Figure 5.16 presents the effects of sintering temperature on the produced current as a function of temperature. It is seen that the best performance is obtained at 1375ºC. At higher temperatures, the performance decrease may be the result of grain growth.

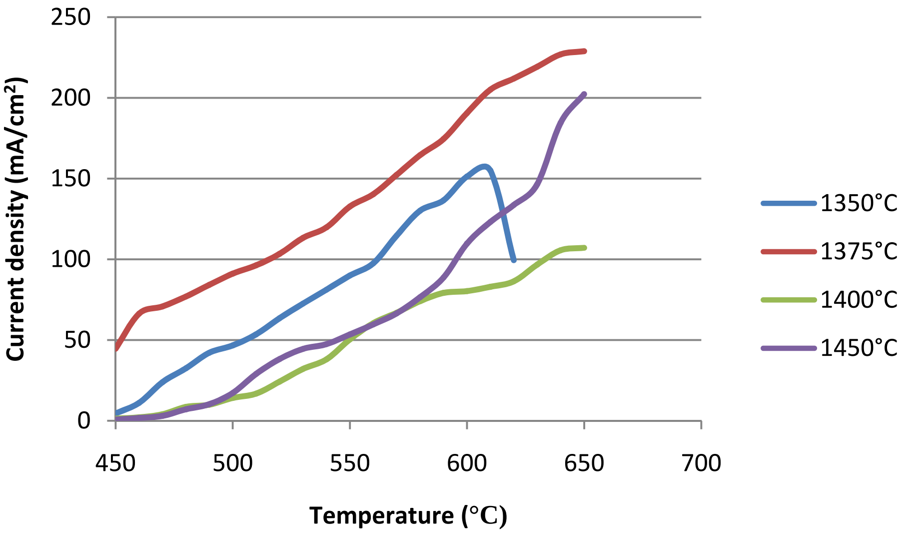

Figure 5.16 Effect of electrolyte sintering temperature on current density at V=0.7V

The OCV values for the electrolytes sintered at different temperatures are presented in Fig. 5.17. It is seen that the electrolytes sintered at higher temperatures perform better. The electrolyte sintered at 1375ºC also performs reasonably well. Since power output is product of current and voltage, the sintering temperature is chosen as 1375ºC for the rest of the PENs produced.

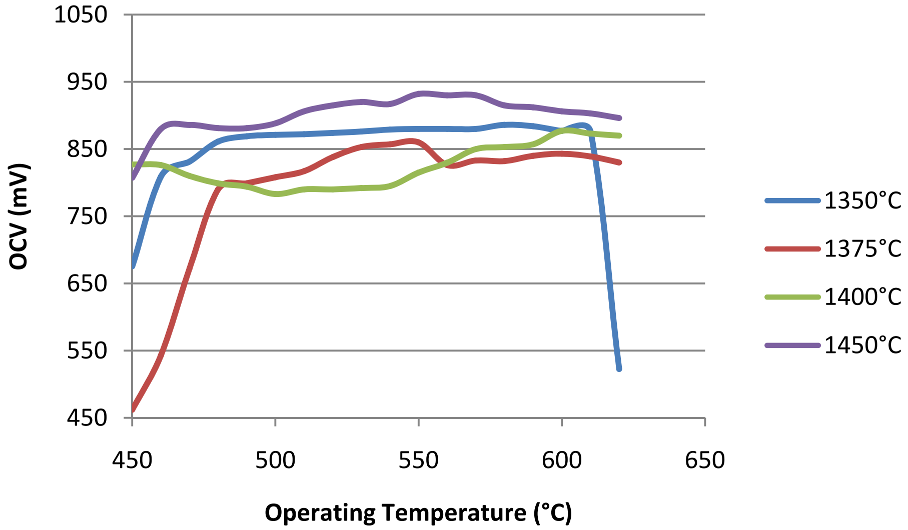

Figure 5.17 Effect of electrolyte sintering temperature on OCV

5.3 Temperature Measurements

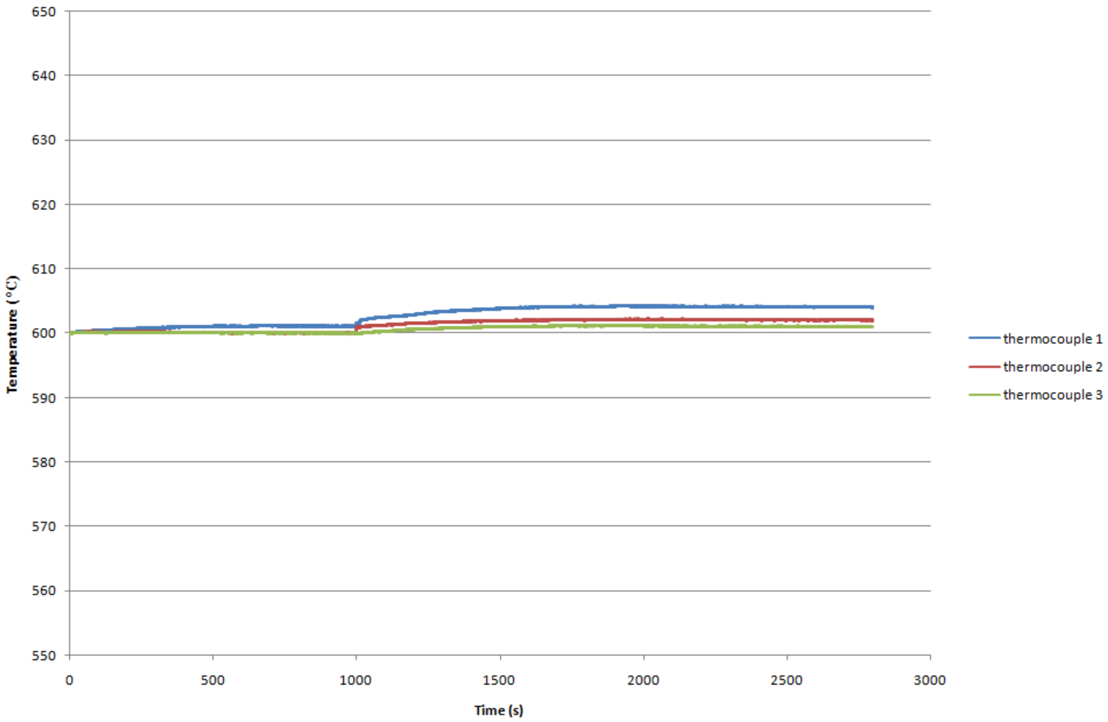

Figure 5.18 Temperature distributions over PEN before and after load ($\dot{m}_{air}$= 2.1x10^{-5} and $\dot{m}_{fuel}$=3.4x10^{-6} kgs^{-1})

During the operation of an SOFC, non-homogenous electrochemical reactions may create a temperature gradient in the cell. This temperature gradient produces a stress development in the system. PENs are very sensitive to stress in the cell due to their brittle ceramic nature. Therefore a series of experiments are conducted in this study to determine the temperature gradient during the operation of an SOFC. The experiments are performed by changing flow rates of the fuel and oxidant with under load and no load conditions to see the effects of the fuel consumption on the temperature gradients.

Figure 5.18 shows the temperature distribution in the system after the system operated at 0.7 V which is the standard operation voltage of SOFCs. First and second locations correspond adjacent to first and second channel and the third location is chosen close to the exit of the fuel channel. The load is applied after around 1700 seconds and as soon as the load is applied an abrupt change in the temperature distribution is observed due to high electrochemical activities. While a gradual change is measured close to mid section and the outlet, a steep change in the vicinity of the first channel from the inlet can be attributed to direct contact of the fresh fuel with the anode catalyst layer. The high temperature gradient between the inlet and the exit section is the result of fuel depletion. Since hydrogen is consumed rapidly starting from the inlet down to the cell, there is less hydrogen left close to the exit section thus the temperature increase slows down at this section.

Figure 5.19 shows the temperature distribution over the PEN at three locations when no load applied to the cell. It is seen that even with a very low electrochemical activity, a temperature gradient develops in the cell. However, the temperature gradient decreases as the system reaches to steady state operation.

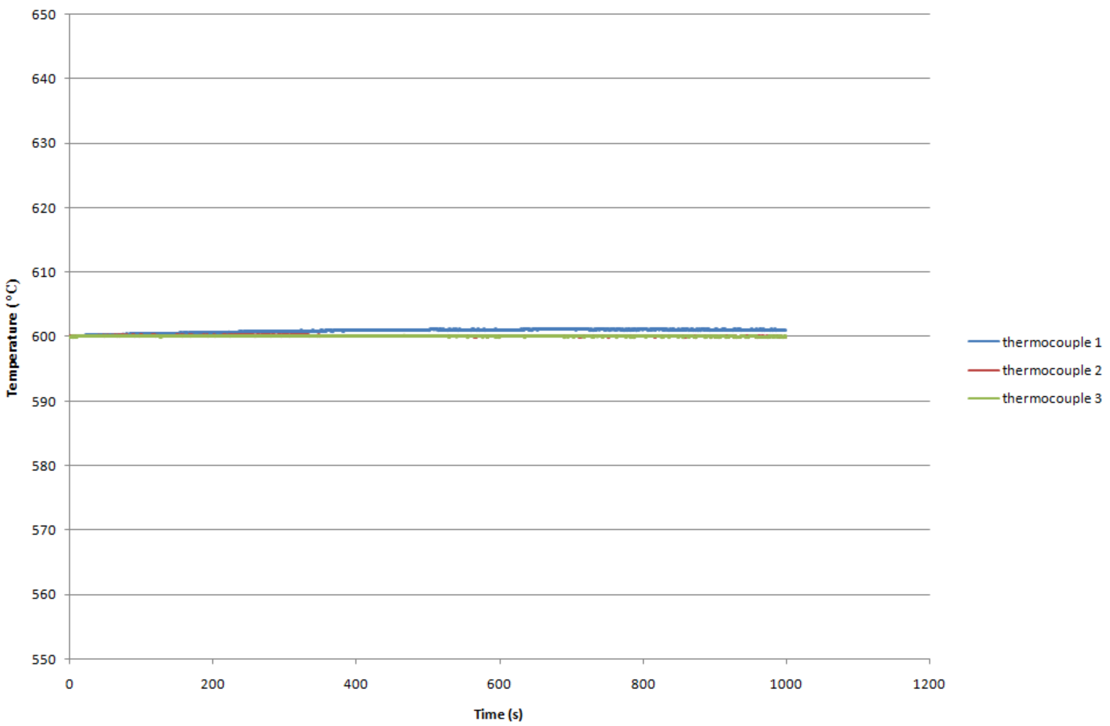

Figure 5.19 Temperature distributions over PEN under no load ($\dot{m}_{air}$= 2.1x10^{-5} and $\dot{m}_{fuel}$=3.4x10^{-6} kgs^{-1})

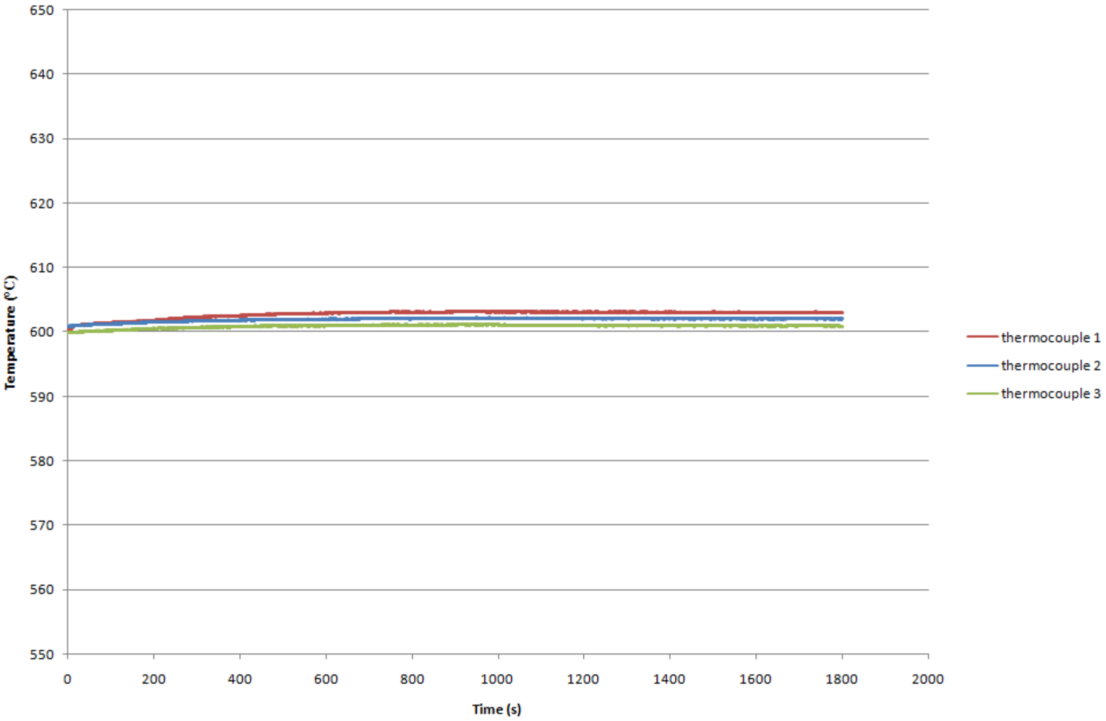

Figure 5.20 Temperature distributions over PEN under load ($\dot{m}_{air}$= 4.2x10^{-6} and $\dot{m}_{fuel}$=6.8x10^{-7} kgs^{-1})

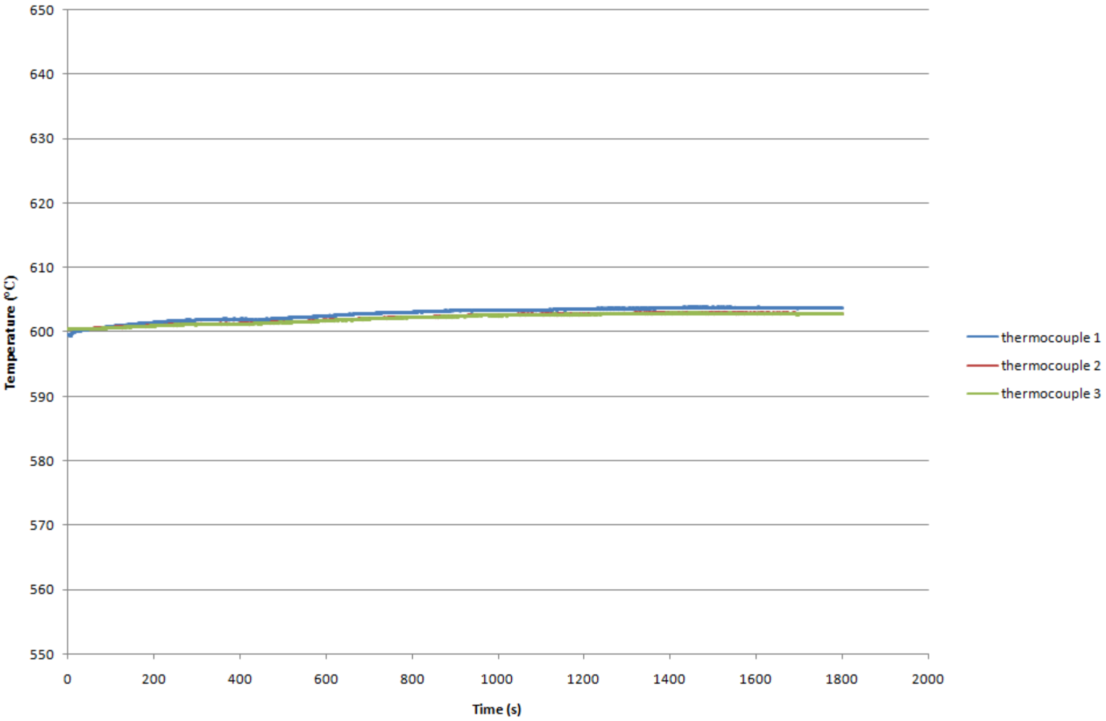

Figure 5.21 Temperature distributions over PEN under load ($\dot{m}_{air}$=3.15x10^{-5} and $\dot{m}_{fuel}$=5.1x10^{-6} kgs^{-1})

The effects of mass flow rate on the temperature gradient are investigated by increasing and decreasing the fuel and oxidant amount supplied to the system.

Figure 5.20 shows the temperature profiles in the system when the mass flow rates of the reaction gases are decreased to 1/5. The changes in the temperatures are not significant. Figure 5.21 shows the temperature gradient in the system when the mass flow rate of fuel and oxidant are increased 1.5 times under the 0.7V operation condition. It is seen that the temperature gradient in the system decreases while the temperature increases in the system. This behavior can be attributed to the enhanced electrochemical reaction in the cell due to more fuel availability for the reaction. The mass flow rates are further increased two times in Fig. 5.22. It is seen that the further increase of mass flow rates results in less temperature gradient and a little increase in the average cell temperature since the electrochemical reactions are limited by the active area. Without increasing the active area, further increase of fuel and oxidant will not result in better performance.

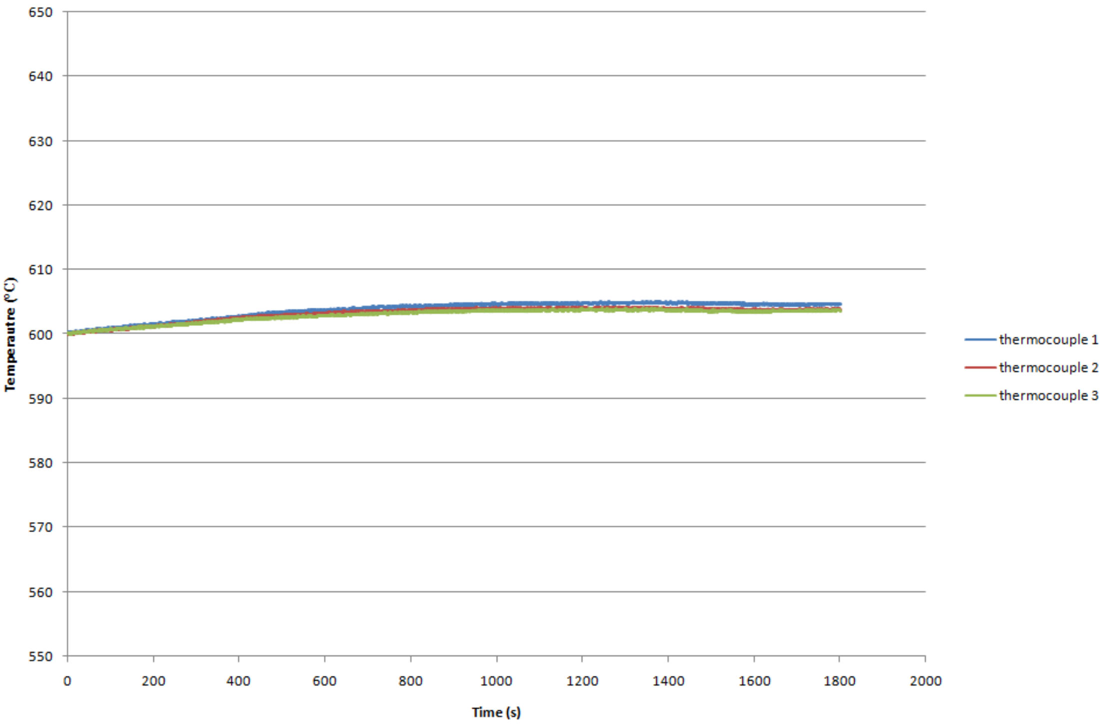

Figure 5.22 Temperature distributions over PEN under load ($\dot{m}_{air}$=4.2x10^{-5} and $\dot{m}_{fuel}$=6.8x10^{-6} kgs^{-1})

CHAPTER 6

COMPARISON OF EXPERIMENTAL AND NUMERICAL RESULTS

To validate and improve the mathematical model, the numerical results are compared with the experimental data considering the anode layer temperature. Figure 6.1 and 6.2 show the temperature on the anode catalyst layer along the anode channel in a range of mass flow rates. The numerical results are plotted with continuous lines while the experimental data is shown by symbols.

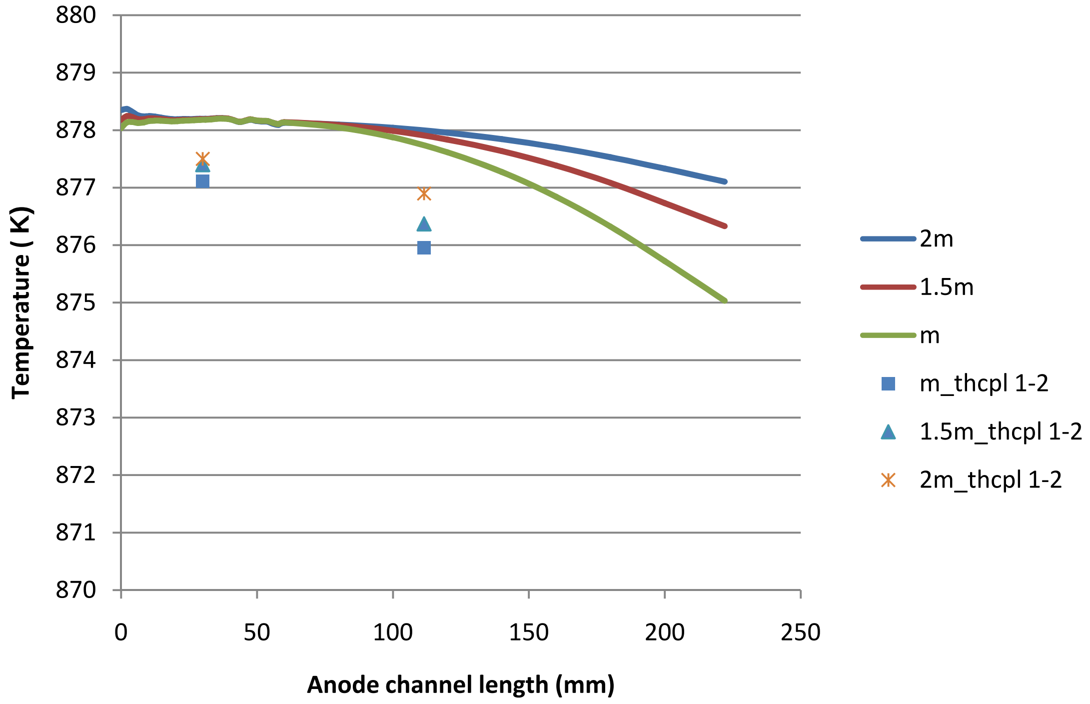

Figure 6.1 Temperature profile on the anode under various mass flow rates ($\dot{m}_{air}$= 2.1x10^{-5} and $\dot{m}_{fuel}$=3.4x10^{-6} kgs^{-1})

It is seen that the temperature in the system decreases along the fuel gas channel due to the fuel consumption and less fuel remains through the exit section of the anode channel. Increasing the mass flow rate does not change the temperature profile at the beginning of the channel since the electrochemical reaction in the anode catalyst depends on the surface area and therefore it is limited. However, with higher mass flow rates, the temperature in the system stabilizes and the thermal gradient decreases since more fuel is available for the electrochemical reactions at the further sections of the anode channel.

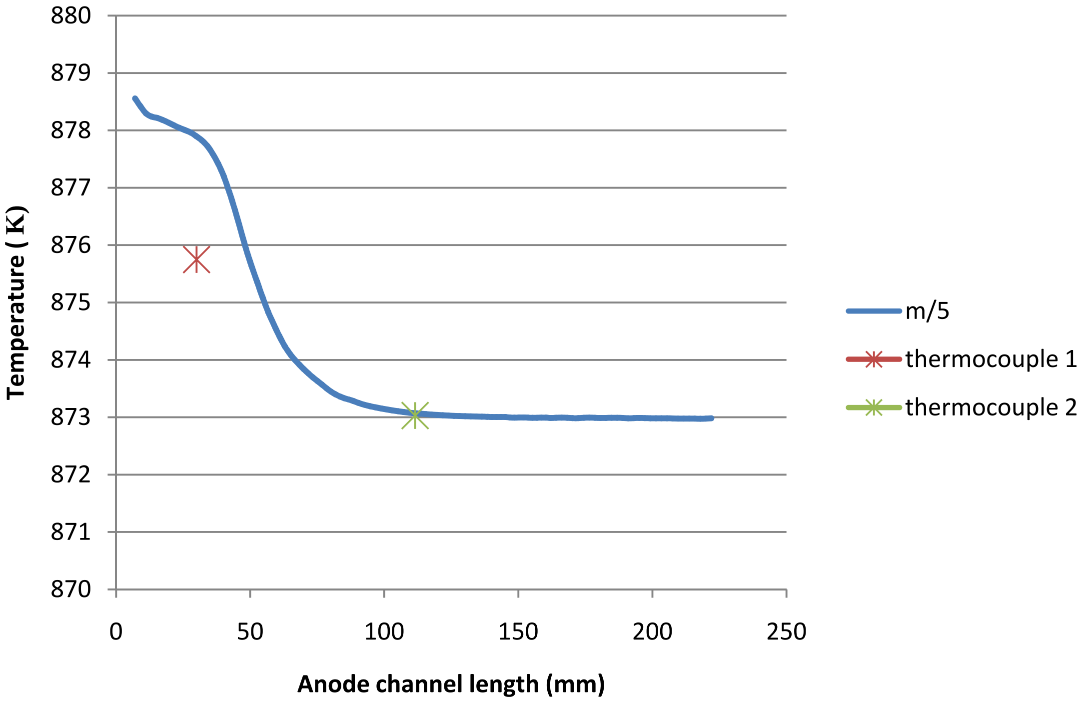

Figure 6.2 Temperature profile on the anode ($\dot{m}_{air}$= 4.2x10^{-6} and $\dot{m}_{fuel}$=6.8x10^{-7} kgs^{-1})

It is seen that with very low fuel feeding, the fuel is consumed rapidly in the first section of the anode channel (Fig. 6.2) and the temperature decreases rapidly along the channel since no or very little fuel is left to change the temperature.

It is observed that the numerical results follow the same trend as that of the experimental measurements. However, the model little over predicts the real temperatures. This may be attributed to the assumption specifically the adiabatic condition at the cell boundaries. Although a very thick isolation layer is applied to all over the furnace, there is some heat loss to the environment. This should be improved in the future studies.

CHAPTER 7

CONCLUSION AND FUTURE STUDIES

Gadolinium doped ceria (GDC) as an electrolyte material instead of Yittria stabilized zirconia (YSZ) significantly reduces operating temperature of the SOFC down to 600ºC. With a GDC based membrane electrode group, it is possible to use cheaper interconnect and sealing materials. Therefore, it is possible to reduce the SOFC system cost with GDC based technology. In this study, fundamental theoretical and experimental analyses were carried out to manufacture GDC based SOFCs, the effects of the major parameters on system performance and parameter space for the optimal operating conditions are investigated theoretically and experimentally.

The major achievements and results are summarized below:

a. A large GDC based PEN having a GDC electrolyte, a NiO/GDC anode and a LSF/GDC cathode with 57 cm^2 active area is manufactured with the tape casting and screen printing methodology.
b. The performance of the PEN is measured with a fuel cell test station at various operating temperatures and it is found that the best results are obtained at 640ºC operating temperature with a 200µm thick GDC electrolyte.
c. An experimental setup is devised to measure the spatial temperature distribution in the SOFC. The temperature distribution is an important parameter in SOFC applications since the ceramic membrane is very sensitive to the stress developed in the system due to the temperature gradients.
d. The experimental results showed that the temperature gradient is more pronounced in the SOFC at low pressure operation under loading condition.

The temperature gradient decreases at high operating pressures due to the enhanced electrochemical reaction at higher pressures.

e. A mathematical model is developed which characterize the fluid flow, the energy and species transport and the electrochemical reactions during the SOFC operation. The mathematical model covers the whole domain in a fuel cell stack including the anode and cathode channels, the electrolyte, the current collectors, and the catalyst layers. Specific nature of each region is characterized with a source term. This approach eliminates the excessive introduction of boundary conditions between each region and simplifies the solution route.
f. The mathematical model is solved with a commercial CFD code which follows on a control volume approach solution methodology. The code allows user incorporation of source terms to the main program with an appropriate FORTRAN coding. The temperature distribution, the species distribution, the charge distribution and flow field are obtained for co-flow SOFC cell which simulates the experimental cell developed in this study. The numerical results showed that the temperature increases close to the inlet section of the cell due to the enhanced electrochemical reaction and decreases close to the exit section due to the depletion of fuel. The model also predicts hydrogen and carbon monoxide depletions and water and carbon dioxide formations along the anode gas channels.
g. A parametric study is performed to investigate the effects of operating parameters on the cell performance. It is found that operating at a high pressure results in a better performance due to the enhanced electrochemical reaction at higher pressures. Since the electrochemical reactions at the anode and the cathode catalyst layers are rate limiting processes the excess fuel cannot be consumed and cannot improve the performance.
h. The numerical results are compared with the experimental data for verification of the mathematical model and for further improvement. It is found that the numerical results agree with the measured experimental data. However, the numerical results over predict the real situation due to the

assumption in the model and corresponding boundary conditions. The model will be improved in further studies.

This comprehensive study provides experimental and numerical data to the literature which is very limited for GDC based SOFCs. Much effort is needed to further improve the PEN performance, the mathematical model and the experimental setup. Therefore following systematic studies are planned for a near future:

- Continue for performance improvement of PEN
- Develop experimental setup for species distribution
- Improve experimental set up for better current collection
- Improve mathematical model
- Add more realistic boundary conditions
- Add radiative heat transfer
- Devise experimental setup for determination of GDC properties (Cp, k, etc)

REFERENCES

[1] Debangsu Bhattacharyya, Raghunathan Rengaswamy, Caine Finnerty, Isothermal models for anode-supported tubular solid oxide fuel cells, Chemical Engineering Science 62 (2007) 4250 – 4267

[2] Hsi-Jen Chen, Shan-Huei Yang, Shun-Hsing Huang, Y.P. Chyou , A paraffin-fueled SOFC system design and integration, Journal of the Chinese Institute of Chemical Engineers, In press

[3] Th. Seitarides, C. Athanasiou, A. Zabaniotou, Modular biomass gasification-based solid oxide fuel cells (SOFC) for sustainable development, Renewable and Sustainable Energy Reviews

[4] D.L. Cresswell, I.S. Metcalfe, Energy integration strategies for solid oxide fuel cell systems, Solid State Ionics 177 (2006) 1905–1910

[5] Mario L. Ferrar, Alberto Traverso, Loredana Magistri, Aristide F. Massardo, Influence of the anodic recirculation transient behavior on the SOFC hybrid system performance, Journal of Power Sources 149 (2005) 22–32

[6] P.F. van den Oosterkamp, Critical issues in heat transfer for fuel cell systems, Energy Conversion and Management 47 (2006) 3552–3561

[7] A. Boudghene Stambouli, E. Traversa, Solid oxide fuel cells (SOFCs): a review of an environmentally clean and efficient source of energy, Renewable and Sustainable Energy Reviews 6 (2002) 433–455

[8] A. Weber, E.I. Tiffee, Materials and concept for solid oxide fuel cells(SOFCs) in stationary and mobile applications, Journal of Power Sources 127(2004) 273-283.

[9] Hengyong Tu, Ulrich Stimming, Advances, aging mechanisms and lifetime in solid-oxide fuel cells, Journal of Power Sources 127 (2004) 284–293.

[10] B.A. Haberman, J.B. Young, Numerical investigation of the air flow through a bundle of IP-SOFC modules, International Journal of Heat and Mass Transfer 48 (2005) 5475–5487

[11] S.C. Singhal, Advances in solid oxide fuel cell technology, Solid State Ionics 135 (2000) 305–313

[12] Roberto Bove, Stefano Ubertini, Modeling solid oxide fuel cell operation: Approaches, techniques and results, Journal of Power Sources 159 (2006) 543–559

[13] Sunil Murthy, Andrei G. Fedorov, Radiation heat transfer analysis of the monolith type solid oxide fuel cell, Journal of Power Sources 124 (2003) 453–458

[14] Subhash C Singhal and Kevin Kendall, High Temperature Solid Oxide Fuel Cells: Fundamentals, Design and Applications (2003), Elsevier Advanced Technology, The Boulevard, Langford Lane, Kidlington Oxford OX5 lGB, UK, p 205

[15] S.H. Chan, X.J. Chen, K.A. Khor, A simple bilayer electrolyte model for solid oxide fuel cells, Solid State Ionics 158 (2003) 29– 43

[16] J. Ma, T.S. Zhang, L.B. Kong, P. Hing, S.H. Chan, Ce0. 8Gd0. 2O2− δ ceramics derived from commercial submicron-sized CeO2 and Gd2O3 powders for use as electrolytes in solid oxide fuel cells, Journal of Power Sources 132 (2004) 71–76

[17] D.-S. Lee, W.S. Kim, S.H. Choi, J. Kim, H.-W. Lee, J.-H. Lee, Characterization of ZrO2 co-doped with Sc2O3 and CeO2 electrolyte for the application of intermediate temperature SOFCs, Solid State Ionics 176 (2005) 33–39

[18] S. Komine, T. Iimure, E. Iguchi, Co-doping effects on crystal structure and electric conduction in ((Y0.75La0.25)1_xGdx)0.18Zr0.82O2_δ, Solid State Ionics 176 (2005) 2535 – 2543

[19] Katsuhiko Yamaji, Teruhisa Horita, Natsuko Sakai, H. Yokokawa, Comparison between La0.9Ba0.1Ga0.8Mg0.2O2.85 and La0.9Sr0.1Ga0.8Mg0.2O2.85 as SOFCs electrolytes, Solid State Ionics 152– 153 (2002) 517– 523

[20] K.A. Khor, L.-G. Yu, S.H. Chan, X.J. Chen, Densification of plasma sprayed YSZ electrolytes by spark plasma sintering (SPS), Journal of the European Ceramic Society 23 (2003) 1855–1863

[21] Kongfa Chen, Zhe Lu, Na Ai, Xiqiang Huang, Yaohui Zhang, Xianshuang Xin, Ruibin Zhu, Wenhui Su, Development of yttria-stabilized zirconia thin films via slurry spin coating for intermediate-to-low temperature solid oxide fuel cells, Journal of Power Sources 160 (2006) 436–438

[22] Sun Dong Kim, Sang Hoon Hyun, Jooho Moon, Jong-Hee Kim, Rak Hyun Song, Fabrication and characterization of anode-supported electrolyte thin films for intermediate temperature solid oxide fuel cells, Journal of Power Sources 139 (2005) 67–72

[23] Yanhai Du, N.M. Sammes, Fabrication of tubular electrolytes for solid oxide fuel cells using strontium- and magnesium- doped LaGaO3 materials, Journal of European Ceramic Society 21 (2001) 727-735

[24] M. Hirano, S. Watanabe, E. Kato, Y. Mizutani, M. Kawai, Y. Nakamura, Fabrication, electrical conductivity and mechanical properties of Sc2O3 doped tetragonal zirconia ceramics, Solid State Ionics 111 (1998) 161-169

[25] N. M. Sammes, G. A. Tompsett, H. Nafe and F. Aldinger, Bismuth Based Oxide Electrolytes Structure and Ionic Conductivity, Journal of the European Ceramic Society 19 (1999) 1801-1826

[26] Sukhvinder P.S. Badwal, Fabio T. Ciacchi, Kristine M. Giampietro, Analysis of the conductivity of commercial easy sintering grade 3 mol% Y2O3–ZrO2 materials, Solid State Ionics 176 (2005) 169–178

[27] Jan Van Herle, Ruben Vasquez, Conductivity of Mn and Ni-doped stabilized zirconia electrolyte, Journal of the European Ceramic Society 24 (2004) 1177–1180

[28] C. Haering, A. Roosen, H. Schichl, Degradation of the electrical conductivity in stabilised zirconia systems Part I: yttria-stabilised zirconia, Solid State Ionics 176 (2005) 253–259

[29] Masatoshi Hattori, Yasuo Takeda, Yoshinori Sakaki, Akihiro Nakanishi, Satoshi Ohara, Kazuo Mukai, Jin-Ho Lee, Takehisa Fukui, Effect of aging on conductivity of yttria stabilized zirconia, Journal of Power Sources 126 (2004) 23–27

[30] M. Hattori, Y. Takeda, J.-H. Lee, S. Ohara, K. Mukai, T. Fukui, S. Takahashi, Y. Sakaki, A. Nakanishi, Effect of annealing on the electrical conductivity of the Y2O3–ZrO2 system, Journal of Power Sources 131 (2004) 247–250

[31] Yaohui Zhang, Xiqiang Huang, Zhe Lu, Zhiguo Liu, Xiaodong Ge, Jiahuan Xu, Xianshuang Xin, Xueqing Sha, Wenhui Su, A screen-printed $Ce_{0.8}Sm_{0.2}O_{1.9}$ film solid oxide fuel cell with a $Ba_{0.5}Sr_{0.5}Co_{0.8}Fe_{0.2}O_{3-\delta}$ cathode, Journal of Power Sources 158 (2006) 1048-1050

[32] Toru Inagaki, Futoshi Nishiwaki, Jirou Kanou, Satoru Yamasaki, Kei Hosoi, Takashi Miyazawa, Masaharu Yamada, Norikazu Komada, Demonstration of high efficiency intermediate-temperature solid oxide fuel cell based on lanthanum gallate electrolyte, Journal of Alloys and Compounds 408–412 (2006) 512–517

[33] S.P. Jiang, X.J. Chen, S.H. Chan, J.T. Kwok, K.A. Khor, (La0.75Sr0.25)(Cr0.5Mn0.5)O3/YSZ composite anodes for methane oxidation reaction in solid oxide fuel cells, Solid State Ionics 177 (2006) 149 – 157

[34] D. Skarmoutsos, A. Tsoga, A. Naoumidis, P. Nikolopoulos, 5 mol% TiO -doped Ni–YSZ anode cermets for solid oxide fuel cells, Solid State Ionics 135 (2000) 439–444

[35] W.Z. Zhu, S.C. Deevi, A review on the status of anode materials for solid oxide fuel cells, Materials Science and Engineering A362 (2003) 228–239

[36] Joon-Ho Koh, Young-Sung Yoo, Jin-Woo Park, Hee Chun Lim, Carbon deposition and cell performance of Ni-YSZ anode support SOFC with methane fuel, Solid State Ionics 149 (2002) 157– 166

[37] Caine M. Finnerty, Neil J. Coe, Robert H. Cunningham, R. Mark Ormerod, Carbon formation on and deactivation of nickel-based/zirconia anodes in solid oxide fuel cells running on methane, Catalysis Today 46 (1998) 137-145

[38] C. Lu, S. An, W.L. Worrell, J.M. Vohs, R.J. Gorte, Development of intermediate-temperature solid oxide fuel cells for direct utilization of hydrocarbon fuels, Solid State Ionics 175 (2004) 47–50

[39] K. Kendall, C.M. Finnerty, G. Saunders, J.T. Chung, Effects of dilution on methane entering an SOFC anode, Journal of Power Sources 106 (2002) 323–327

[40] Shaowu Zha, Philip Tsang, Zhe Cheng, Meilin Liu, Electrical properties and sulfur tolerance of La0.75Sr0.25Cr1_xMnxO3 under anodic conditions, Journal of Solid State Chemistry 178 (2005) 1844–1850

[41] V. Esposito, D.Z. de Florio, F.C. Fonseca, E.N.S. Muccillo, R. Muccillo, E. Traversa, Electrical properties of YSZ/NiO composites prepared by a liquid mixture technique, Journal of the European Ceramic Society 25 (2005) 2637–2641

[42] Yanhong Yin, Shaoyu Li, Changrong Xia, Guangyao Meng, Electrochemical performance of gel-cast NiO–SDC composite anodes in low-temperature SOFCs, Electrochimica Acta 51 (2006) 2594–2598

[43] Masashi Mori, Yoshiko Hiei, Hibiki Itoh, Geoff A. Tompsett, Nigel M. Sammes, Evaluation of Ni and Ti-doped Y2O3 stabilized ZrO2 cermet as an anode in high-temperature solid oxide fuel cells, Solid State Ionics 160 (2003) 1 – 14

[44] K.-R. Lee, Y.S. Pyo, B.S. So, S.M. Kim, B.K. Lee, J.H. Hwang, J. Kim, J.-H. Lee, H.-W. Lee, Interpretation of the interconnected microstructure of an NiO-YSZ anode composite for solid oxide fuel cells via impedance spectroscopy, Journal of Power Sources 158 (2006) 45–51

[45] Hiroshi Mori, Ching-ju Wen, Junichiro Otomo, Koichi Eguchi, Hiroshi Takahashi, Investigation of the interaction between NiO and yttria-stabilized zirconia (YSZ) in the NiO/YSZ composite by temperature-programmed reduction technique, Applied Catalysis A: General 245 (2003) 79–85

[46] J. Wan, J.H. Zhu, J.B. Goodenough, La0.75Sr0.25Cr0.5Mn0.5O3−δ+Cu composite anode running on H2 and CH4 fuels, Solid State Ionics 177 (2006) 1211–1217

[47] Teruhisa Horita, Haruo Kishimoto, Katsuhiko Yamaji, Yueping Xiong, Natsuko Sakai, Manuel E. Brito, Harumi Yokokawa, Materials and reaction mechanisms at anode/electrolyte interfaces for SOFCs, Solid State Ionics 177 (2006) 1941–1948

[48] M. Radovic, E. Lara-Curzio, Mechanical properties of tape cast nickel-based anode materials for solid oxide fuel cells before and after reduction in hydrogen, Acta Materialia 52 (2004) 5747–5756

[49] Xiqiang Huang, Zhe Lu, Li Pei, Zhiguo Liu, Yuqiang Liu, Ruibin Zhu, Jipeng Miao, Zhiguo Zhang, Wenhui Su, A n anode for solid oxide fuel cells: NiO1(Ce Ca O) (YSZ) solid solution, Journal of Alloys and Compounds 360 (2003) 294–297

[50] P. Vernoux, M. Guillodo, J. Fouletier, A. Hammou, Alternative anode material for gradual methane reforming in solid oxide fuel cells, Solid State Ionics 135 (2000) 425–431

[51] Steven McIntosh, John M. Vohs, Raymond J. Gorte, An examination of lanthanide additives on the performance of Cu_YSZ cermet anodes, Electrochimica Acta 47 (2002) 3815_3821

[52] Seungdoo Park, Raymond J. Gorte, John M. Vohs, Applications of heterogeneous catalysis in the direct oxidation of hydrocarbons in a solid-oxide fuel cell, Applied Catalysis A: General 200 (2000) 55–61

[53] A. Gunji, C. Wen, J. Otomo, T. Kobayashi, K. Ukai, Y. Mizutani, H. Takahashi, Carbon deposition behaviour on Ni–ScSZ anodes for internal reforming solid oxide fuel cells, Journal of Power Sources 131 (2004) 285–288

[54] A.L. Sauvet, J.T.S. Irvine, Catalytic activity for steam methane reforming and physical characterisation of La1_xSrxCr1_yNiyO3_d, Solid State Ionics 167 (2004) 1 –8

[55] Nobuyoshi Nakagawa, Hitoei Sagara, Kunio Kato, Catalytic activity of Ni-YSZ-CeO2 anode for the steam reforming of methane in a direct internal-reforming solid oxide fuel cell, Journal of Power Sources 92 (2001) 88-94

[56] M. Wisniewski, A. Bore´ave, P. Ge´lin, Catalytic CO2 reforming of methane over Ir/Ce0.9Gd0.1O2-x, Catalysis Communications 6 (2005) 596–600

[57] Wei Zhu, Changrong Xia, Jue Fan, Ranran Peng, Guangyao Meng, Ceria coated Ni as anodes for direct utilization of methane in low-temperature solid oxide fuel cells, Journal of Power Sources 160 (2006) 897–902

[58] A. Martınez-Arias, A.B. Hungrıa, M. Fernandez-Garcıa, A. Iglesias-Juez, J.C. Conesa, G.C. Mather, G. Munuera, Cerium–terbium mixed oxides as potential materials for anodes in solid oxide fuel cells, Journal of Power Sources 151 (2005) 43–51

[59] S. An, C. Lu, W.L. Worrell, R.J. Gorte, J.M. Vohs, Characterization of Cu–CeO2 direct hydrocarbon anodes in a solid oxide fuel cell with lanthanum gallate electrolyte, Solid State Ionics 175 (2004) 135–138

[60] Zhe Cheng, Shaowu Zha, Luis Aguilar, Meilin Liu, Chemical, electrical, and thermal properties of strontium doped lanthanum vanadate, Solid State Ionics 176 (2005) 1921 – 1928

[61] Olga Costa-Nunes, Raymond J. Gorte, John M. Vohs, Comparison of the performance of Cu–CeO2–YSZ and Ni–YSZ composite SOFC anodes with H2, CO, and syngas, Journal of Power Sources 141 (2005) 241–249

[62] Hiraad Taherparvar, John A. Kilner, Richard T. Baker, Mortaza Sahibzada, Effect of humidification at anode and cathode in proton-conducting SOFCs, Solid State Ionics 162– 163 (2003) 297– 303

[63] Tatsuya Takeguchi, Ryuji Kikuchi, Tatsuya Yano, Koichi Eguchi, Kazutoshi Murata, Effect of precious metal addition to Ni-YSZ cermet on reforming of CH4 and electrochemical activity as SOFC anode, Catalysis Today 84 (2003) 217–222

[64] G.C. Mather, F.M. Figueiredo, J.R. Jurado, J.R. Frade, Electrochemical behaviour of Ni-cermet anodes containing a proton-conducting ceramic phase on YSZ substrate, Electrochimica Acta 49 (2004) 2601–2612

[65] Q.X. Fu, F. Tietz, P. Lersch, D. Stöver, Evaluation of Sr- and Mn-substituted LaAlO3 as potential SOFC anode materials, Solid State Ionics 177 (2006) 1059–1069

[66] M.A. Haldane, T.H. Etsell, Fabrication of composite SOFC anodes, Materials Science and Engineering B 121 (2005) 120–125

[67] Zhen Xie, Wei Zhu, Baichuan Zhu, Changrong Xia, FexCo0.5−xNi0.5–SDC anodes for low-temperature solid oxide fuel cells, Electrochimica Acta 51 (2006) 3052–3057

[68] Shizhong Wang, Masaki Ando, Tatsumi Ishihara, Yusaku Takita, High performance Ni–Sm0.15Ce0.85O2_d cermet anodes for intermediate temperature solid oxide fuel cells using LaGaO3 based oxide electrolytes, Solid State Ionics 174 (2004) 49–55

[69] Sung Pil Yoon, Jonghee Han, Suk Woo Nam, Tae-Hoon Lim, Seong-Ahn Hong, Improvement of anode performance by surface modification for solid oxide fuel cell running on hydrocarbon fuel, Journal of Power Sources 136 (2004) 30–36

[70] Khaliq Ahmed, Karl Foger, Kinetics of internal steam reforming of methane on Ni/YSZbased anodes for solid oxide fuel cells, Catalysis Today 63 (2000) 479–487

[71] Joseph Sfeir Philippe A. Buffat, Pedro Mockli, Nicolas Xanthopoulos, Ruben Vasquez, Hans Joerg Mathieu, Jan Van herle and K. Ravindranathan Thampi, Lanthanum Chromite Based Catalysts for Oxidation of Methane Directly on SOFC Anodes, Journal of Catalysis 202 (2001), 229–244

[72] A. Hartley, M. Sahibzada, M. Weston, I.S. Metcalfe, D. Mantzavinos, La0 ⋰6Sr0 ⋰4Co0 ⋰2Fe0 ⋰8O3 as the anode and cathode for intermediate temperature solid oxide fuel cells, Catalysis Today 55 (2000) 197–204

[73] G. Pudmich[a], B.A. Boukamp, M. Gonzalez-Cuenca, W. Jungen, W. Zipprich, F. Tietz, Chromite/ titanate based perovskites for application as anodes in solid oxide fuel cells, Solid State Ionics 135 (2000) 433–438

[74] A.-L. Sauvet, J. Fouletier, Catalytic properties of new anode materials for solid oxide fuel cells operated under methane at intermediary temperature, Journal of Power Sources 101 (2001) 259-266

[75] Hongpeng He, Yingyi Huang, John M. Vohs, Raymond J. Gorte, Characterization of YSZ–YST composites for SOFC anodes, Solid State Ionics 175 (2004) 171–176

[76] H.Z. Song, H.B. Wang, S.W. Zha, D.K. Peng, G.Y. Meng, Aerosol-assisted MOCVD growth of Gd2O3-doped CeO2 thin SOFC electrolyte film on anode substrate, Solid State Ionics 156 (2003) 249– 254

[77] Xianshuang Xin, Zhe Lu, Xiqiang Huang, Xueqing Sha, Yaohui Zhang, Wenhui Su, Anode-supported solid oxide fuel cell based on dense electrolyte membrane fabricated by filter-coating, Journal of Power Sources, in press

[78] S. Sarat, N. Sammes, A. Smirnova, Bismuth oxide doped scandia-stabilized zirconia electrolyte for the intermediate temperature solid oxide fuel cells, Journal of Power Sources 159 (2006) 1158–1161

[79] M. Sahibzada, B.C.H. Steele, K. Zheng, R.A. Rudkin, I.S. Metcalfe, Development of solid oxide fuel cells based on a Ce(Gd) 02-X electrolyte film for intermediate temperature operation, Catalysis Today 38 (1997) 459-466

[80] Yong Jun Leng, Siew Hwa Chan, Khiam Aik Khor, San Ping Jiang, Philip Cheang, Effect of characteristics of Y2O3/ZrO2 powders on fabrication of anode-supported solid oxide fuel cells, Journal of Power Sources 117 (2003) 26–34

[81] Xian-Jin Ning, Cheng-Xin Li, Chang-Jiu Li, Guan-Jun Yang, Effect of powder structure on microstructure and electrical properties of plasma-sprayed 4.5 mol% YSZ coating, Vacuum 80 (2006) 1261–1265

[82] Bin Zhu, Ingvar Albinsson, Camilla Andersson, Karin Borsand, Monika Nilsson, Bengt-Erik Mellander, Electrolysis studies based on ceria-based composites, Electrochemistry Communications 8 (2006) 495–498

[83] Guangyao Meng, Haizheng Song, Qiang Dong, Dingkun Peng, Application of novel aerosol-assisted chemical vapor deposition techniques for SOFC thin films, Solid State Ionics 175 (2004) 29–34

[84] Yeong Yoo, Fabrication and characterization of thin film electrolytes deposited by RF magnetron sputtering for low temperature solid oxide fuel cells, Journal of Power Sources 160 (2006) 202–206

[85] C. Haering, A. Roosen, H. Schichl, M. Schnfller, Degradation of the electrical conductivity in stabilised zirconia system Part II: Scandia-stabilised zirconia, Solid State Ionics 176 (2005) 261–268

[86] Toshiaki Matsui, Minoru Inaba, Atsushi Mineshige, Zempachi Ogumi, Electrochemical properties of ceria-based oxides for use in intermediate-temperature SOFCs, Solid State Ionics 176 (2005) 647–654

[88] J.H. Hirschenhofer, D.B. Stauffer, R.R. Engleman and M.G. Klett, Fuel Cell Handbook, 4th Edition, prepared for the U.S. Department of Energy under contract no. DE-AC21-94MC31166, November, 1988, 5-24

[89] K. Kordesh and G. Simader, Fuel Cells and Their Applications, VCH Publishers, New York, NY, 1996, p.133

[90] S.C. Singhal, Solid oxide fuel cells for stationary, mobile and military applications, Solid State Ionics, 2002, 405–410

[91] Gemma Crawley, Solid Oxide Fuel Cells (SOFC), Fuel Cell Today – January 2007

[92] Kerry-Ann Adamson and Gemma Crawley, Fuel Cell Today Military Survey 2006, Fuel Cell Today – June 2006

[93] Alexandra Baker and David Jollie, Fuel Cell Market Survey: Military Applications, Fuel Cell Today – 13 April 2005

[94] Roberto Bove, Stefano Ubertini, Modeling solid oxide fuel cell operation: Approaches, techniques and results, Journal of Power Sources 159 (2006) 543–559

[95] Sadik Kakaç, Anchasa Pramuanjaroenkij, XiangYang Zhou, Areviewof numerical modeling of solid oxide fuel cells, International Journal of Hydrogen Energy 32 (2007) 761 – 786

[96] M.M. Hussain, X. Li, I. Dincer, Mathematical modeling of planar solid oxide fuel cells, Journal of Power Sources 161 (2006) 1012–1022

[97] LehnertW, Meusinger J, Thom F. Modeling of gas transport phenomena in SOFC anodes. J Power Sources 2000;87:57–63

[98] Yakabe H, Hishinuma M, Uratani M, Matsuzaki Y, Yasuda I. Evaluation and modeling of performance of anode-supported solid oxide fuel cell J Power Sources 2000;86:423–31

[99] Virkar AV, Chen J, Tanner CW, Kim J. The role of electrode microstructure on activation and concentration polarizations in solid oxide fuel cells, Solid State Ionics 2000;131:189–98

[100] Yan Ji, Kun Yuan, J.N. Chunga, Yen-Cho Chen, Effects of transport scale on heat/mass transfer and performance optimization for solid oxide fuel cells, Journal of Power Sources 161 (2006) 380–391

[101] Jinliang Yuan, Masoud Rokni, Bengt Sunden, Three-dimensional computational analysis of gas and heat transport phenomena in ducts relevant for anode-supported solid oxide fuel cells, International Journal of Heat and Mass Transfer 46 (2003) 809–821

[102] E. Achenbach, Three-dimensional and time-dependent simulation of a planar solid oxide fuel cell stack, J Power Sources 49 (1994) 333–348

[103] Yau-Pin Chyou, Tsang-Dong Chung, Jong-Sheng Chen, Ri-Fong Shie, Integrated thermal engineering analyses with heat transfer at periphery of planar solid oxide fuel cell, Journal of Power Sources 139 (2005) 126–140

[104] P.W. Li, S.P. Chen, M.K. Chyu, Novel gas distributors and optimization for high power density in fuel cells, Journal of Power Sources 140 (2005) 311–318

[105] Iwata M, Hikosaka T, Morita M, Iwanari T, Ito K, Onda K. et al. Performance analysis of planar-type unit SOFC considering current and temperature distributions. Solid State Ionics 132 (2000) 297–308

[106] Costamagna P., The benefit of solid oxide fuel cells with integrated air pre-heater. Journal of Power Sources 69 (1997) 1–9

[107] M. Lockett, M.J.H. Simmons, K. Kendall, CFD to predict temperature profile for scale up of micro-tubular SOFC stacks, Journal of Power Sources 131 (2004) 243–246

[108] A.C. Burt, I.B. Celik, R.S. Gemmenb, A.V. Smirnov, A numerical study of cell-to-cell variations in a SOFC stack, Journal of Power Sources 126 (2004) 76–87

[109] Tae Won Song, Jeong Lak Sohn, Jae Hwan Kim, Tong Seop Kim, Sung Tack Ro, Kenjiro Suzuki, Performance analysis of a tubular solid oxide fuel cell/micro gas turbine hybrid power system based on a quasi-two dimensional model, Journal of Power Sources 142 (2005) 30–42

[110] K. P. Recknagle, R. E. Williford, L. A. Chick, D. R. Rector, M. A. Khaleel, Three-dimensional thermo-fluid electrochemical modeling of planar SOFC stacks, Journal of Power Sources 113 (2003) 109-114

[111] Sunil Murthy, Andrei G. Fedorov, Radiation heat transfer analysis of the monolith type solid oxide fuel cell, Journal of Power Sources 124 (2003) 453–458

[112] K.J. Daun, S.B. Beale, F. Liu, G.J. Smallwood, Radiation heat transfer in planar SOFC electrolytes, Journal of Power Sources 157 (2006) 302–310

[113] X. Xue, J. Tang, N. Sammes, Y. Du, Dynamic modeling of single tubular SOFC combining heat/mass transfer and electrochemical reaction effects, Journal of Power Sources 142 (2005) 211–222

[114] David L. Damm, Andrei G. Fedorov, Radiation heat transfer in SOFC materials and components, Journal of Power Sources 143 (2005) 158–165

[115] David L. Damm, Andrei G. Fedorov, Reduced-order transient thermal modeling for SOFC heating and cooling, Journal of Power Sources 159 (2006) 956–967

[116] Y. Inui, N. Ito, T. Nakajima, A. Urata, Analytical investigation on cell temperature control method of planar solid oxide fuel cell, Energy Conversion and Management 47 (2006) 2319–2328

[117] L. Petruzzi, S. Cocchi, F. Fineschi, A global thermo-electrochemical model for SOFC systems design and engineering, Journal of Power Sources 118 (2003) 96–107

[118] Yixin Lu, Laura Schaefer, Peiwen Li, Numerical study of a flat-tube high power density solid oxide fuel cell Part I. Heat/mass transfer and fluid flow, Journal of Power Sources 140 (2005) 331–339

[119] B.A. Haberman, J.B. Young, Numerical investigation of the air flow through a bundle of IP-SOFC modules, International Journal of Heat and Mass Transfer 48 (2005) 5475–5487

[120] D. Sanchez, R. Chacartegui, A. Munoz, T. Sanchez, Thermal and electrochemical model of internal reforming solid oxide fuel cells with tubular geometry, Journal of Power Sources 160 (2006) 1074–1087

[121] S.H. Chan, O.L. Ding, Simulation of a solid oxide fuel cell power system fed by methane, International Journal of Hydrogen Energy 30 (2005) 167 – 179

[122] R. Suwanwarangkul, E. Croiset, E. Entchev, S. Charojrochkul, M.D. Pritzker, M.W. Fowler, P.L. Douglas, S. Chewathanakup, H. Mahaudom, Experimental and modeling study of solid oxide fuel cell operating with syngas fuel, Journal of Power Sources 161 (2006) 308–322

[123] Dayadeep S. Monder, K. Nandakumar, Karl T. Chuang, Model development for a SOFC button cell using H2S as fuel, Journal of Power Sources 162 (2006) 400–414

[124] Jin Hyun Nam, Dong Hyup Jeon, A comprehensive micro-scale model for transport and reaction in intermediate temperature solid oxide fuel cells, Electrochimica Acta 51 (2006) 3446–3460

[125] Costamagna P, Costa P, Antonucci V. Micro-modeling of solid oxide fuel cell electrodes, Electrochimica Acta 43 (1998) 375–94

[126] Chen XJ,Chan SH, Khor KA, Simulation of a composite cathode in solid oxide fuel cells. Electrochimica Acta 49 (2004) 1851–61

[127] S.H. Chan, K.A. Khor, Z.T. Xia, A complete polarization model of a solid oxide fuel cell and its sensitivity to the change of cell component thickness, Journal of Power Sources 93 (2001) 130-140

[128] James Larminie and Andrew Dicks (2003), Fuel Cell System Explained, 2nd edition, John Wiley & Sons Ltd., p 53

[129] James Larminie and Andrew Dicks (2003), Fuel Cell System Explained, 2nd edition, John Wiley & Sons Ltd., p 60

[130] Subhash C Singhal and Kevin Kendall, High Temperature Solid Oxide Fuel Cells: Fundamentals, Design and Applications (2003), Elsevier Advanced Technology, The Boulevard, Langford Lane, Kidlington Oxford OX5 lGB, UK, p 300